Engineering Kidney Organoids Derived from Human Induced Pluripotent Stem Cells under 3-Dimensional Conditions

Iryna Vykhlyantseva

Thesis to obtain the Master of Science Degree in

Biotechnology

Supervisor: Doctor Cláudia Daniela Canelas Miranda Simões

Examination Committee

Chairperson: Doctor Miguel Nobre Parreira Cacho Teixeira

Supervisor: Doctor Cláudia Daniela Canelas Miranda Simões

Members of the Committee: Doctor Tiago Paulo Gonçalves Pinheiro Fernandes

October 2022

Preface

This document was written and made publicly available as an institutional academic requirement and as a part of the evaluation of the MSc thesis in Biotechnology of the author at Instituto Superior Técnico. The work described herein was performed at the Institute for Bioengineering and Biosciences of Instituto Superior Técnico (Lisbon, Portugal), during the period September 2021 - October 2022, under the supervision of Doctor Cláudia Miranda.

An electronic version of this thesis is available at:
https://fenix.tecnico.ulisboa.pt/cursos/mbiotec/dissertacoes

Acknowledgements

I would like to thank Professor Joaquim Cabral for welcoming me and all the master students so warmly, and for all his interest in all the work being done at SCERG, and most importantly, for caring about the people in his group.

To my amazing supervisor Dr. Cláudia Miranda, I cannot thank enough for first accepting me as her master student, then for her guidance and utmost patience in teaching me everything about pluripotent stem cells, kidney organoids, and all the lab techniques related. I appreciate her readiness to answer all my doubts and concerns, with compassion and honesty. I also really enjoyed her good sense of humor and the jokes that got me every time! I appreciate her help, encouragement and truly, I could not have produced this thesis without her. I am grateful for everything.

I want to thank Prof. Cláudia Lobato da Silva for awakening my passion for stem cells in the classes at IST, for her gentleness to her students. I am thankful for the help that she provided in finding a master thesis theme that I am passionate about.

I also want to express my gratitude to Prof. Tiago Fernandes, not only for his lectures in classes but also for his answering my questions, which turn into very interesting lessons.

I want to express my gratitude to PhD student Miguel Tenreiro for being my company to go to the lab at weekends and for being my role model as a PhD student. His hard work and lab ethic inspired me so much and made an impact in me. I trust everything he does at the lab, his honesty, and cannot thank enough for all those times at the lab, when he saved me from making mistakes and helped me to solve problems.

I want to say thank you to my thesis brothers and sisters at SCERG from room 16.8: Ana Luísa Rayagra, Beatriz Soares, Tiago Nunes and João Henriques. Thank you for the good memories: lunch breaks, coffee breaks, laughs, shuttle rides, adventures at Taguspark. It truly wouldn't be the same without you guys.

I also acknowledge all the rest of SCERG members for the amazing work that they do, their friendliness and indications where things are in the lab.

To all my friends who kept me entertained during my breaks, shared their thesis experiences, and helped me feel less alone in this. My special thanks go to my bestie Andreia Graça for her friendship and support. For his (British) check and his encouragement I want to thank Tiago Gil. For the helpful feedback and being my company in some of the writing process, I want to thank Tomás Hernandez.

To my family here, I thank them for their support. To my grandpa and grandma that I adore and esteem so much, thank them for their encouragement and believing in my work, this thesis is for you. You are the reason for me to strive further.

Abstract

Human induced pluripotent stem cells (iPSCs) are a powerful tool for conducting research, as they have the potential to differentiate into all three germ layers, which can serve as the basis for generating organoids. In the last decade, progress has been made in developing protocols to generate kidney organoids from iPSCs, as *in vitro* kidney models can enable disease modelling, drug screening, and potentially organ regeneration. This study aims to investigate the initial phase of renal differentiation and the influence of culture medium, spatial configuration, and the effect of various small molecules in the final cell population. To achieve this, the Morizane, Takasato, and Uchimura protocols have been fully adapted to 3D conditions. Furthermore, this project proposes the development of a novel hybrid protocol "Morisato", inspired by the concept of separately inducing the kidney progenitor populations and then co-culturing them to form complex structures. Finally, the utility of the resulting renal organoids as an option to model drug-injury responses was evaluated. Obtained kidney organoids showed heterogeneity in shape and size but demonstrated capably of self-organize into impressive tubular structures, found to be distal tubes, early proximal tubules, and showed existence of glomeruli cells. However, organoids revealed to be immature, with an inconclusive drug-injury response and no collecting duct formation. As main conclusions, kidney organoids can be generated from human iPSCs under fully 3D conditions and demonstrate that development of different populations within the kidney is a highly dynamic process that can be controlled by external factors.

Keywords: Human induced pluripotent stem cells; Kidney organoids; Renal differentiation; 3D culture; 2D culture

Resumo

As células estaminais pluripotentes induzidas humanas (iPSCs) são uma ferramenta útil para a investigação: têm o potencial de diferenciação em cada uma das três camadas germinais, que por sua vez podem servir como base para gerar organoides. Na última década, houve progresso no desenvolvimento de protocolos de geração de organoides de rim, uma vez que os modelos renais *in vitro* facilitam a modelação de doenças, triagem de fármacos e potencialmente permitir a regeneração de órgãos. Este estudo intende investigar a fase inicial da diferenciação renal e a influencia do meio de cultura, configuração espacial e o efeito de várias pequenas moléculas na população celular final. Os protocolos de Morizane, Takasato e Uchimura foram totalmente adaptados para condições 3D. Este projeto propõe o desenvolvimento de um novo protocolo híbrido “Morisato”, inspirado no conceito da indução separada de populações progenitoras de rim e posterior co-cultura, de forma a permitir a formação de estruturas complexas. Por último, foi avaliada a utilidade dos organoides renais resultantes como modelo de dano por drogas. Organoides de rim obtidos mostraram ser heterogéneos em forma e tamanho, mas demonstraram capacidade de auto-organização em estruturas tubulares impressionantes, incluindo túbulo proximal, túbulo distal e também glomérulos. Contudo, os organoides revelaram-se imaturos, com resposta a drogas inconclusiva e sem formar ductos coletores. Conclui-se que os organoides de rim podem ser gerados a partir de iPSCs em condições totalmente 3D e revelar que o desenvolvimento de diferentes populações renais é um processo altamente dinâmico, possível de ser controlado por fatores externos.

Palavras-chave: Células estaminais pluripotentes induzidas; Organoides de rim; Diferenciação renal; Cultura 3D; Cultura 2D

Table of Contents

List of Figures

List of Tables

List of Acronyms & Abbreviations

2D	Two-dimensional
3D	Three-dimensional
AIM	Anterior intermediate mesoderm
AKI	Acute kidney injury
AQP1	Aquaporin 1
ASCs	Adult Stem Cells
BMP	Bone Morphogenetic Protein
BRN1	POU transcription factor Brn1
BSA	Albumin Bovine Serum
Cas9	CRISPR associated protein 9
CASP3	Caspase-3
CD9	Cluster of differentiation 9
CD24	Cluster of differentiation 24
cDNA	Complementary Deoxyribonucleic acid
CDX2	Caudal type homeobox 2
CHIR	CHIR99021
CK8	Cytokeratin-8
c-Myc	Cellular Myelocytomatosis
CO_2	Carbon dioxide
c-Ret	Cellular Receptor tyrosine-protein kinase
CRISPR	Clustered regularly interspaced short palindromic repeats
CUBN	Cubilin
DAPI	4',6-Diamidino-2-phenylindole
DMEM	Dulbecco's modified Eagle's medium-F12
DMSO	Dimethyl Sulfoxide
EB	Embryoid body
ECAD	E-cadherin 1
ECCs	Embryonic carcinoma cells
EDTA	Ethylenediaminetetraacetic acid
EGCs	Embryonic germ cells
EGF	Epidermal Growth Factor
EMT	Epithelial-to-mesenchymal transition
ESCs	Embryonic stem cells
EYA1	Eyes absent homolog 1
FACS	Fluorescence-Activated Single Cell Sorting
FBS	Fetal Bovine Serum
FGF	Fibroblast growth factor
FOXD1	Forkhead box D1
GAPDH	Glyceraldehyde-3-Phosphate Dehydrogenase
GATA3	GATA binding protein 3
GDNF	Glial cell line-derived neurotrophic factor
GSK-3	Glycogen Synthase Kinase-3 β
HOX4-11	Homeobox proteins 4-11
HOXD11	Homeobox Hox-D11
ICM	Inner cell mass
ICs	Intercalated cells
IFT140	Intraflagellar Transport 140
IgG	Immunoglobulin G
IM	Intermediate mesoderm
iPSC	Induced Pluripotent Stem Cell
KDR	Kinase insert domain receptor
KIM-1	Kidney Injury Molecule-1
Klf4	Kruppel-like factor 4
KSP	Kinesin spindle protein
LDN	LDN193183
Lgr5	Leucine-rich repeat-containing G-protein coupled receptor 5
LHX1	LIM Homeobox 1
LIF	Leukaemia Inhibitory Factor
LIN28	Lin-28 homolog A
L-Myc	L-myc-1 proto-oncogene protein
LTL	Lotus Tetragonolobus Lectin
MKD	Mucin-1 kidney disease
MM	Metanephric mesenchyme
MSCs	Mesenchymal stem cells
MUC1	Mucin 1
Nanog	Nanog homeobox
NEPH1	Kin of IRRE-like protein 1
NGAL	Neutrophil gelatinase-associated lipocalin

NPCs	Nephron progenitor cells
NPH	Ciliopathic nephronophthisis
NPHS1	Nephrin
O_2	Oxygen
OCT4	Octamer-binding transcription factor 4
OSR1	Odd-skipped-related 1
PAN	Puromycin aminonucleoside
PAX2	Paired box 2
PAX8	Paired box 8
PBS	Phosphate-buffered saline
PCs	Principal cells
PCR	Polymerase Chain Reaction
PDGFR-α	Platelet-derived growth factor receptor α
PE	Phycoerythrin
PFA	Paraformaldehyde
PIM	Posterior intermediate mesoderm
PKD	Polycystic kidney disease
PSC	Pluripotent stem cell
qPCR	Quantitative Polymerase Chain Reaction
RA	Retinoic acid
REX-1	ZFP42 zinc finger protein
RNA	Ribonucleic acid
ROCKi	ROCK inhibitor
RPMI1640	Roswell Park Memorial Institute medium 1640
RT	Real Time
SALL1	Spalt-like transcription factor 1
SC	Stem cell
SD	Standard deviation
SIX2	Sine oculis-related homeobox 2
SOX2	SRY-Box Transcription Factor 2
SOX17	SRY-box Transcription Factor 17
SSEA	Stage Specific Embryonic Antigen
SV40 T	SV40 large T antigen
TBST	Tris-buffered saline and tween solution
THY-1	Thy-1 Cell Surface Antigen
TRA-1-60	Tumor related antibody 1-60
TRA-1-81	Tumor related antibody 1-81
UB	Ureteric bud
UMOD	Uromodulin
WD	Wolffian duct
WNT	Wingless-Type mouse mammary tumor virus integration site
WT1	Wilms' tumor 1

List of Symbols

°C	Degrees Celsius
µg	Microgram
µL	Microliter
µM	Micromolar
h	Hours
M	Molar
mg	Miligram
mL	Milliliter
min	Minutes
mM	Milimolar
ng	Nanogram
rpm	Rotations per minute

Introduction

1. Stem Cells

Stem cells are the foundation of life, building blocks of all organs, tissues, blood, and immune system. From conception to death, stem cells are responsible for the generation of all cells and structures within multicellular organisms (National Stem Cell Foundation).

In humans, stem cells exist both in embryos and in some adult tissues (**Figure 1**). During embryogenesis, stem cells can give rise to cells from all three germ layers, including the mesoderm, endoderm, and ectoderm (Bradley et al., 1984). In adults, they have a remarkable function as an internal repair system in many tissues, renewing to replace lost or damaged cells in order to maintain life.

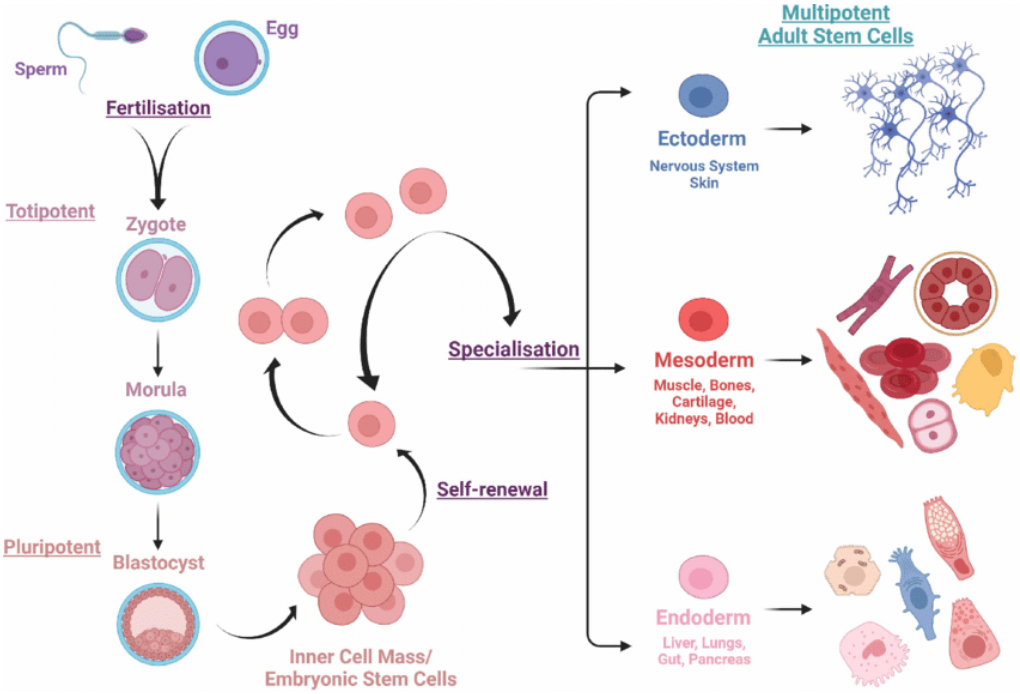

Figure 1 - Illustration of stem cells and their respective potency, from the zygote to adult stem cells. Adapted from (Stewart, 2021).

Laboratory research on stem cells over the last few decades has allowed to understand about their key features and what distinguishes them from specialized cell types. One of the fundamental properties of a stem cell is that it does not possess any tissue-specific structures that allow it to perform specialized functions. Stem cells are unspecialized and undifferentiated (Evans & Kaufman, 1981). These characteristics of stem cells makes them a valuable tool with potential in scientific research and therapeutic applications.

Other fundamental characteristics of stem cells are the ability of self-renewal and potency. Self-renewal is the process by which cells give rise to identical new stem cells leading to maintenance of the stem cell pool. Potency, in the other hand, depends on the types of cells that a precursor cell can form. This

means that stem cells can give rise to specialized cells with a particular function, while undergoing mitotic cell division. When an unspecialized cell produces a specialized cell, the process is called differentiation (Thomson et al., 1998). When a cell's fate is set, the cell is said to be determined. Differentiation refers to the actual expression of the fraction of the genome that still remains available to a determined cell and generates the process of phenotypic cell specialization.

Categorized by the scope of their capacity for differentiation, stem cells can be divided into five main types, according to their potency: totipotent, pluripotent, multipotent, oligopotent and unipotent, as can be seen in **Table 1**.

Table 1 - Characterization of stem cells based on their potency and differentiation potential. ESCs: Embryonic stem cells, iPSCs: Induced pluripotent stem cells, EGCs: Embryionic germ cells. HSCs: Hematopoietic stem cells. Retrieved from Loya et al., 2014.

Type	Characteristic	Example
Totipotent	can differentiate into all cell types including extra-embryonic tissue, ability to from a fully functional complete organism	cells of the zygote
Pluripotent	can differentiate into all three germ layers, ability to form any of the fetal or adult cell types	ESCs, iPSCs, EGCs, and fetal stem cells
Multipotent	usually consist of progenitor cells, ability to differentiate into only a limited number of cell types	adult stem cells such as HSCs and neural stem cells
Oligopotent	usually consist of cells that reside in the tissue, ability to terminally differentiate into cells of a specific tissue	stem cells present on the mammalian ocular surface, lymphoid or myeloid stem cells
Unipotent	have the ability to differentiate into a single type of cells	progenitor cells present during postnatal prostate development

1.1. Pluripotent stem cells

Pluripotency can be defined as capacity to differentiate into tissues of all three germ layers: ectoderm, mesoderm, and endoderm, as well as the germ lineage; but not extraembryonic structures (Bradley et al., 1984). The capability of pluripotent stem cells to give origin to any type of cell of the human body is demonstrated throughout embryonic development (van den Brink et al., 2014). Previously, pluripotent stem cells were thought to be only found during the earliest stages of embryogenesis and then become rapidly depleted as embryonic development proceeds (Carpenedo & McDevitt, 2013), as pluripotency is a transient characteristic of cells of the early embryo (de Miguel et al., 2010). Currently, different types of PSCs have been identified, including:

- Embryonic carcinoma cells (ECCs), derived from teratocarcinomas, a malignant tumor that originates in the gonads from germ cells and is capable of giving rise to cells from all three germ lineages within the tumor (Martin & Evans, 1975);

- Embryonic stem cells (ESCs), derived from the inner cell mass of blastocysts (Thomson et al., 1998);
- Epiblast-derived stem cells (EpiSCs), also known as embryonic germ cells (EGCs), possess similar phenotypic markers to those of ESCs and are derived from primordial germ cells found within gonadal ridges and mesenteries of fetuses. (Shamblott et al., 1998);
- Induced pluripotent stem cells (iPSCs), produced by forcing the expression of specific transcription factors in adult somatic cells (Takahashi et al., 2007).

Characteristically, this type of cells expresses the transcription factors OCT4, SOX2, and Nanog, which are involved in maintaining the undifferentiated state. The gold standard to assess the *bona fide* pluripotency of stem cells is the teratoma formation assay. This *in vivo* assay that can be resumed in the injection of the test-cells into immunocompromised mice and expect the formation of a teratoma, a non-malignant tumor comprised of cells from all three of the embryonic germ-layers (Wesselschmidt, 2011). Pluripotent stem cells were also shown to form chimeras through cell aggregation with eight-cell embryos or cell injection into blastocysts (Peli et al., 1996), demonstrating their ability to contribute to all tissue of an organism but not the trophoblast-derived cell lineages.

In vitro, PSCs can be induced to differentiate into other cell types with the use of specific biochemical and physical signals, also can be forced to form into embryoid bodies (EBs), which are three-dimensional aggregates composed by the three embryonic germ layers (Martin & Evans, 1975).

In research, there are many immortal cell lines of pluripotent stem cells that can be grown indefinitely under specific conditions. The ECC lines were the first pluripotent cell lines to be established and are considered the malignant equivalent of ESCs, as they share the same pluripotency markers but are usually aneuploid (de Miguel et al., 2010).

Although human ESC and EGC lines were established at approximately the same time, researchers have more regularly worked with and reported on ESCs, which have indeed served as the foundation for the majority of what is now known about human pluripotent cell biology (Carpenedo & McDevitt, 2013). The preferred model systems of pluripotent stem cells are the ESCs and iPSCs, due to their dynamics and practical availability.

1.2. Embryonic stem cells

Embryonic stem cells (ESCs) are derived from the inner cell mass (ICM) of blastocyst, which is formed during the embryonic development, at approximately 5 days after fertilization (Carpenedo & McDevitt, 2013). Molecular characterization of ESCs shows the express surface markers such as CD9, CD24, and alkaline phosphatase, and several genes involved with pluripotency, including OCT4, REX-1, SOX2, Nanog, LIN28, THY-1, SSEA-3, and SSEA-4 (Loh et al., 2006). ESCs confirm defined characteristics of PSCs that were previously remarked: they are pluripotent, capable of differentiating into cells derived from all three germ layers (Akutsu et al., 2006).

In 1998, the first human ESC line was isolated and cultured from frozen embryos that were obtained from excess samples of *in vitro* fertilization (Thomson et al., 1998). In culture, ESCs can retain their ability to self-renew, can be propagated indefinitely for several hundred passages in the undifferentiated state while also maintaining a normal chromosomal composition. Expression of high levels of telomerase explains their immortality in culture (Chagastelles & Nardi, 2011). This feature allowed ESCs to become *in vitro* model system for initial stages of mammalian development without the need to harvest peri-implantation embryos, used to dissect the basic mechanisms underlying pluripotency, cell lineage specification and respective potential clinical use for regenerative cell therapies (Rippon & Bishop, 2004).

However, there is a major ethical debate about the moral status of the embryo in human embryonic stem cell research. Since harvesting embryonic stem cells requires destroying the 5-day-old preimplantation embryo from which those cells are obtained, opponents of human ESC use consider that because embryos have the potential to develop into a human being, it has important moral standing, and hence its destruction is unacceptable. Some human ESC researchers deny that the embryo has any moral status; others award it some moral status, but it is outweighed by the potential advantages of human ESC research (King & Perrin, 2014).

Induced pluripotent stem cells (iPSC) emerged an alternative to ESCs, since the first option does not require blastocysts as a source of cells, but rather adult somatic cells. Indeed, iPSCs are a viable alternative to embryonic stem cells since they avoid the ethical issues associated with their use.

1.3. Induced pluripotent stem cells

The knowledge of genetic hallmarks in pluripotent stem cell populations let to an important breakthrough in stem cell technology: the method of nuclear reprogramming adult cells into pluripotent stem cells. This discovery shifted the stem cell research paradigm by demonstrating that differentiation is not a unidirectional process.

Induced pluripotent stem cells were obtained for the first time in 2006 by Shinya Yamanaka's lab. iPSCs were attained through the introduction of the expression of transcription factors, found to be increased in ESCs and other pluripotent stem cells (specifically, OCT4, SOX2, c-Myc, and Klf4), delivered by retroviral vector constructs. After the insertion of the transgenes of the four transcription factors, the cells will continue to drive transcription of their downstream genes which leads to the activation of other transcriptional network signaling that induces a cascade of transcriptional activity that consequently reprograms the potency of the cell (Takahashi et al., 2007). These differentiated cells were reverted into a less differentiated state with an efficiency of 0.1% (de Miguel et al., 2010). Initially, cellular reprogramming was only done from skin fibroblasts but soon it was performed with other somatic cells (Staerk et al., 2010).

This reprogramming technique provided an unparalleled opportunity to model human disease, undertake gene repairs, and conduct personalized drug screens from iPSCs created from patient cells

with known mutations and phenotypes (J. Wu & Izpisua Belmonte, 2016). Furthermore, the ability to generate patient-derived iPSCs leads to a significant advancement in autologous transplantation and the application of the technique in medicine. Since they are obtained from the cells of the patient, there is low possibility of problems associated with transplant rejection.

Despite not being identical, iPSCs closely resemble embryo derived human ESCs. Recent experiments have demonstrated that human ESCs and human iPSC differ in the expression of genes are linked to epigenetic memory (Votteler et al., 2010). Human iPSCs, like other pluripotent stem cells, can undergo differentiation into virtually any cell type of interest by the establishment of induction protocols. iPSCs can be transformed to any types of cells (**Figure 2**).

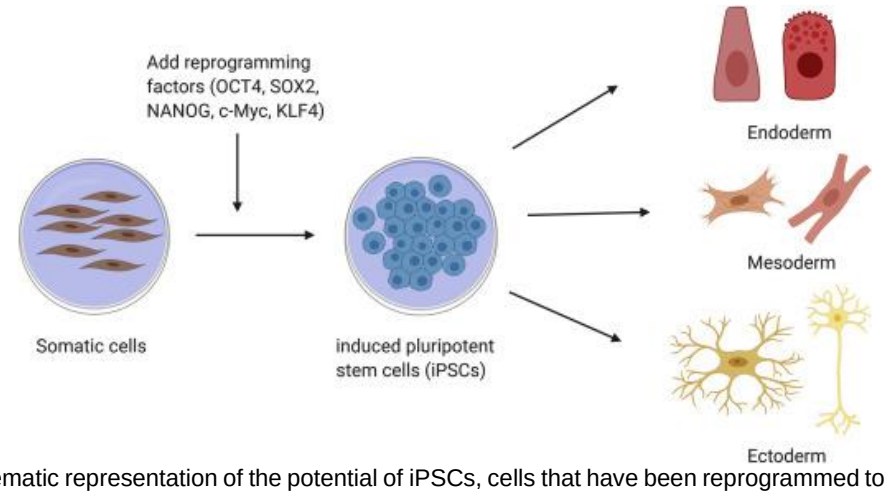

Figure 2 – Schematic representation of the potential of iPSCs, cells that have been reprogrammed to the pluripotent state, which in proper culture conditions can be induced to differentiate into any cell type. Retrieved from (Deinsberger & Weber, 2021).

2. Organoids

Organoids have been a topic of research that predates the first isolation of pluripotent stem cells. The earliest foundations of organoids research can be traced back to the basic method of cell disaggregation, followed by reaggregation which concluded that simple sponges had the ability to self-organize (Wilson, 1910). Later, disaggregation-reaggregation assays were replicated with suspensions of kidney cells of the chick embryo. After aggregation, epithelial cells formed small clusters and exhibited structures such as tubules bounded by mesenchyme-derived stroma that resembled the small-scale anatomy of kidney during mesonephros stage (Moscona & Moscona, 1952). These experiments proved that cells of embryonic chicks, as well as the cells of sponges contained enough information to arrange themselves accurately even after their initial spatial associations were lost (Davies, 2018).

The interest in organoid systems increased in the beginning of the 21st century, driven by the rapid developments in stem cell differentiation and the attempts to recreate organs *in vitro* (Davies, 2018). Indeed, it was observed that when stem cells form teratomas *in vivo* and embryoid bodies *in vitro*, differentiated cells can arrange into diverse patterns matching those present in many tissue types (Martin & Evans, 1975). However, it was not until 2009 that the modern organoid systems emerged when Hans Clevers' lab demonstrated the possibility of creating gut organoids with a crypt-villus architecture from 3D Lgr5+ stem cells cultured in Matrigel (Sato et al., 2009).

The modern-day definition of organoid is that of a three-dimensional structure of cells that fulfils standards such as multiple organ-specific cell types, basic tissue-level functions of an organ (e.g., excretion, neural activity, contraction) and 3D spatial organization that can recapitulate the anatomy of the same organ. These characteristics make organoids different from organotypic cultures, simple cell aggregates and embryoid bodies. In many ways, organoids reflect the evolution of the *in vitro* system known as embryoid body. However, embryoid bodies are 3D aggregates of PSCs that in culture spontaneously give rise to all three germ layers, undergoing the initial developmental specification in much the same manner as the pre-gastrulating embryo (Weitzer, 2006), while organoids are usually originated from one germ layer and mimic organogenesis.

During their formation, organoids replicate two key self-organization mechanisms during development: cell sorting and spatially restricted lineage commitment (Lancaster & Knoblich, 2014). This means that they can recreate some organogenesis principles *in vitro* and provide simpler and easily available systems for assessing the relative contributions of different tissue components to complex organ development processes (Rossi et al., 2018). Organoid systems are an extremely appealing prospect for scientists because they resemble the composition and functions of organs, which means more *in vivo*-like outcomes in research (Lancaster et al., 2013).

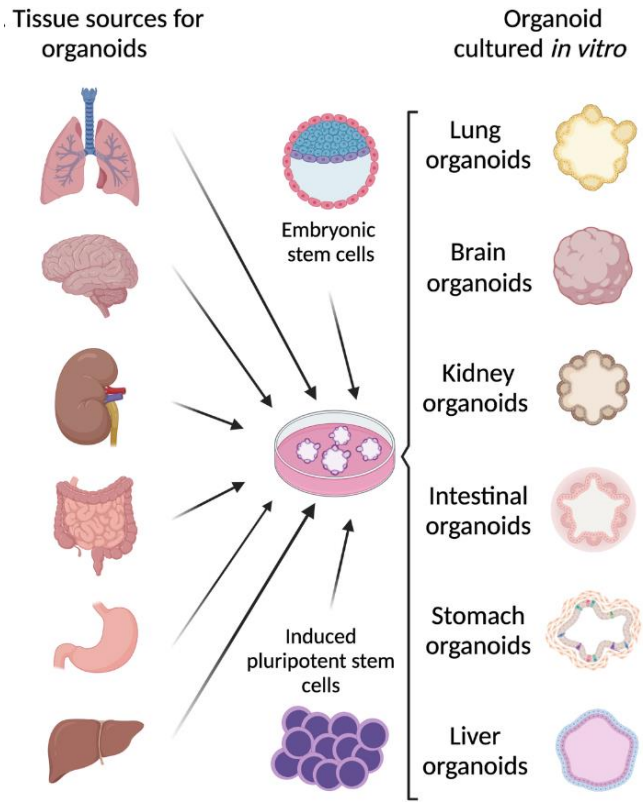

Figure 3 – Sources of cells to able to generate organoids *in vitro*: adult stem cells, embryonic stem cells or induced pluripotent stem cells. Adapted from (Ramírez-Flores & Knoll, 2021).

Organoids have been successfully generated from both adult stem cells and pluripotent stem cells (**Figure 3**). They can be derived from either from tissue-resident adult stem cells (ASCs), directly

sourced from biopsy samples, or from pluripotent stem cells (PSCs), such as embryonic stem cells (ESCs) or induced pluripotent stem cells (iPSCs) or even fetal progenitor cells. This opened the possibility of organoids generated from pluripotent stem cells or organ progenitors of diseased adult tissue-specific stem cells. This means that organoids can be used as tools to answer a range of biological and medical questions and even help to redefine, reduce, or replace the use of animals in research (Davies, 2018).

2.1. Organoids derived from induced pluripotent stem cells

iPSC-derived organoids have taken the spotlight of stem cell research because, in comparison to adult tissue-derived organoids, they are not limited to accessibility to tissues. In fact, iPSCs offer an unlimited source of stem cells after genetic reprograming of any adult cell and the establishment of the respective cell line (Lancaster & Huch, 2019). Furthermore, iPSCs circumvent the ethical problems of human ESCs isolation that implied the destruction of human embryos at the blastocyst stage (de Wert & Mummery, 2003).

Protocols of generation of iPSC-derived organoids usually begin with adequate germ-layer induction (endoderm, mesoderm, or ectoderm), then followed by maturation and cell propagation in a three-dimensional environment. Initial attempts of production of *in vitro* organoids centered on the differentiation of iPSCs into a particular cell type and its culture in two dimensions (Takahashi et al., 2007; Yu et al., 2007). Advanced culture techniques tried to replicate the organogenesis in different 3D culture systems, which enabled derivation of more cell types within the organoid and consequently increased its complexity (Li et al., 2016).

The current rational of *in vitro* organoid generation from iPSC is based on closely mimicking the complete process of the organ development during embryogenesis, in which the first step is the germ layer specification into ectoderm, mesoderm or endoderm. What triggers the iPSC differentiation is the introduction of specific combinations of exogenous agents like small molecules and growth factors, even though it is impossible the exact imitation of all biochemical factors that drive cell differentiation at the right timing, concentration, and localization at which they occur throughout embryogenesis. Luckily, this process is facilitated by the nearly autonomous differentiation trajectory that the stem cells follow, displayed both *in vivo* and *in vitro*. The innate self-organization capacity of these cells leads towards differentiation into potentially any organ-specific tissue. Thus, to recapitulate of organogenesis *in vitro,* one must understand the principles and pathways underlying that process and apply them into differentiation protocols. For example, kidney organoids were observed to differentiate and self-assemble spontaneously in response to environmental stimuli similar to those seen in the developing kidney (Grobstein & Dalton, 1956; Takasato & Little, 2016). Therefore, in order to successfully recapitulate the development of the kidney in iPSC-derived organoids, one must first understand the key-player cell populations and their interactions during nephrogenesis.

3. Early embryonic development

Around 6-7 days after fertilization, the embryo begins to form a strong attachment to the endometrial epithelial lining (**Figure 4B**). The first stage of implantation involves the attachment of the enlarged multi-cellular blastocyst to tiny surface projections of endometrial epithelial cells. During implantation to the uterine epithelium, the blastocyst comprises of the inner cell mass, from which the body of the proper embryo develops, and the outer trophoblast, which delineates the future extraembryonic tissues (Marieb et al., 2012).

The inner cell mass is source of pluripotent stem cells that is initially homogenous until the beginning of the subdivision process known as gastrulation. Gastrulation starts with the formation of the primitive streak, a linear midline condensation of cells derived from the epiblast (primitive ectoderm) in the embryo's posterior region, induced by cells at the border of the embryonic disk in that region. The migration of cells through the primitive streak causes the creation of a groove (primitive groove) along the primitive streak's midline (**Figure 4B**). WNT3 and BMP4 have been identified as inducers of primitive streak development and their gradient guides the anterior-posterior axis of the embryo (Carlson & Kantaputra, 2018).

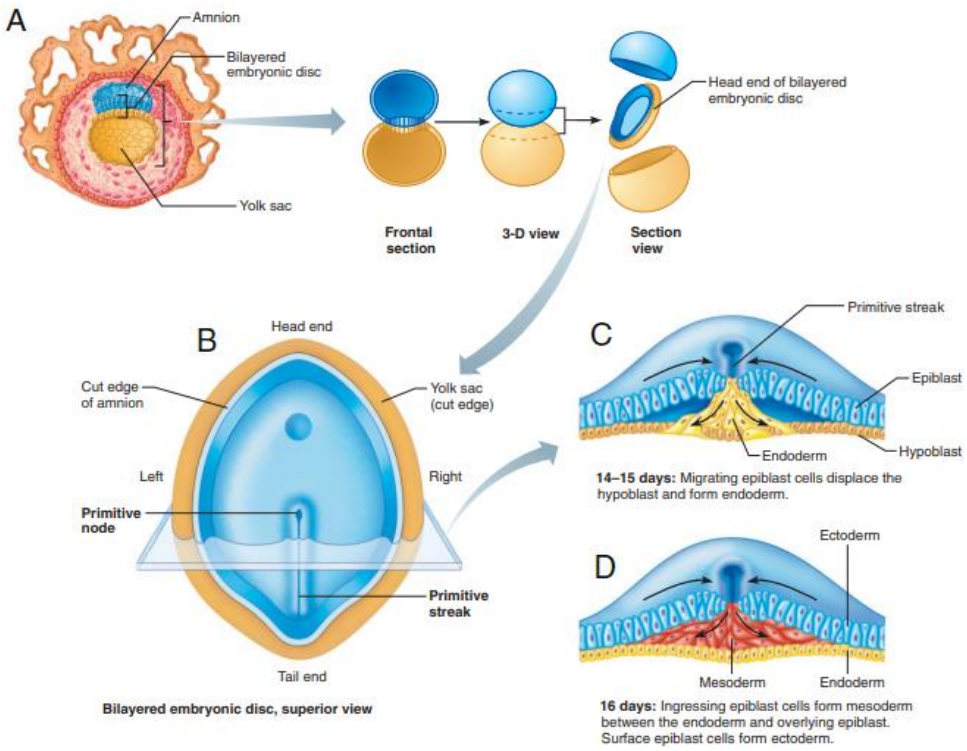

Figure 4 - The primitive streak stage. A) Implanted blastocyst in the trophoblast at circa day 11 of embryonic age. B) The primitive streak appears on the epiblast on about day 14. C) Sections through the embryonic disc at the location shown in (B). D) Formation of the mesoderm from the primitive streak. Retrieved from (Marieb et al., 2012).

A primitive node formation in front of the primitive streak and it is a signaling center that expresses a potent combination of secreted factors for establishing the body axes and left-right asymmetry. This structure is important for the development because it is the area through which cells flow in a stream toward the embryo's anterior end. These cells, known as mesendoderm, quickly separate into a rod-like

mesodermal notochord and the endodermal dorsal wall of the forming gut. The primitive streak, which is initially triangular, quickly becomes linear and elongates, owing to a combination of proliferation, migration, and internal cellular rearrangements known as convergent-extension events (**Figure 4C**)(Carlson & Kantaputra, 2018). Ultimately this results in an embryonic body that contains the three primary embryonic germ layers: the ectoderm (outer layer), mesoderm (middle layer), and endoderm (inner layer) (**Figure 4D**).

3.1. Intermediate mesoderm specification

Mesoderm is a primary germ layer positioned in between the ectoderm and the endoderm. In the future it gives rise to muscle, bone, connective tissue, blood vessels, red and white blood cells, and various organs such as the kidney and gonads.

Mesoderm be classified in four types: the axial mesoderm (notochord), the paraxial mesoderm, the intermediate mesoderm, and the lateral plate mesoderm. The location of cells in the primitive streak defines the subsequent differentiation into paraxial mesoderm, intermediate mesoderm, and lateral plate mesoderm. Cells migrating from the primitive streak during earlier stages of embryonic development differentiate into the more anterior mesoderm, whereas those migrating from the late stage of the primitive streak differentiate into the posterior mesoderm. Importantly, the primitive streak cell locations determine future differentiation into paraxial or lateral plate mesoderm (**Figure 5**) (Sweetman et al., 2008).

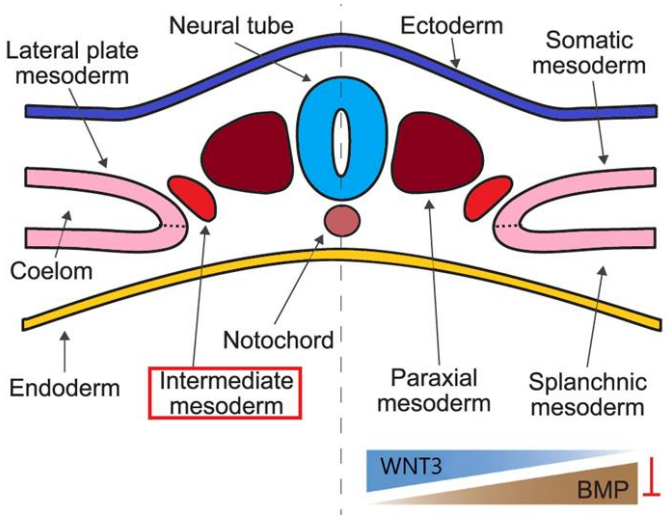

Figure 5 - Scheme of the mesoderm patterning along the mediolateral axis by gradients of specific signalling molecules, as WNT3 and BMP. Adapted from (Iberite et al., 2022).

Indeed, the cells located at the anterior part of the primitive streak differentiate into paraxial mesoderm while the posterior cells in the primitive streak become the lateral plate mesoderm. Specifically, the mammalian kidney originates from intermediate mesoderm, in a region of mesoderm located between the paraxial mesoderm and the lateral plate mesoderm. Thus, the progenitor cells of the intermediate mesoderm are located at the center of the primitive streak. (Lengerke et al., 2008)

The gradient of WNT3A and BMP4 guides the anterior-posterior axis of the primitive streak. Furthermore, higher levels of BMP4 induce the posterior primitive streak in humans and mice (Lengerke et al., 2008; Liu et al., 1999). Thus, these results suggested that adjusting the BMP4 signal levels was important to induce cells that could mimic those at the center of the primitive streak, the origin of the intermediate mesoderm.

3.2. Nephrogenesis

The mammalian kidney develops from the intermediate mesoderm of the urogenital ridge, a tissue present in the developing fetus along the posterior wall of the abdomen (**Figure 6A,B**) (Saxén, 1987). Kidney development, also called nephrogenesis, compromises three sequential developmental phases: pronephros, mesonephros, and metanephros (**Figure 6C**). Interestingly, the only section that gives rise to the definitive mature kidney is the metanephros, which is derived from the late-stage mid primitive streak cells, while the pronephros and mesonephros structures degrade before birth (Saxén & Sariola, 1987). Regardless, several signaling pathways and genes that are critical in the metanephric kidney appear to serve comparable functions in the pronephros and mesonephros, during early stages of renal development (Sainio & Raatikainen-Ahokas, 1999; Taal et al., 2012).

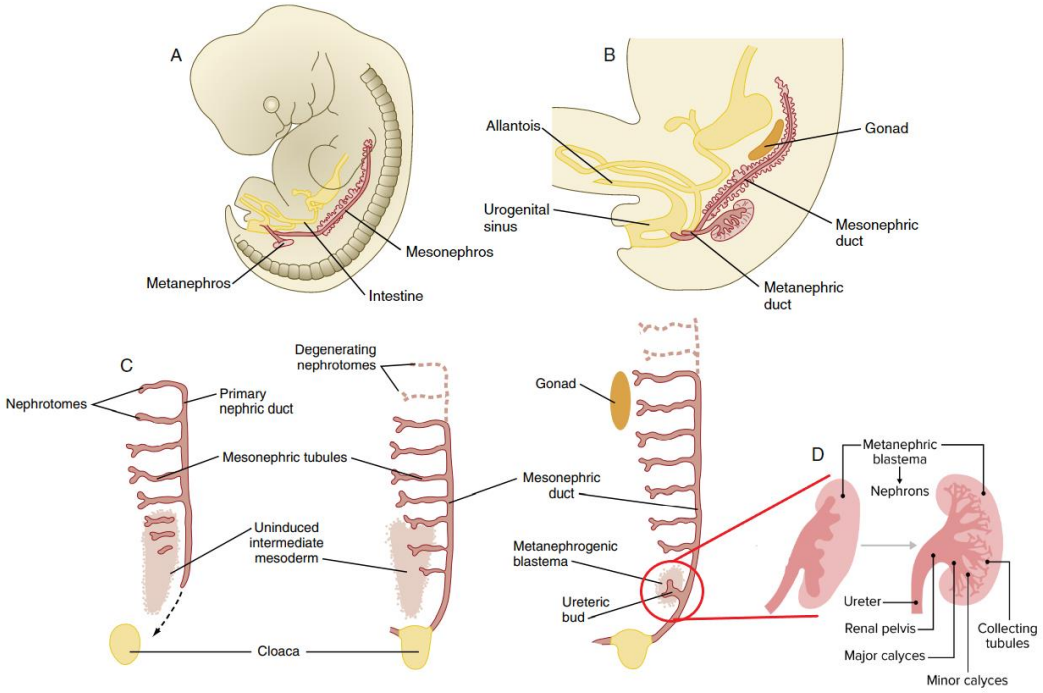

Figure 6 - Stages in the formation of the metanephros. A) At 6 weeks. B) At 7 weeks. C) Caudal progression of formation of the mesonephros and degeneration of the most cranial segments of the primitive kidney. D) The ureteric bud forms a peduncle that develops into the ureter. Its cranial expansion becomes the renal pelvis while the mesenchymal cells of the metanephric blastema gradually evolve into the primordial nephrons. Adapted from Carlson & Kantaputra, 2018.

During the pronephros stage there is formation of nephrotomes, which are an extended pair of excretory structures that differentiate from anterior intermediate mesoderm. The nephrotomes connect laterally with a pair of primary nephric ducts that grow toward the embryonic cloaca. This early stage depends

on the expression of HOX4-11 genes that determine the cranial-caudal limits of the organ system (Dressler, 2006; Wellik, 2011).

The primary nephric ducts elongate caudally, influenced by transcription factor GATA3 (Labastie et al., 1995), and stimulates the intermediate mesoderm to form additional segmental sets of tubules (denominated mesonephric tubules) which form along a cranial-caudal gradient. The first pairs of mesonephric tubules (and the pronephric tubules) arise as extensions from the primary nephric ducts (Carlson & Kantaputra, 2018). The expression of PAX2 is important to the conversion of the mesenchymal cells of the intermediate mesoderm into epithelial tubules. If there is deficiency of such molecule, there is no further development of mesonephric tubules (Bouchard et al., 2002; Dressler et al., 1990).

In the end of the week 4 of gestation, in the posterior (caudal) portion of the intermediate mesoderm, the mesonephric ducts attach to the embryonic cloaca. Near to this attachment site, an epithelial outgrowth forms the ureteric bud (UB), also known as metanephric diverticulum. The ureteric bud growth induces the surrounding mesoderm to form the metanephric blastema (the precursor of metanephric duct), through the action of WNT secreted from the bud and plays a central role in the regulation of mesenchymal to epithelial transitions (Carroll et al., 2005). Simultaneously, the GDNF (gonadal derived neurotrophic factor) produced by the metanephric blastema stimulates the growth of the ureteric bud (UB) (Basson et al., 2005; Saxén, 1987).

There is an anteroposterior polarity in intermediate mesoderm (**Figure 7**). The anterior intermediate mesoderm differentiates into mesonephric duct (Wolffian duct) and the posterior intermediate mesoderm gives rise to the metanephric mesenchyme (MM) (the nephron progenitor) and to mesonephric mesenchyme (Takasato & Little, 2016; Xu et al., 2014).

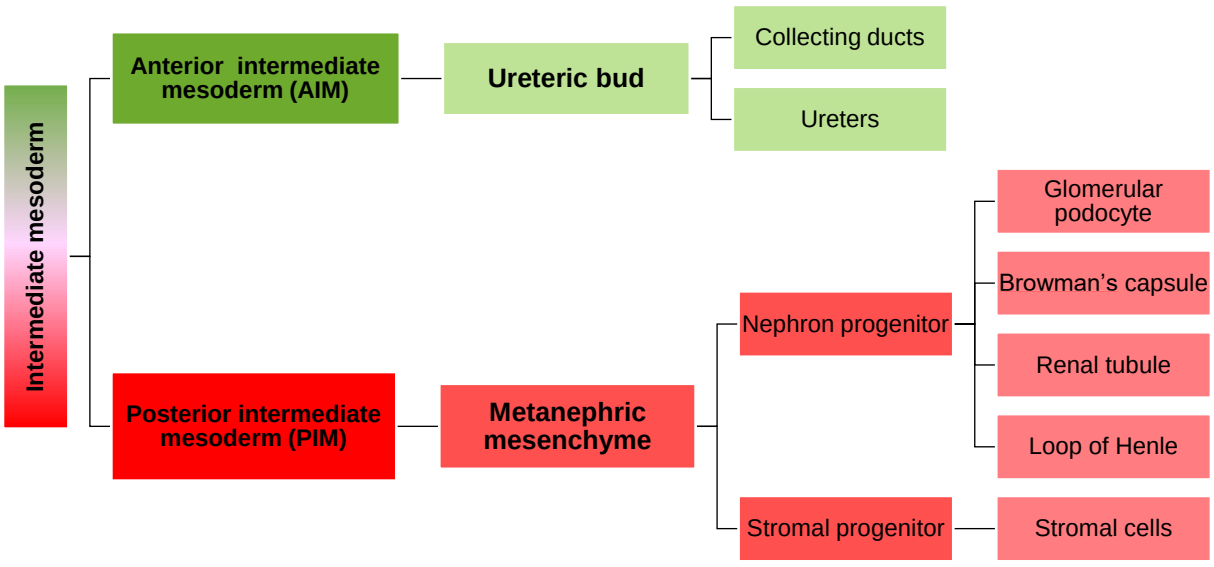

Figure 7 – Schematic summary of lineage relationships in mammalian kidneys, where the metanephric mesoderm (MM) and ureteric bud (UB) share a common origin, the intermediate mesoderm.

In the last stage of development, the metanephros, depends on several inductive interactions that occur between the MM and the UB in the posterior (caudal) section of the urogenital ridge. This inductive signal is influenced by c-Ret on the ureteric bud (Batourina et al., 2001). Additionally, Fibroblast growth factor 2 (FGF2), BMP7, and leukemia inhibitory factor (LIF), secreted by the ureteric bud, stimulate the further formation of renal tubules in the metanephric mesenchyme. This sets up a series of continuous mutual interactions between the ureteric bud and the metanephric blastema that lead to the development of the kidney and its excretory system. (Carlson & Kantaputra, 2018; Grobstein & Dalton, 1956)

In the developing metanephros, nephrons (which are the functional units of the kidney) are generated from three sources: the metanephric blastema, the ureteric bud, and in growing cells endothelial of vasculature (**Figure 6D**). Nephrons continue to form throughout the fetal development, at the tips of the ureteric bud. The induction of nephrons involves reciprocal inductions between terminal branches of the collecting duct system (ureteric bud) and the metanephric mesoderm (Saxén & Sariola, 1987). Even though all elements of the nephron are present before birth and filtration occurs during pregnancy, tubule and nephron maturation continues following birth (Taal et al., 2012). Summary of kidney development *in vivo* can be seen in **Figure 8**.

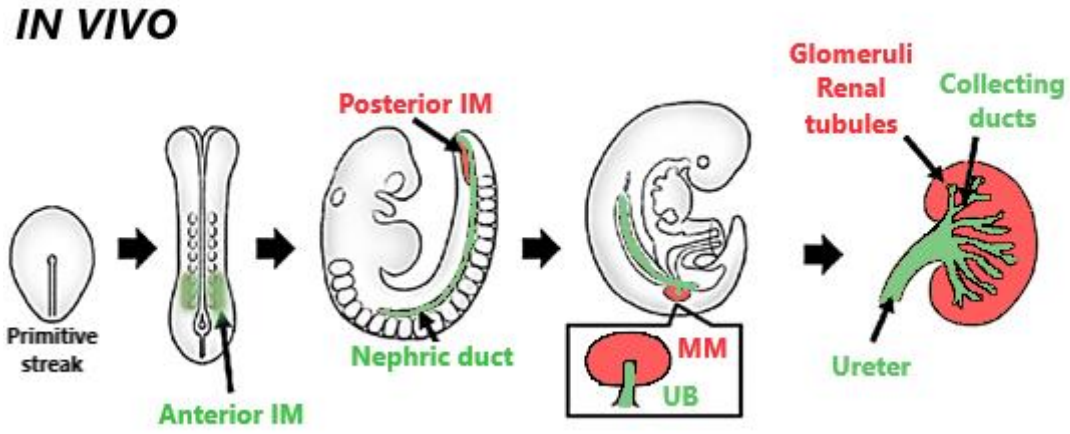

Figure 8 - Schematic diagram of *in vivo* kidney development. Adapted from (Osafune, 2021).

4. Differentiation of pluripotent stem cells into renal lineage

Early protocols towards *in vitro* expansion of kidney cell populations were based on 2D monolayer culture or embryoid body culture formats. Usually of single or few-steps nature, these differentiation protocols used mouse ESCs and/or mouse iPSCs and explored the growth factors that induced the expansion of renal lineage cells.

Differentiation of kidney cells from PSCs can be accomplished by the introduction of specific factors that can induce differentiation and recapitulate nephrogenesis (Kim & Dressler, 2005). The conventional approach was initial the induction of the primitive streak, following mesoderm induction and the generation of anterior intermediate mesoderm (wrongly thought as common to all kidney cell populations) and then finally the metanephric mesenchyme formation.

Generally, nephrogenic factors such as activin A, retinoic acid (RA), and bone morphogenetic proteins (BMPs) were used since previously they were found to be important in development and specification of kidney populations in the anterior intermediate mesoderm (Dressler, 2006; Moriya et al., 1993). Most of these studies, however, used undefined components like fetal bovine serum (FBS) while other required transplantation of differentiated cells into mice to obtain kidney cell phenotypes (Kim & Dressler, 2005).

By mimicking nephrogenesis, the first step on the differentiation protocol is late primitive steak induction, that can be achieved with the presence of WNT signaling. CHIR99021, a GSK-3 inhibitor, is used to induce late primitive streak via canonical WNT signaling pathway activation (Nusse, 2008).

Because there are no specific markers to identify late-stage mid primitive streak cells during *in vitro* directed differentiation of PSCs, the best timing, and treatments of WNT and BMP4 modulators to use were sought by examining the subsequent differentiation of PSCs into $WT1^+$ $HOXD11^+$ posterior intermediate mesoderm cells. Indeed, differentiation protocols attempt to induce the specific differentiation pathway of intermediate mesoderm and obtain cell types of the renal lineage. In addition, it is crucial to undertake tissue characterization to confirm if the cells are undertaking the right differentiation course, and this is achieved with the analysis of different renal developmental markers. Markers such as PAX2 and WT1 were both found to be expressed during kidney organogenesis and then downregulated (Georgas et al., 2008). Yet, WT1 seems also be expressed in the final stage of nephron formation, in the podocytes. The transcription factor OSR1 is upregulated in the intermediate mesoderm, HOX11 and GDNF is expressed in the metanephric mesenchyme. GATA3 is expressed the ureteric epithelium (Labastie et al., 1995). The simultaneous expression of SIX2, SALL1, WT1, EYA1 and PAX2 is characteristic of a nephron progenitor cell (Moribana & Lam, 2015).

In 2005, one of the first protocol of mouse ESCs differentiation in kidney cell types was established. Kim and Dressler used the molecules activin A, BMP7 (bone morphogenetic protein 7), and RA (retinoic acid) in their protocol to induce embryoid body (EB) formation and consequent differentiation into $PAX2^+$, $WT1^+$ and $GDNF^+$ cells, which are known markers the early stage of metanephric mesenchyme (Kim & Dressler, 2005). In 2009, Morizane *et al*. differentiated mouse iPSC and ESCs into embryoid bodies that were seeded afterwards into gelatin-coated plates. Activin, GDNF, and BMP7 or only activin was supplemented to the differentiation media. The results reported that GDNF and BMP7 enhanced the differentiation to metanephric mesenchyme in ESCs, Activin enhanced the differentiation of tubular cells in both ESCs and iPSCs. In the end, kidney cells that expressed SIX2, WT1, PAX2, nephrin, and KSP (tubular specific marker) were obtained (Morizane et al., 2009). In 2013, Xia et al. demonstrated the induction of $PAX2^+$ $LHX1^+$ intermediate mesoderm cells from iPSCs, with the use of BMP2-4, FGF2, RA and Activin A. This resulted in an enrichment of ureteric bud progenitor-like cells, but not nephron progenitor cells (Xia et al., 2013). Indeed, the differentiation of PSCs into renal lineage had demonstrated limited success until Taguchi *et al.* proposed a novel approach based in the newly identified origin of the kidney populations.

4.1. Kidney organoids

4.1.1. Protocols of PSC-derived kidney organoid generation

The progress in understanding kidney organogenesis facilitated the generation of advanced differentiation and culture techniques that allowed the generation of complex 3D structures with multiple renal cell types. However, the generation of nephron progenitors that can fully reconstitute the 3D nephron structure and function *in vitro* remained a challenge. Different modern protocols of kidney organoid generation were developed over time that were able to induce metanephric mesenchyme (MM) or ureteric bud (UB) epithelium, or both at the same time. The most successful and widely applied protocols can be seen in **Table 2**.

Table 2 – Most impactful studies and protocols of kidney cell linage generation from human PSCs. Retrieved from Takasato & Wymeersch, 2020.

Authors and Year	Culture format	Stepwise protocol	Outcome
Taguchi et al. 2014	Embryoid body	Epiblast: 2d activin A Late primitive streak: 2d BMP4, CHIR99021 Posterior nascent mesoderm: 4d BMP4, CHIR99021 Posterior IM: 2d activin A, BMP4, CHIR99021, RA Metanephric mesenchyme: CHIR99021, FGF9	$SIX2^+$, $WT1^+$, $SALL1^+$, $PAX2^+$ metanephric mesenchyme. When metanephric mesenchyme cells were culture with mouse dorsal spinal cord, the cells self-organized nephrons segmenting into glomerulus, proximal tubule and distal tubule
Takasato et al. 2014	Monolayer	Posterior primitive streak: 2d CHIR99021 Intermediate mesoderm: 4d FGF9, Heparin Metanephric mesenchyme and ureteric epithelium: 6d FGF9, Heparin followed by 6d no growth factors	Simultaneous induction of $WT1^+$ $SIX2^+$ metanephric mesenchyme and $PAX2^+$ $GATA3^+$ ureteric epithelium. When metanephric mesenchyme and ureteric epithelium cells were aggregated, the cells self-organized into renal structures including collecting ducts, proximal and distal tubules
Takasato et al. 2015	Monolayer then 3D	Mid primitive streak: 4d CHIR99021 Anterior and posterior intermediate mesoderm: 3d FGF9, Heparin Kidney organoid: 1h CHIR99021 pulse followed by 5d FGF9, Heparin and then 13d no growth factors	Kidney organoid containing nephrons segmenting into glomerulus, proximal tubule and distal tubule that were associated with a collecting duct network surrounded by renal interstitium and endothelial cells.
Morizane et al. 2015	Monolayer then 3D	Late primitive streak: 4d CHIR99021, ± Noggin Posterior intermediate mesoderm: 3d activin A Metanephric mesenchyme: 2d FGF9 Self-organizing nephrons: 2d FGF9, CHIR99021 followed by 3d FGF9 and then no growth factor	Nephron organoid containing nephrons segmenting into glomerulus, proximal tubule, and distal tubule

Taguchi et al. 2017	Embryoid body	Epiblast: 1d activin A, BMP4 Early primitive streak: 1.5d CHIR99021, BMP4 Anterior IM: 2d RA, FGF9, BMP inhibitor, TGFb inhibitor WD progenitor: 1.75d RA, FGF9, CHIR99021, BMP inhibitor Ureteric bud: 2d RA, FGF9, CHIR99021, GDNF, FGF1, BMP inhibitor followed by 2d RA, CHIR99021, GDNF, FGF1, BMP inhibitor	Budding structures of ureteric bud, expressing PAX2, ECAD, CK8 and SOX9. A combination with human iPSCs-derived MM (from a protocol of 2014) did not successfully induce branching, whereas it was very successful using mouse ESCs derived UB and MM with primary renal stroma.

4.1.1.1. Taguchi protocol (2014)

In 2014, work by Taguchi *et al.* presented a revised model of early-stage kidney specification. They suggested distinct spatially and temporal origins of two major kidney components: anterior intermediate mesoderm (that originates ureteric bud cell populations) and posterior intermediate mesoderm (that originates metanephric mesenchyme). They achieve it by showing distinction of the T^-, $OSR1^+$, $PAX2/8^+$, $LHX1^+$ intermediate mesoderm at embryonic-day 8.5 and the $OSR1^+$, $WT1^+$, $PAX2^-$, $SIX2^-$, $HOX11^+$ intermediate mesoderm at embryonic-day 9.5 (**Figure 9**).

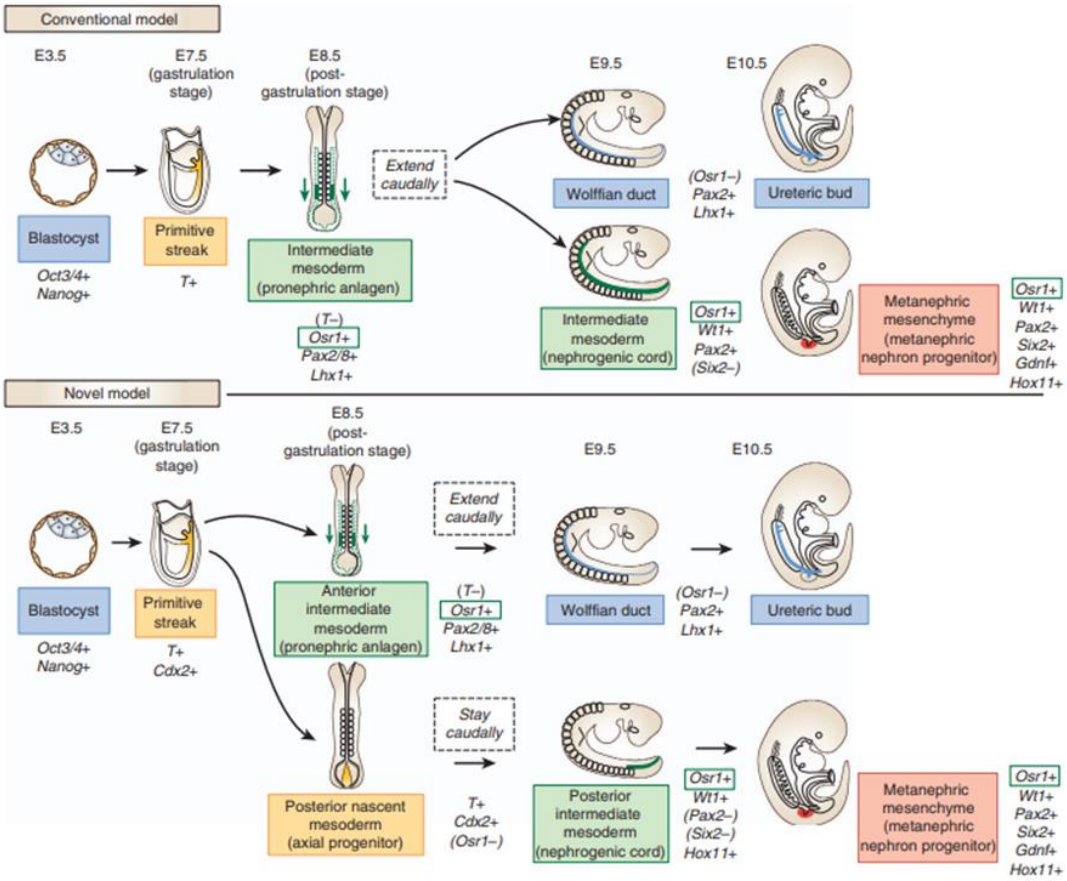

Figure 9 - Conventional and novel model for lineage segregation of the ureteric bud (UB) and the metanephric mesenchyme (MM). Conventional model shows MM and UB originate from common intermediate mesoderm at embryonic stage 8.5. Novel model proposes the spatiotemporally distinct intermediate mesoderm gives rise to the MM and UB. Retrieved from Taguchi & Nishinakamura, 2015.

Moreover, at the post-gastrulation stage, precursors of the ureteric bud transiently express *Brachyury* (T) protein during gastrulation and give rise to the T^-, $OSR1^+$, $PAX2/8^+$, $LHX1^+$ anterior intermediate and the precursors of the metanephric mesenchyme are not derived from this anterior intermediate mesoderm but are maintained as a caudal T^+, $CDX2^+$, $OSR1^-$ cell population until the post-gastrulation stage. This suggests that both two major kidney components: the ureteric bud (UB) and metanephric mesenchyme (MM) are evidently distinct populations (Taguchi et al., 2014; Taguchi & Nishinakamura, 2015).

4.1.1.2. Takasato protocol (2015)

In 2015, Takasato et al. pioneered in the development of a differentiation protocol that allowed the generation of proper kidney organoids with a 3D environment, with the use of the factors CHIR99021, FGF9, and heparin. First, posterior primitive streak was induced with 4 days of CHIR99021 exposure, then FGF9 and heparin was supplemented to allow the formation of anterior and posterior intermediate mesoderm for 3 days. At day 7, cells were transferred to a transwell plate and treated with a 1-hour pulse of CHIR99021, followed by 5 days with FGF9 and heparin, and finally 7 days with no growth factors added. This allowed to generate kidney organoids generated had more than 500 nephrons segmenting into glomerulus (WT1+ cells), proximal tubule (LTL+, ECAD- cells) and distal tubule (GATA3-, LTL-, ECAD+ cells) that were associated with a collecting duct (GATA3+ ECAD+ cells) network surrounded by renal interstitium and endothelial cells. Overall, the organoids had structures that resembled *in vivo* kidney tissue organization, the proximal tubule possessed an endocytosis function and revealed acute apoptosis in response to the drug cisplatin. (Takasato et al., 2015, 2016; Takasato & Little, 2016). Nevertheless, the resulting organoids remain immature, and the protocol did not induce the dichotomously branching ureteric structure or the progenitor niche, indicating that the induced populations are not fully functional (Taguchi & Nishinakamura, 2017).

4.1.1.3. Morizane protocol (2015)

Morizane et al. established a protocol which CHIR99021 and Noggin were used to induce the late primitive streak in iPSCs, then activin A was used for 3 days to induce the posterior intermediate mesoderm, with and the metanephric mesenchyme was formed with the help of FGF9. At day 9, the monolayer culture was then transferred to 3D culture condition in low-attachment plates. CHIR99021 was employed for 2 days to produce spontaneously organized in elongated epithelial nephron structures, followed by 3 days of FGF9 and then no further growth factors were added. This protocol generated nephron progenitor cells (NPCs) in 90% efficiency and that expressed cell markers SIX2+, WT1+, SALL1+, PAX2+ and EYA1+. NPCs also contained epithelial nephron-like structure like loops of Henle (ECAD+ (E-cadherin), UMOD+ (uromodulin), BRN1+ and AQP1+), distal tubules (ECAD+, UMOD-), glomerular podocytes (PODXL+ WT1+), and proximal tubules (LTL+, AQP1+). The proximal tubule revealed cell death in response to the nephrotoxicants gentamicin and cisplatin. However, cells of the collecting duct, renal interstitium and endothelial cells are not generated from this protocol.

4.1.1.4. Taguchi and Nishinakamura protocol (2017)

In 2017, Taguchi and Nishinakamura reported a new method to develop more mature kidney organoids *in vitro*. The two primary kidney populations, MM and UB, were separately generated from mouse ESCs and subsequently cocultured. The organoids generated mimicked the organotypic 3D architecture of embryonic kidney with nephrons interconnected by branched epithelium (Taguchi & Nishinakamura, 2017). This protocol joined both the recent understanding of the early-stage nephrogenesis (Taguchi et al., 2014), and the previously known dissociation-reaggregation technique that involved the mouse embryonic kidney dissociation and then culturing the cells ex vivo, which demonstrated the reconstitution of the mouse kidney (Grobstein & Dalton, 1956; Unbekandt & Davies, 2010).

4.1.1.5. Tsujimoto protocol (2020)

Protocol from Tsujimoto *et al.* involved separate induction of multiple mesoderm progenitors from human iPSCs including the metanephric nephron progenitors, mesonephric nephron progenitor-like cells, and the ureteric bud (UB) were induced. Only ureteric bud cells and metanephric nephron progenitors were combined. The organoids generated had glomeruli and tubules as well as collecting duct and could become vascularized after transplantation *in vivo* into mouse (Tsujimoto et al., 2020).

4.1.1.6. Uchimura protocol (2020)

Uchimura *et al.* established a different protocol of separate induction of both metanephric mesenchyme (MM) and ureteric bud (UB) progenitors from human PSCs. Combination of these progenitors resulted in structures similar to collecting duct, that, with the addition of the hormones vasopressin and aldosterone, developed differentiation of collecting duct cell types including both principal cells (PCs) and intercalated cells (ICs). The organoids showed improved maturation and reduced off-target cell populations (Uchimura et al., 2020).

4.1.2. Kidney organoid applications

Organoids are already in use as primary research tool to investigate human developmental biology, disease modeling and for drug development. In many aspects, they are superior to animal models, due to the availability, transferability, and possibility of adaptation to specific problems, frequently referred as “mini-organs” in a lab dish.

Kidney organoids hold a huge potential as *in vitro* models of the human kidney, Furthermore, modifications to kidney organoid culture format can be made to address specific applications. Establishment of iPSC-derived organoids as models to study disease can be achieved by either the insertion of disease-specific mutations in iPSCs (with molecular manipulation) or make use of patient-derived iPSCs to precisely model the disease. In addition, patient-derived kidney organoids also have

potential as a tool for the screening of potential therapeutic drugs. However, effective use of kidney organoids for properly explore the impact of illnesses and large-scale production for high-throughput screening needs a baseline organoid methodology. Despite the availability of other protocols published afterwards, the main protocols used are of Taguchi *et al*., Freedman *et al*., Morizane *et al.*, and Takasato *et al*., which are adapted to applications of kidney organoids from PSCs.

The use of kidney organoids to model disease was firstly pioneered by Freedman *et al.* that modelled the polycystic kidney disease (PKD). This autosomal dominant genetic disease is based by mutations in *PKD1* or *PKD2* genes and causes cyst formation in the collecting duct of the kidneys, and progressive renal failure. Freedman et al. used the CRISPR-Cas9 genome editing tool to knock-out the PKD1 and PKD2 genes in human iPSCs and established organoids that formed cysts spontaneously formed within the tubule structures but not in the isogenic control organoids, thus validated the organoid culture to model PKD (Freedman et al., 2015). This approach was further improved in sequent study where systematic substitution of certain physical components increased from 6% to 75% cyst formation in organoids in comparison with the previous study (Freedman et al., 2015) and underlined the importance of microenvironment in PKD (Cruz et al., 2017).

Another disease successfully modelled is the ciliopathic nephronophthisis (NPH) in which the downstream cellular pathways responsible for disease origin were unknown, only the knowledge that IFT140 protein plays a key role in retrograde intraflagellar transport. Forbes *et al.* generated human iPSC-derived organoids from a patient with mutations in the IFT140 gene and isogenic mutation-corrected iPSCs with CRISPR-Cas9 technique and revealed that IFT140 mutations cause defects in primary cilia and alter apico-basal polarity in tubular cells (Forbes et al., 2018).

Mucin-1 kidney disease (MKD) is another genetic disease that arises from a mutation (premature stop codon) in the MUC1 gene, leads to the synthesis of a short mutant protein that is intracellularly accumulated in the cytoplasm of the kidney cells and consequently causes activation of several stress response pathways and ultimately cell death (Kirby et al., 2013). To study this disease, Dvela-Levitt *et al.* created complementary organoid models and demonstrated accumulation of mutant MUC1 protein in tubular cells of human MKD samples and iPSC-derived organoids from patients. Additionally, they tested the effectiveness of the drug BRD4780, selected from a primary screen using mutant MUC1 immortalized tubular epithelial cell line. When applied to organoids, the drug showed promising results for the treatment of MKD because it targeted the mutant protein and increased lysosomal degradation (Dvela-Levitt et al., 2019).

Acute kidney injury (AKI) induced by chemotherapeutic drugs causes toxic effects on kidneys (nephrotoxicity) and it is nowadays increasing each year (Barnett & Cummings, 2018). Indeed, kidney toxicity accounts up to 8% of preclinical safety closures and drawbacks of new drugs (Cook et al., 2014). Therefore, there is demand of kidney models for nephrotoxicity analysis of each drug before it enters the market. Keeping this in mind, kidney organoids can be a great tool to be applied in toxicological studies. Comparing with 2D kidney cell lines, organoids have more maturity and morphology that provides a better platform system to the evaluation the simultaneous responses of multiple cell types and gather more biologically relevant data. Nephrotoxic drugs like cisplatin have already shown toxicity

for proximal tubular cells in mature organoids (Freedman et al., 2015; Morizane et al., 2015; Takasato et al., 2015), similar to previously assessed *in vivo* response and thus, provided proof-of-concept of how protocols for organoid generation can be applied for toxicology studies.

With the objective of performing toxicology studies, Yoshimura *et al.* established a method for selective induction of human podocytes, by optimized the cell differentiation conditions. *In vitro* podocytes created were treated with puromycin aminonucleoside (PAN), used as a model of podocyte injury and nephrotic syndrome. Results presented a significant reduction of proteins NEPH1 and Podocin at sub-lethal doses, meanwhile other podocyte markers remained unaltered, exhibiting consistency with the phenotype of PAN-induced podocyte injury *in vivo* (Yoshimura et al., 2019). Overall, the studies imply that kidney organoids are suitable to evaluate nephrotoxic drugs on the basis of their phenotypical characteristics.

The usage of iPSC-derived kidney organoids as a model for preclinical toxicity research may enhance the chance of new candidate pharmaceuticals be successful in the clinical context while also lowering drug research and development expenses (**Figure 10**). iPSC-derived organoids, however, are still immature and reflect a fetal stage of the kidney, despite successful attempts at nephrotoxicity testing utilizing these organoids. Further research is required to make kidney organoids a more complete model for drug screening.

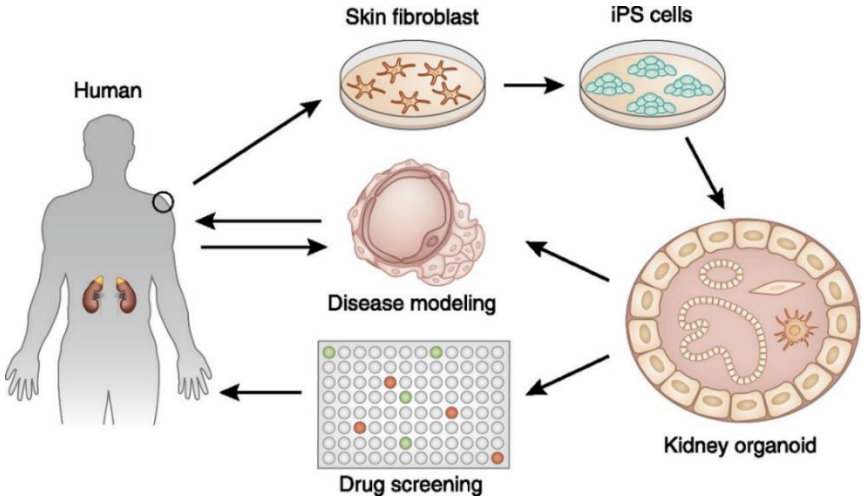

Figure 10 - Scheme illustrating the therapeutic potential of kidney organoids: they can be used for patient-specific disease modelling and drug screening. Retrieved from (H. Wu & Humphreys, 2020).

Aim of Studies

The first part of this study focuses on the initial phase of renal differentiation up to the intermediate mesoderm stage, as this is the most critical stage of renal differentiation in terms of primitive streak induction and later the anteroposterior fate of the intermediate mesoderm. This work aims to examine the relative proportions of the two main populations in kidney development, anterior intermediate mesoderm (AIM) and posterior intermediate mesoderm (PIM). Factors influence the trajectory of the differentiation, such as culture medium and supplementation with different small molecules will be studied to assess their effect in the final generated cell population, by following protocols of Morizane, Takasato and a novel hybrid protocol “Morisato”.

Another important factor explored in each protocol is the spatial conditions of the culture. Like most protocols for kidney organoid generation that have been developed, Morizane and Takasato protocols initially start with 2-dimentional (2D) conditions and only thereafter progress to 3-dimentional (3D) conditions. Although 2D culture is reported to control anteroposterior cell fate of the primitive streak precisely, these types of cultures present several limitations related to the lack of cell-to-cell interactions. Aggregate culture systems will be tested as they mimic *in vivo* conditions more closely and avoid the use of adhesion matrices such as Matrigel, thereby reducing the number of components within the culture (Miranda et al., 2018).

AIM differentiates into ureteric bud (UB), whilst PIM gives rise to the metanephric mesenchyme (MM), the nephron progenitor and to posterior mesonephric mesenchyme. The reciprocally inductive interactions between these two populations are key to nephrogenesis. Therefore, to mimic kidney development *in vivo*, it is crucial to recapitulate the interactions between AIM and PIM populations. This precise concept is used in the Uchimura protocol, which is examined and applied in this study under fully 3D conditions. In addition, special attention is given to the type of populations present in intermediate mesoderm phase and the structures they give rise to in future kidney organoids.

Additionally, this project aims to develop a framework for a novel hybrid protocol “Morisato”. Different conditions will be tested to determine which are most favorable for producing each of the two main populations: AIM and PIM. Then, the concept of the Uchimura protocol will be applied to develop a protocol that uses fewer small molecules and a more cost-effective culture medium.

Materials & Methods

1. Expansion of Human Induced Pluripotent Stem Cells

1.1. Cell culture

1.1.1. Cell Line

All the experiments employed the human iPSC line DF6-9-9T.B (DF6) obtained from WiCell Research Institute (Wisconsin, United States of America). The DF6 cell line was generated from a healthy donor's foreskin fibroblasts with a normal karyotype (44+XY) through retroviral transduction using seven reprogramming factors (OCT4, SOX2, Nanog, LIN28, L-Myc, Klf4 and SV40 T). It was certified free from mycoplasma and other vectors. Cell passages between 48 and 64 were used for all experiments.

1.1.2. Adhesion Substrate

For the 2D culture of human iPSCs, Matrigel (Corning) was used as adhesion substrate. The aliquots of Matrigel stored at -20ºC were thawed on ice and diluted 1:100 (v/v) in Dulbecco's Modified Eagle Medium: Nutrient Mixture F-12 (DMEM-F12, Gibco). Matrigel was used to coat 6-well tissue culture plates (Corning/Falcon) that were left at room temperature least at for two hours or 30 minutes in the humified incubator at 37°C. The Matrigel-coated 6-well tissue culture plates could also be stored at 4ºC for later use up to 2 weeks.

1.1.3. Culture medium

mTeSR Plus (STEMCELL Technologies) was used as cell culture medium for the DF6 iPSCs. mTeSR Plus 5x supplement (STEMCELL Technologies) was thawed at room temperature or at 4ºC overnight and mixed with mTeSR Plus basal medium (STEMCELL Technologies). Aliquots stored at -20ºC were thawed overnight at 4ºC and supplemented with 0.5% (v/v) penicillin/streptomycin (Invitrogen). mTeSR Plus was stored at 4ºC and pre-warmed at room temperature before use.

1.1.4. Cell Thawing

Each cryovial (Thermo Fisher Scientific) with cryopreserved cells in liquid nitrogen at -196ºC were thawed at 37ºC for 30 seconds. The cell content was gently resuspended in pre-warmed washing medium, then centrifuged at 1000 rpm for 3 minutes. Cell pellet was resuspended in culture medium mTeSR Plus supplemented with 10 mM Rho kinase inhibitor (ROCKi, Y-27632, STEMCELL Technologies) and seeded into 6-well tissue culture plates coated with Matrigel.

1.1.5. Maintenance of human iPSC

In order to maintain a state of pluripotency, the cell culture in the 6-well tissue culture plates coated with Matrigel using mTeSR Plus was kept in a humified incubator at 37°C, 5% CO_2, 20% O_2 and culture medium was changed daily. Human iPSCs were passaged at 1:3-1:5 split ratio when 50%-60% cell confluence was achieved by using 0.5 mM EDTA solution (Invitrogen) diluted in phosphate-buffered saline (PBS, Sigma-Aldrich).

1.1.6. Cell Cryopreservation

For cryopreservation, human iPSCs were washed twice and then incubated with 0.5 mM EDTA at room temperature for 5 min. Then, cells were rinsed with washing medium and centrifuged at 1,000 rpm for 3 min. Cells were resuspended in mTeSR Plus and 10% (v/v) dimethyl sulfoxide (DMSO, Sigma-Aldrich) and distributed in cryovials at a final volume of 250 µL. Cryovials first were stored at -80ºC for 24 hours and then transferred to liquid nitrogen at -196ºC for long term storage.

1.1.7. Cell Counting

Cell counting was performed to access the density of viable cells for seeding. Cells were treated with Accutase (Sigma-Aldrich) prior to their re-suspension in mTeSR Plus supplemented with 10 mM ROCKi Y-27632. A sample of the cells in suspension were diluted at 1:20 with 0.4% Trypan Blue staining solution (Gibco). Only 10 µL of Trypan Blue-treated cell suspension was collected and loaded into a haemocytometer (Superior Marienfield). Blue-stained viable cells were observed and counted through an inverted optical microscope and at least two independent counts were performed for each sample. Total number of viable cells was determined by **Equation 1**:

Equation 1

$$Total\ viable\ cell\ number = \frac{\Sigma\ Viable\ cell\ count}{\#\ Independent\ counts} \times \frac{Dilution\ factor \times Cell\ suspension\ volume}{\#Squares\ \times Square\ volume}$$

2. Differentiation of human induced pluripotent stem cells into renal lineage

2.1. Culture media

In all experiments of differentiation of human iPSCs into renal linage, one of the following culture media was used: Advanced Roswell Park Memorial Institute medium 1640 (Advanced RPMI 1640, Gibco) or STEMdiff APEL 2 (STEMCELL Technologies). Both media were supplemented with 0.5% (v/v) penicillin/streptomycin, stored at 4ºC and pre-warmed at room temperature before use.

Advanced RPMI 1640 medium is a commonly used basal medium that allows the culture of mammalian cells. This medium does not require Fetal Bovine Serum (FBS) supplementation since its composition includes ethanolamine, glutathione, ascorbic acid, insulin, transferrin and AlbuMAX I lipid-rich bovine serum albumin for cell culture. Due to the lack of L-glutamine in this content, the medium was supplemented with 1:100 (v/v) GlutaMAX-I (100X) (Gibco) before use. Advanced RPMI 1640 medium was used during Morizane and “Morisato” protocols.

STEMdiff APEL 2 medium is a fully defined, serum-free and animal component-free medium. It is based on Dr. Andrew Elefanty's APEL formulation and lacks unspecified components such as protein-free hybridoma media. This medium was used during Takasato and Uchimura protocols.

2.2. Adherent monolayer 2D culture setting

For the differentiation of DF6 human iPSCs in monolayer culture, cells were passaged with Accutase and seeded on Matrigel-coated 6-well plates at a density of 15,000 cells per cm^2 in mTeSR Plus supplemented with 10μM ROCKi Y-27632. Upon successful seeding, cells were kept in a humified incubator at 37°C, 5% CO_2, 20% O_2. In the following day, culture media was replaced with the differentiation media depending on the protocol implemented. The concentration of CHIR99021 (Stemgent) used in the first stage supplementation to differentiation medium which is a common first step to all differentiation protocols applied and it was defined as 8 μM, respecting the physiological gradients of cells in monolayer.

2.3. Aggregate 3D culture setting

For the 3D differentiation of DF6 human iPSCs and their promotion to assemble into cell aggregates, AggreWell 800 plates (STEMCELL Technologies) were used (Ungrin et al., 2008). This high-throughput platform allowed the generation of approximately 300 cellular aggregates in each well of 24-plate with V-shaped bottom microwells of exactly 800 μm of length. Each well of AggreWell 800 plate was rinsed with DMEM-F12 and centrifuged at 3,500 rpm for 3 minutes in order to remove air bubbles formed inside the microwells, prior to cell seeding.

For the process of cell seeding, iPSCs were collected, dissociated into single cells using Accutase. Then, resuspended in mTeSR Plus supplemented with 10μM ROCKi and the adequate number of cells was transferred into AggreWell 800 and spun down at 1,000 rpm for 3 minutes, in order to force cells to settle into the microwells. Upon successful seeding, cells were kept in a humified incubator at 37°C, 5% CO_2, 20% O_2. After a 24-hour period, the differentiation protocol was initiated with the change into adequate differentiation treated with 11 μM CHIR99021, respecting the physiological gradients of cells in the aggregate.

The size of the aggregates inside microwells in terms of number of cells depends on the total number of iPSCs applied into each well during cell seeding can be seen in **Table 3**.

Table 3 -Total cell number seeded into each well and its correspondence with the approximate number of cells per aggregate generated in the microwells, used throughout this experimental work.

Total cell number per well	Number of cells per aggregate
$3.0x10^5$	1,000
$4.5x10^5$	1,500
$6.0x10^5$	2,000
$9.0x10^5$	3,000

2.3.1. Aggregate size measurement

Firstly, bright-field images of cell aggregates were acquired at day 0 of differentiation (24h after seeding) taken with a digital camera Leica DFC7000T (Leica Microsystems GMbH, Germany) and through microscope Leica DMI3000B (Leica Microsystems GMbH, Germany). Images were then uploaded to ImageJ (Fiji) imaging processing software for the assessment of aggregate limit area. Assuming that the cell aggregate had a spheroid structure, the diameter of each was calculated using **Equation 2**, in which D represents the aggregate's diameter, in µm, and A represents its area, in μm^2.

Equation 2

$$D = 2 \times \sqrt{\frac{A}{\pi}}$$

2.4. Air-liquid interface 3D culture setting

Air-liquid interface 3D culture or Transwell culture was possible with the use of 6-well Costar Transwell 3450 clear plates (Corning) that in which each well contains a 24 mm polyester membrane with 0.4 µm pore, treated for optimal cell attachment. Transwell culture setting was only applied during the Morizane modified protocol (Morisato protocol) and Uchimura protocol after day 7 of differentiation in aggregate culture. Each Transwell filter was seeded with 5 different aggregates with $5x10^5$ cells each.

2.5. Differentiation protocols of human iPSCs into renal lineage

This work was mainly based on protocols previous developed: Morizane et al., (2015), Takasato et al., (2015) and Uchimura et al., (2020). These protocols also suffered modifications and optimization to achieve different goals which yielded the following novel adaptation: "Morisato" protocol.

2.5.1. Morizane protocol

At day 0 of differentiation (24h after seeding) cells were cultured in Advanced RPMI1640 supplemented CHIR99021 (8 or 11 µM) for 2-4 days to induce late primitive streak cells. For the intermediate mesoderm induction, cells were cultured with Activin A (10 ng/ml, R&D Systems) for 3-5 days. The medium was replaced every other day. Both in the monolayer differentiation and in 3D culture differentiation, the protocol was stopped at day 7 timepoint prior to fixation in 4% (v/v) Paraformaldehyde (PFA, Sigma) in PBS at 4ºC, for 20 min and stored in PBS for posterior analysis. Additionally, approximately $1x10^6$ whole cells were recovered and stored at -80ºC for RNA extraction.

2.5.2. Takasato protocol

At day 0 of differentiation (24h after seeding) culture media was replaced with STEMdiff APEL-2 medium supplemented with CHIR99021 (8 or 11 µM) for 4 days, followed by APEL-2 supplemented with 200 ng ml^{-1} FGF9 (R&D Systems) and 1 µg ml^{-1} heparin (Sigma-Aldrich) for another 3 days, replacing the medium every other day. Both in the monolayer differentiation and in 3D culture differentiation aggregates, the protocol was halted at day 7 timepoint prior to fixation in 4% (v/v) PFA in PBS at 4ºC, for 20 min and stored in PBS for posterior analysis. Additionally, approximately $1x10^6$ whole cells were recovered and stored at -80ºC for RNA extraction.

2.5.3. “Morisato”: Novel hybrid protocol

“Morisato” is a portmanteau of the words “Morizane” and “Takasato”, which reflects on its hybrid nature as it was created based on both protocols referenced. The medium used during this differentiation protocol is the Advanced RPMI1640, which was supplemented with 11 µM CHIR99021 for 2-4 days, followed by the same medium supplemented with 200 ng ml^{-1} FGF9 and 1 µg ml^{-1} heparin for another 3-5 days, replacing the medium every other day. The protocol was halted at day 7 timepoint prior to aggregate fixation in 4% (v/v) PFA in PBS at 4ºC, for 20 min and stored in PBS for posterior analysis. Additionally, approximately $1x10^6$ whole cells were recovered and stored at -80ºC for RNA extraction.

2.5.4. Uchimura protocol

For Uchimura protocol two independent but simultaneous differentiations were undertaken which have the objective of induction the two renal linages from iPSCs: AIM and PIM. Firstly, both AIM and PIM cultures followed in the Aggregate 3D culture setting until day 7.

For the PIM linage differentiation, Takasato protocol was followed until day 7. Briefly, cells were treated with 11 µM CHIR99021 in basal medium STEMdiff APEL 2 for 4 days, followed by FGF9 (200 ng/mL) and heparin (1mg/mL) for another 3 days.

The AIM linage differentiation started with 11 μM CHIR99021 treatment for one day, followed by treatment with CHIR99021 (11 μM), Activin A (10 ng/mL), and BMP4 (1 ng/mL, R&D Systems) for two days, followed by FGF9 (200 ng/mL), heparin (1mg/mL), Activin A (1 ng/mL), Retinoic Acid (100 nM, Sigma-Aldrich), and LDN193189 (100 nM, StemGent) for 4 days with the exception that LDN193189 was reduced to 30 nM after two days.

In order to generate kidney organoids, the AIM and PIM lineage cells were dissociated into single cell suspension using Accutase, at day 7. A total of $5x10^5$ cells of each lineage and also a combination of the two lineages at 3:1 ratio was mixed and spun down at 1,000 rpm for 3 min to form a pellet. The pellets were transferred onto a Transwell membrane and incubated with CHIR99021 (5 μM) for 1 hour, then cultured with FGF9 (200 ng/mL), heparin (1mg/mL), Retinoic Acid (100 nM), GDNF (10 ng/mL, PeproTech), and EGF (10 ng/mL, R&D Systems) for 5 days. For the next 17 days, the organoids were cultured in only basal medium that was changed three times a week.

2.5.5. "Morisato" in Transwell protocol

Morizane "long" protocol follows a similar principle of independent but simultaneous induction of the two renal linages AIM and PIM in 3D conditions.

For the first 7 days of differentiation for the PIM aggregates, the "Morisato" protocol was applied. Firstly, Advanced RPMI1640 supplemented with 11 μM CHIR99021 for 4 days, followed by the same medium supplemented with 200 ng ml^{-1} FGF9 and 1 μg ml^{-1} heparin for another 3 days.

In terms of AIM linage differentiation, the protocol Morizane was followed in the first 7 days. Aggregates were cultured in Advanced RPMI1640 supplemented with 11 μM CHIR99021 for 2 days, following supplementation with Activin A (10 ng/ml) for the next 5 days.

At day 7 of differentiation, both AIM and PIM aggregates were collected and dissociated into single cell suspension using Accutase. A total of $5x10^5$ cells of each lineage and also a combination of the two lineages at 3:1 ratio was mixed and spun down at 1,000 rpm for 3 min to form a pellet. The pellets were transferred onto a Transwell membrane and incubated with CHIR99021 (5 μM) for 1 hour, then cultured with FGF9 (200 ng/mL for 5 days. For the next 17 days, the organoids were cultured in only basal medium that was changed three times a week.

3. Cell characterization

3.1. Intracellular flow cytometry

Human iPSCs were dissociated using Accutase for 5 min at 37ºC, resuspended with 2% PFA and incubated overnight at 4ºC. Cells were fixed in cold Methanol (90% v/v, Sigma-Aldrich) at 4ºC for 15 minutes. Then, cells were washed twice in a solution of 10% (v/v) Fetal Bovine Serum (FBS) in PBS to remove the residues of Methanol. After that, cells were resuspended in a solution of 0.1% (v/v) Triton

X-100 (Sigma-Aldrich), 10% (v/v) Bovine Serum Albumin (BSA, Invitrogen) in PBS and incubated for 1 hour at room temperature with the primary antibody at adequate dilution (**Table 4**). Cells were washed with the previous solution but without primary antibody and then incubated incubated with 1:1000 dilution of secondary antibody Alexa Fluor 488 anti-mouse IgG (Invitrogen) for 30 minutes at room temperature and in the dark. Cells were washed twice with 10% BSA in PBS to remove non-binding antibodies. Flow cytometry was performed using a FACSCalibur flow cytometer (Becton Dickinson) and data analysis using Flowing Software 2.0.

3.2. Extracellular flow cytometry

Human iPSCs were dissociated using Accutase for 5 min at 37ºC, and then resuspended in 2% PFA at 4ºC. Cells were washed with PBS and resuspended in 10% (v/v) Fetal Bovine Serum (FBS, Invitrogen). Cells were incubated with primary antibody SSEA-1-PE (Miltenyi Biotec) at 1:5 dilution (**Table 4**) and then washed in PBS three times. Flow cytometry was performed using a FACSCalibur flow cytometer and data analysis using Flowing Software 2.0.

Table 4 - Primary antibody, secondary antibodies solutions and isotype control used for intracellular and extracellular flow cytometry with their correspondent dilutions.

Intracellular markers	**Primary antibody**		**Secondar antibody**	
	Antibody	**Dilution**	**Antibody**	**Dilution**
OCT4	Anti-OCT4, Mouse IgG (Milipore)	1:300	Goat anti-Mouse IgG Alexa Fluor-488 (Invitrogen)	1:1000
SOX2	Anti-SOX2 Mouse IgG (R&D Systems)	1:300		
Extracellular markers	**Primary antibody**		**Isotype control**	
	Antibody	**Dilution**	**Isotype**	**Dilution**
SSEA-1	Anti-human SSEA-1-phycoerythrin (PE)-conjugated (BioLegend)	1:5	REA control (S)-PE (Miltenyi Biotec)	1:20

3.3. 3D Cellular aggregates cryosectioning

Cell aggregates were collected at day 7 or 30 of differentiation and fixed in 4% (v/v) PFA in PBS at 4ºC for 20 minutes. After fixation, cell aggregates were incubated in 5% (w/v) Sucrose (Sigma-Aldrich) in PBS, overnight at 4ºC. Sequentially, aggregates were incubated for 1 hour at 37ºC in a solution of 15% (w/v) Sucrose and 7.5% (w/v) Gelatin from porcine skin (Sigma-Aldrich) in PBS. Gelatin blocks were attained by the transfer of cell aggregates on to a previously solidified Gelatin layer and settled with

another layer of Gelatin on top. After the solidification, Gelatin blocks were cut and frozen by submersion in -80ºC Isopentane (VWR) and stored at -80ºC. Frozen Gelatin blocks were sectioned into 12 µm thick slices by cryostat-microtome (Leica CM3050 S) at -24ºC and placed on adhesive Superfrost Plus glass slides (Thermo Scientific). Glass slides with cell aggregate sections were stored at -20ºC until further immunofluorescence staining.

3.4. Immunocytochemistry

Cell cultures in 6-well plates were previously fixed in 4% PFA at 4ºC for 20 minutes. Sectioned cell aggregates in glass sides required de-gelatinization step accomplished thought incubation in pre-warmed PBS at 37ºC for 1 hour.

Fixed and sectioned cells were washed with 0.1 M Glycine (Sigma-Aldrich) in PBS to remove any residues. Then, permeabilized with 0.1% (v/v) Triton X-100 in PBS, at room temperature for 10 minutes, and washed with PBS three times. Cells were then blocked with blocking solution composed with 10% (v/v) fetal bovine serum in TBST, constituted by 20 mM Tris-HCl pH 8.0 (Sigma), 150 mM NaCl (Sigma) and 0.05% (v/v) Tween-20 (Sigma-Aldrich) in PBS, at room temperature for 30 min. Cells were incubated with the primary antibody (**Table 5**) diluted in blocking solution at 4ºC overnight. After incubation, cells were washed three times with TBST for 5 minutes each or left 48h in TBST for maximum antibody removal. Secondary antibody (**Table 5**) was diluted in blocking solution and incubated with the cells, in the dark, at room temperature for 30 minutes. Cells were once again washed three times with TBST for 5 minutes each. After this, cells were incubated with 15:10000 dilution of 4',6-diamidino-2-phenylindole (DAPI) dye (Sigma-Aldrich) at room temperature for 5 min. Then, cells were again washed three times with TBST for 2 minutes each. Mowiol (Sigma-Aldrich) was added using a glass-cover and was left overnight to dry. Cells were examined using a fluorescence microscope Leica DMI3000B and a digital camera Leica DFC7000T, or with Zeiss LSM 710 Confocal Laser Point-Scanning Microscope using 20x objective and a digital zoom of 80%.

Table 5 - Primary and secondary antibodies for intracellular staining and their respective dilution.

Marker	**Primary antibody**		**Secondar antibody**	
	Antibody	**Dilution**	**Antibody**	**Dilution**
OCT4	Anti-OCT4, Mouse IgG (Milipore)	1:750	Goat anti-Mouse IgG Alexa Fluor-488 (Invitrogen)	1:500
HOXD11	Anti-HOXD11, Mouse IgG2a (Santacruz Biotechnology)	1:100	Goat anti-Mouse IgG Alexa Fluor-546 (Invitrogen)	
GATA3	Anti-GATA3, Mouse IgG1 (Santacruz Biotechnology)	1:100	Goat anti-Mouse IgG1 Alexa Fluor-488 (Invitrogen)	

ECAD	Anti-ECAD, Mouse IgG2ak (BD Biosciences)	1:100	Goat anti-Mouse IgG Alexa Fluor-546 (Invitrogen)	
PAX8	Anti-PAX8, Rabbit IgG (ProteinTech)	1:100	Goat anti-Rabbit IgG Alexa Fluor-488 (Invitrogen)	
WT1	Anti-WT1, Rabbit IgG (ThermoFisher Scientific)	1:100	Goat anti-Rabbit IgG Alexa Fluor-546 (Invitrogen)	
NPHS1	Anti-NPHS1, Rabbit IgG (ThermoFisher Scientific)	1:100	Goat anti-Rabbit IgG Alexa Fluor-488 (Invitrogen)	
KIM-1	Anti-KIM-1, Rabbit IgG (Invitrogen)	1:200	Goat anti-Rabbit IgG Alexa Fluor-488 (Invitrogen)	
LTL	Biotin-conjugated LTL (Vector Labs)	1:100	Streptavidin Alexa Fluor-647 (Invitrogen)	

3.5. Quantitative RT-PCR

Total RNA from cell samples of both in monolayer and in 3D cultures were extracted using High Pure RNA Isolation Kit (Roche Diagnostics) following manufacturer's instructions. After RNA quantification with nanodrop, 1 µg of RNA was converted into cDNA with High-Capacity cDNA Reverse Transcription Kit (Applied Biosystems) also following manufacturer's instructions. The RNA-cDNA conversion was done resorting to a T100™ Thermal Cycler (Bio-Rad) with the following program: 10 minutes at 25℃, 120 minutes at 37℃, 5 minutes at 85℃ and then, 4℃ until storage (at -20℃).

All PCR reactions were run in triplicate on Step One Plus Real-time PCR System (Applied Biosystems) or on ViiA™ 7 RT-PCR Systems (Applied Biosystems) using NZY Supreme qPCR Green Master Mix Rox Plus (NZYTech), with 12.5 ng of cDNA and 250 µM of each primer of each gene (**Table 6**). Data obtained was first normalized to housekeeping gene GAPDH and then normalized to control samples (day 0) by applying the ΔΔCt method. The final results of gene expression are represented as $2^{-\Delta\Delta CT}$. Graphs were made using GraphPad Prism version 8.0.1 for Windows (GraphPad Software, San Diego, USA).

Table 6 - Sequence of primers for each gene used for the quantitative RT-PCR.

Gene	**Primer sequence**	
GAPDH	Forward 5'-3'	GAGTCAACGGATTTGGTCGT
	Reverse 5'-3'	TTGATTTTGGAGGGATCTCG
PAX2	Forward 5'-3'	GACTATGTTCGCCTGGGAGATTC
	Reverse 5'-3'	AAGGCTGCTGAACTTTGGTCCG

HOXD11	Forward 5’-3’	CAGTCCCTGCACCAAGGCGAC
	Reverse 5’-3’	GGTATAGGGACAGCGCTTTTTCC
GATA3	Forward 5’-3’	ACCACAACCACACTCTGGAGGA
	Reverse 5’-3’	TCGGTTTCTGGTCTGGATGCCT
WT1	Forward 5’-3’	CCAGCCCGCTATTCGCAATC
	Reverse 5’-3’	CGAGTACTGCTGCTCACCCA
OCT4	Forward 5’-3’	GAGAACCGAGTGAGAGGCAACC
	Reverse 5’-3’	CATAGTCGCTGCTTGATCGCTTG
KDR	Forward 5’-3’	AGCGGTCAACAAAGTCGGGA
	Reverse 5’-3’	AGTGGGCTGCATGTCAGGTT
PDGFR-α	Forward 5’-3’	GATTAAGCCGGTCCCAACCT
	Reverse 5’-3’	GGATCTGGCCGTGGGTTT
OSR1	Forward 5’-3’	GCGTGTCCGGCGCTTG
	Reverse 5’-3’	GGTTTTGCTGCCCATTTCGGT
SOX17	Forward 5’-3’	CTCCGGTGTGAATCTCCCC
	Reverse 5’-3’	CACGTCAGGATAGTTGCAGTAAT
KIM-1	Forward 5’-3’	CGACAACGACTGTTCCAATG
	Reverse 5’-3’	AAAGGCATTGGAGGAACAAA

Results & Discussion

1. Pluripotency marker assessment of human iPSC line DF6

The quality of a cell culture is highly important towards the consistency of the outputs. Therefore, it is important to start with high-quality pluripotent cells that still retain their full pluripotency (Chen et al., 2014). To succeed in human iPSC differentiation protocols, it is mandatory to start with robust, undifferentiated human iPSC colonies. Generally, the most straightforward way of monitoring human iPSC culture quality can be achieved by observing its morphology (Maddah et al., 2014). Healthy, mature human iPSC colonies have clearly defined borders, tightly clustered cells with uniform morphology and border spikiness (**Figure 11A**). In contrast, spontaneously differentiating colonies show loss of defined edges, possess large, differentiated cells with a heterogeneous central core that is not typical of pluripotent stem cells, and smaller cells with different sizes grow outwards from the main core of the colony. To avoid unwanted differentiations, it was critical to passage the cells at 60-70% confluence, with a split rate of 1:3-1:6, before large colonies completely merged, as this can compromise viability and pluripotency marker expression.

The expression of markers in pluripotent stem cells can be detected in iPSCs at a similar level to ESCs. Normally, pluripotent stem cells express the transcription factors OCT4, SOX2, and Nanog, which are involved in maintaining their undifferentiated state by suppressing cell determination factors. Cell-specific surface antigens SSEA-3, SSEA-4, tumour related antigens TRA-1-60, TRA-1-81, and TRA-2-49/6E (alkaline phosphatase) are also characteristic of pluripotent stem cells (Adewumi et al., 2007).

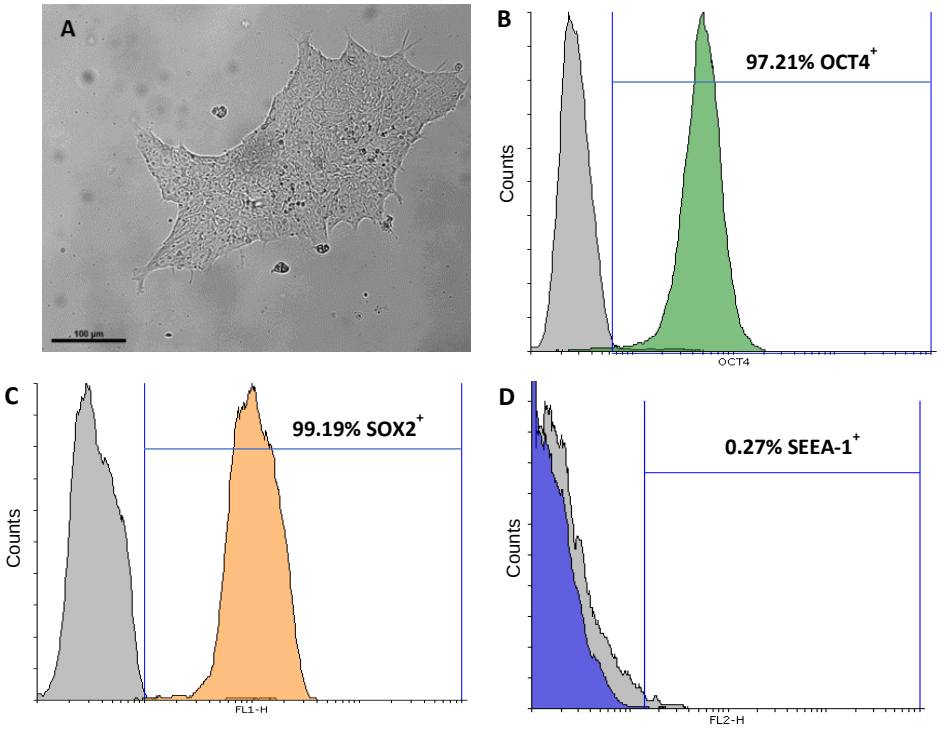

Figure 11 - Human iPSC line DF6 characterization. (A) Bright-field image of healthy undifferentiated human iPSC colony cultured under adherent monolayer conditions with mTeSR Plus, 48h after passaging. Quantification of pluripotency markers by flow-cytometry for analysis for (B) OCT4, (C) SOX2, and early differentiation marker (D) SSEA-1 on human iPSC DF6 cell line.

Flow cytometry and immunocytochemistry were used to assess the existence of pluripotency markers in the iPSC line DF6. Intracellular flow cytometry analysis revealed that 97.21% of the cells were $OCT4^+$ (**Figure 11B**) and 99.19% were $SOX2^+$ (**Figure 11C**). Expression of SSEA-1 was also examined and showed a residual expression of 0.27% of cells positive for this extracellular marker (**Figure 11D**). This result was expected as SSEA-1 is known to be expressed in mouse embryonic stem cells (ESCs), and murine and human germ cells, but not in human ESCs or in iPSCs (Draper et al., 2002).

Immunocytochemistry OCT4 and SSEA-1 markers were also used to confirm the cell's pluripotency. In this case, immunostaining revealed the localized expression of pluripotency marker OCT4 in the cell nuclei (**Figure 12B**), in the same localization as the DAPI expression (**Figure 12A**), but expression of maker SSEA-1 was not possible to be assessed (**Figure 12D**). These results are corroborated by the results of flow cytometry.

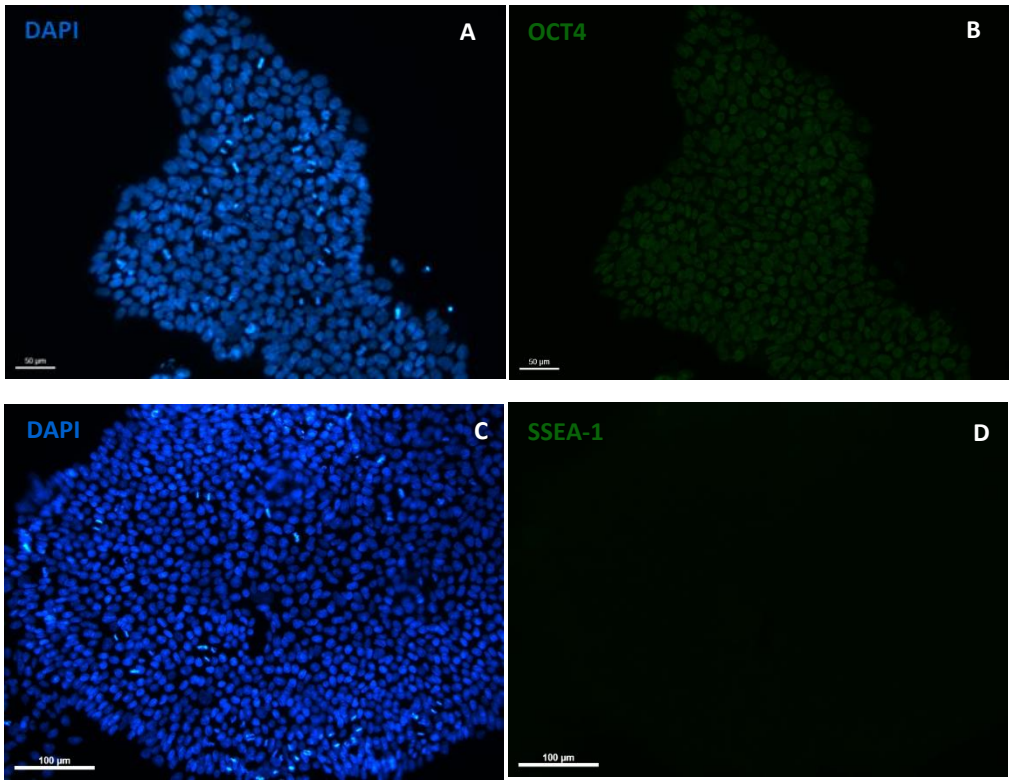

Figure 12 - Immunofluorescent staining of human iPSC line DF6 for (B) OCT4 and (D) SSEA-1 in green. Nuclei in blue stained with DAPI (A,C). Scale bars represent 100 µm.

2. Evaluation of cell lineage fate in renal differentiation protocols

The first 7 days of differentiation of kidney organoids are the most critical for establishment of the correct mesodermal lineage and anteroposterior cell fate. Day 7 represents the stage of intermediate mesoderm, already considered to include progenitors of ureteric epithelium and/or progenitors of metanephric mesenchyme (Mugford et al., 2008).

Morizane, “Morisato”, and Takasato protocols were followed until the stage of intermediate mesoderm, in order to evaluate the effects of different culture systems (2D adherent monolayer culture and 3D aggregate conditions) in cell lineage fate.

2.1. Differentiation of human iPSCs into renal linage in 2D conditions

Previously, it has been reported that cell cultures under monolayer culture conditions control anteroposterior cell fate of the primitive streak more precisely than in embryoid bodies (Takasato et al., 2016). Originally, both protocols of Morizane and Takasato start under 2D conditions until day 9 and day 7 respectively.

In monolayer approaches, the initial cell density is critical for controlling PSC commitment (Peerani et al., 2007). Indeed, plating density is critical to achieve hight efficiency of differentiation. All experiments started with a density of 15,000 cells per cm^2, since it was reported as the optimal density for iPSC lines (Morizane & Bonventre, 2017; Takasato et al., 2015).

A first common stage to all protocols is the induction of primitive streak with induction of WNT signaling, by GSK-3β inhibitor CHIR (CHIR99021). At day 0 of differentiation in monolayer culture, colonies of pluripotent cells appeared to be broken apart into single or small groups of cells with a spiky, triangular morphology (**Figure 13**). This singularization of cells is attributed to the addition of ROCK inhibitor during cell seeding the day before. After 2 days under the influence of CHIR, cells exhibited a morphological change to more round cells, a sign of primary epithelial-to-mesenchymal transition (EMT) expected in iPSC differentiation into primitive streak (**Figure 14A**).

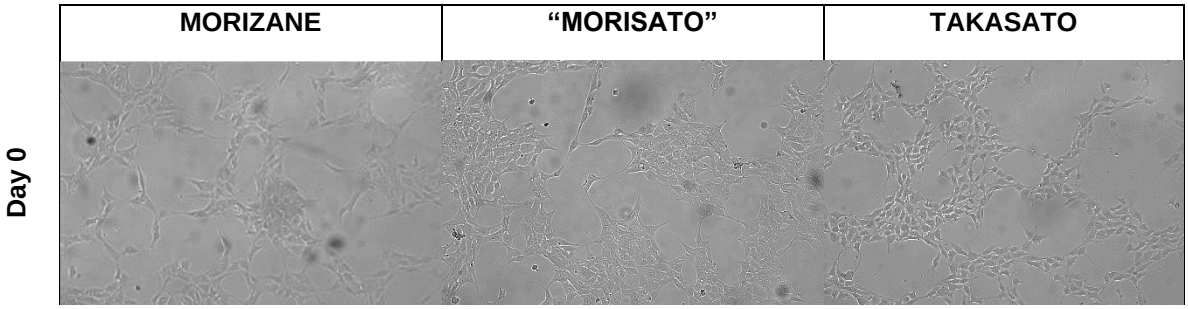

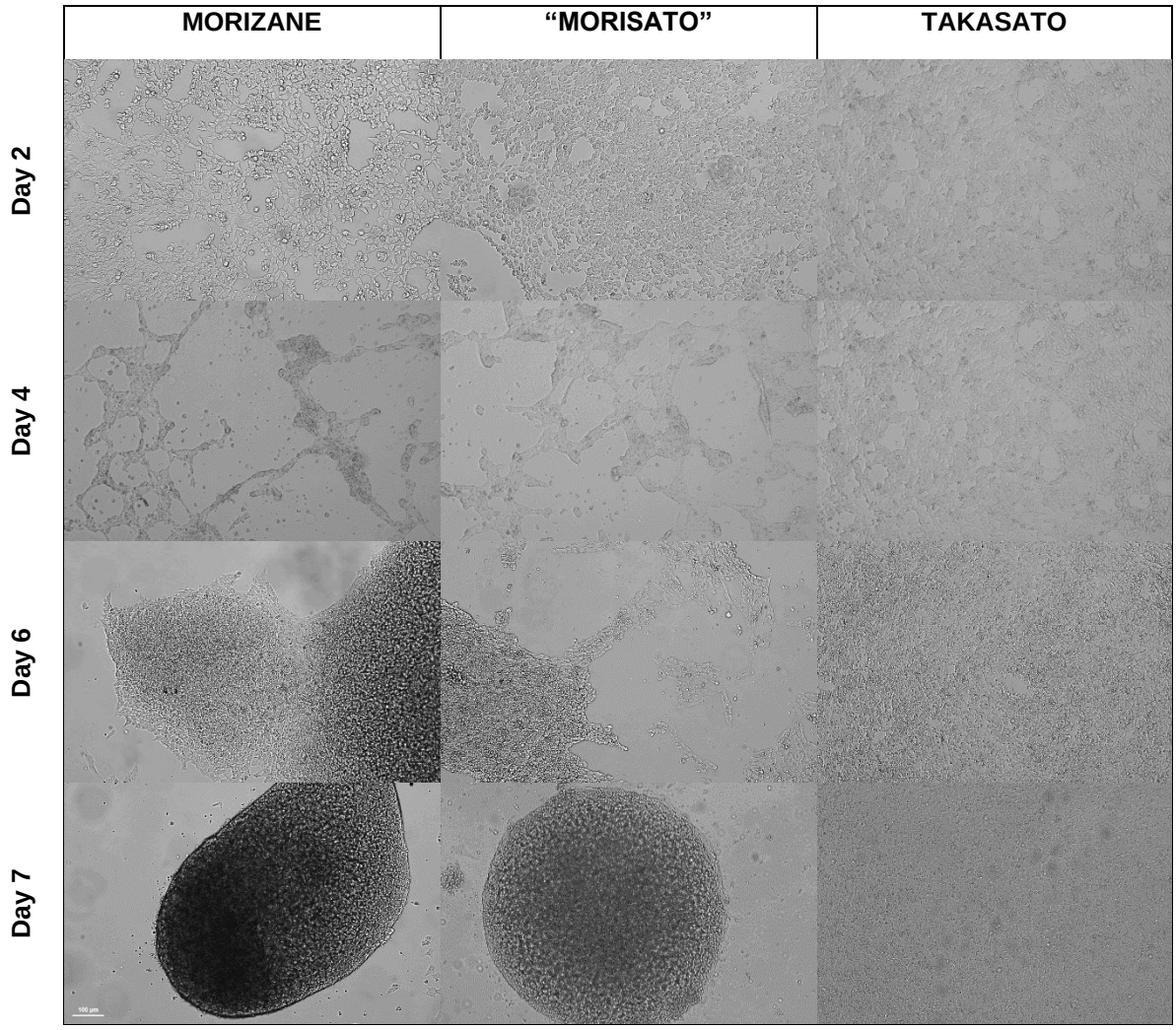

Figure 13 - Brightfield images of human iPSCs at day 0 and differentiating cells after the application of protocols of Morizane, “Morisato”, and Takasato until day 7. Scale bars represent 100 µm.

After 4 days of CHIR treatment, the protocols diverged in terms of molecules applied. Following Takasato and “Morisato” protocols, at day 4 the culture medium was supplemented with FGF9 and heparin. In the case of Morizane differentiation, at day 4 cells were supplemented with Activin A. By day 7 of differentiation of Takasato protocol, the borders of the cells became more subtle, and cells started growing rapidly, as a result they reached almost 100% confluence. This was not observed to the cells under “Morisato” and Morizane protocols: although under the influence of different molecules, cells formed clusters by day 7 of differentiation. This result suggest that the differentiation medium used have as much effect on the cell density as the small molecules applied on the differentiation.

At day 7, markers of the anterior intermediate mesoderm (GATA3) and posterior intermediate mesoderm (HOXD11) were monitored by quantitative RT-PCR and compared relatively to day 0 expression (**Figure 14B**). Previous research found that at day 7 of differentiation, monolayer cell cultures exposed to CHIR for longer periods of time induced less anterior intermediate mesoderm but more posterior intermediate

mesoderm, whereas shorter periods of CHIR exposure induced more anterior intermediate mesoderm and less posterior intermediate mesoderm (Takasato et al., 2016)

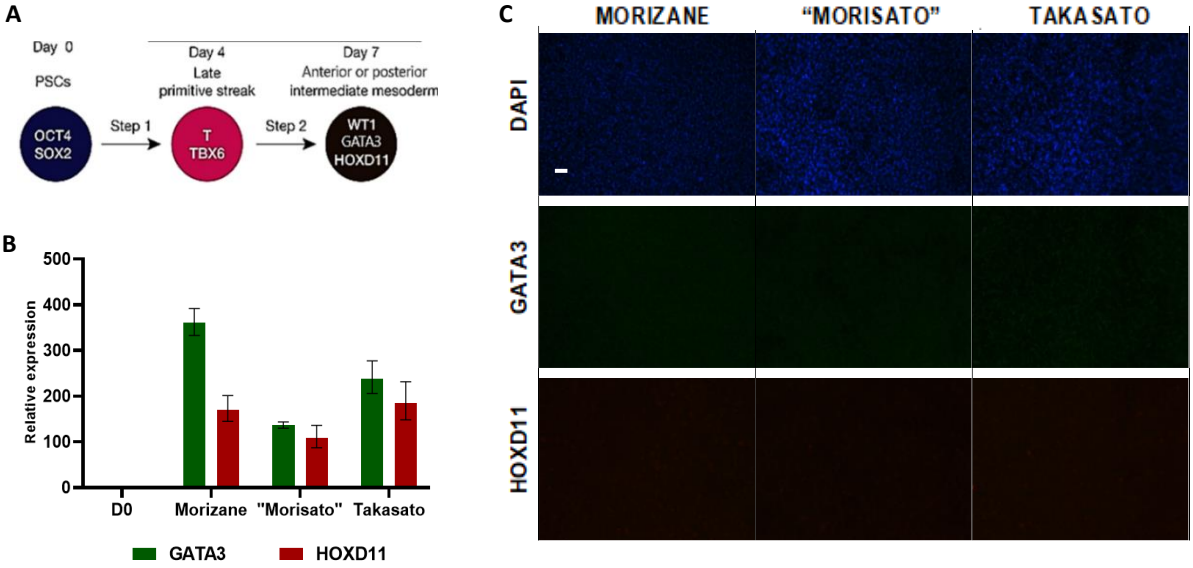

Figure 14 - (A) Diagram and the protocol of differentiation of human PSCs sequentially into late primitive streak and posterior and anterior intermediate mesoderm (IM) with markers identifying their presence. Adapted from Morizane et al., 2015. (B) Relative expression profiles of intermediate mesoderm markers during renal differentiation under monolayer conditions at day 7. Values are normalized to GAPDH expression and plotted relative to gene expression levels in iPSCs (D0). Data are represented as means ± SD from technical triplicates. (C) Immunofluorescence staining of cells differentiated using Morizane, "Morisato", and Takasato protocols at day 7. GATA3 in green and HOXD11 in red. Nuclei in blue stained with DAPI. Scale bars represent 100 µm.

Cells under Morizane protocol shown to have more relative gene expression of GATA3 than HOXD11, resulting in a more anterior IM fate. This result is not expected since Morizane protocol hypothesises the specific induction of only posterior intermediate mesoderm cells that would lead to the induction of nephron progenitor cells (Morizane & Bonventre, 2017).

Takasato *et al.* reported in their protocol that 3-4 days of CHIR exposure is meant to induce both the anterior and the posterior intermediate mesoderm at the same time. The optimal period of CHIR administration must be adjusted depending on PSC line used; therefore, it needs to be optimized to avoid obtaining a one-sided intermediate mesoderm population of either $GATA3^+$ or $HOXD11^+$ cells at day 7 of the differentiation (Takasato et al., 2015). Both "Morisato" and Takasato protocol yielded approximately equal levels of expression of GATA3 and HOXD11, as 4 days of CHIR exposure seem to be adequate. Nevertheless, the relative revels of gene expression were overall lower in "Morisato" protocol.

These results were confirmed by immunofluorescence analysis (**Figure 14C**), which showed both $GATA3^+$ or $HOXD11^+$ cells in each protocol applied.

2.2. Differentiation of human iPSC into renal lineage in 3D conditions

Most of the studies regarding intermediate mesoderm specification are done under monolayer adherent condition or in suspension on low-attachment plates. The main obstacle of suspension aggregate cultures are their heterogeneity and disorganization that results from uncontrolled cell aggregation, which ultimately leads to low differentiation efficiency (Miranda et al., 2018).

This problem can be solved by controlling the initial aggregate size and by providing uniform and adequate chemical cues (Kinney et al., 2012). Microwells are the most effective tool to control initial cell number in aggregates and by consequence the initial aggregate diameter. Increase of aggregate uniformity can be achieved by forcing cell aggregation in microwells that will lead to homogeneous populations formation inside aggregates (Ungrin et al., 2008).

Thus, distinct protocols were adapted into 3D culture with the goal of developing size-controlled iPSC aggregates that can be efficiently guided towards intermediate mesoderm lineage (**Figure 15A**). Seeding was done 24 hours before day 0 of differentiation, resulting in ≈1,500 cells in each microwell, which would yield an aggregate with approximately same number of cells (**Figure 15B**).

It was reported in the past that there is a correlation between size of the aggregate at the beginning of the differentiation and presence of structures in latter stages of differentiation: 90% of aggregates with diameters between 200 to 399 µm have the presence of tubules at day 14 of differentiation (Przepiorski et al., 2018). The number of cells per aggregate was particularly chosen since it produces 200 µm-diameter aggregates whilst also accounting for eventual diameter increase during differentiation (**Figure 15C**).

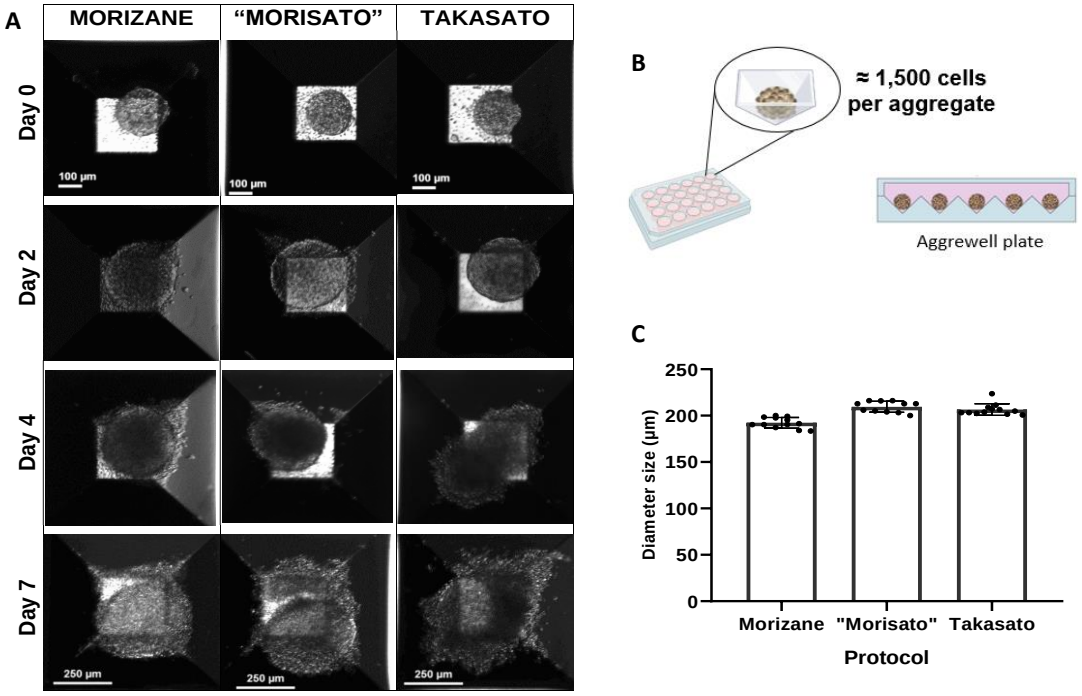

Figure 15 - (A) Brightfield images of human iPSCs aggregate at day 0 and differentiating cells in aggregates after the application of protocols of Morizane, "Morisato", and Takasato until day 7. Scale bars represent 100 or 250 µm. (B) Schematic representation of cell aggregate inside the Aggrewell 800. (C) Diameter size of the aggregates at day 0 of differentiation across distinct protocols applied. Error bars represent ± SD.

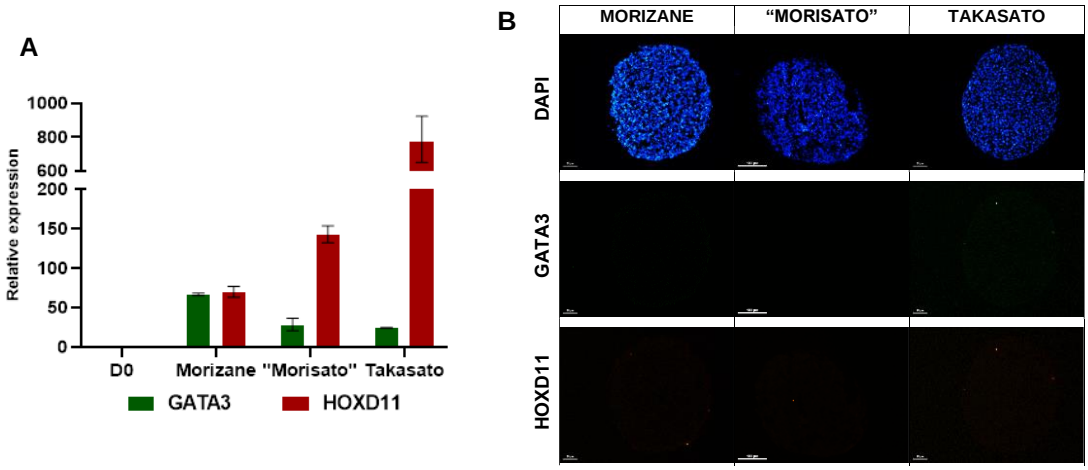

Figure 16 -(A) Relative expression profiles of intermediate mesoderm markers during renal differentiation under monolayer conditions at day 7. Values are normalized to GAPDH expression and plotted relative to gene expression levels in iPSCs (D0). Data are represented as means ± SD from technical triplicates. (B) Immunofluorescence staining of cells differentiated using Morizane, “Morisato”, and Takasato protocols at day 7. GATA3 in green and HOXD11 in red. Nuclei in blue stained with DAPI. Scale bars represent 100 µm.

At day 7, markers of the anterior intermediate mesoderm (GATA3) and posterior intermediate mesoderm (HOXD11) were monitored by quantitative RT-PCR and compared relatively to day 0 expression (**Figure 16A**). Results showed that aggregates following Morizane protocol have approximately equal levels of expression of GATA3 and HOXD11.

It was observed that aggregates yielded from “Morisato” and Takasato protocols were biased towards a more posterior IM fate, with higher expression of HOXD11. This data suggests from aggregate 3D conformation is suitable for posterior IM induction. Immunofluorescence analyses (**Figure 16B**) were inconclusive but in theory there should be expression of HOXD11 in Takasato protocol.

3. Uchimura protocol in fully 3D conditions

The following sets of experiments aim to adapt the Uchimura protocol in fully 3D conditions, analyse closely the first 7 days of differentiation, examine resulting kidney organoids, and apply the cisplatin assay to confirm their viability as drug-injury model.

3.1. Intermediate mesoderm specification

During primitive streak formation, the timing of migration of mesendoderm cells determines their fate. It is critical to determine if these protocols generate the appropriate primitive streak subtype (anterior, mid, or posterior) that is primed to produce the desired downstream differentiation outcome (**Figure 17A**).

The original Uchimura protocol starts with separate induction of anterior intermediate mesoderm (AIM), the progenitor of metanephric mesenchyme and posterior intermediate mesoderm (PIM), progenitor to ureteric bud-like cells. PIM induction, based on the Takasato protocol, and AIM protocol induction, a novel procedure, were followed till day 7.

To access off-target populations at day 7 of differentiation, pluripotency marker OCT4, several mesoderm markers (KDR, PDGFRA-α, OSR1, PAX2 and WT1) and endoderm marker SOX17 were analyzed (**Figure 17B**).

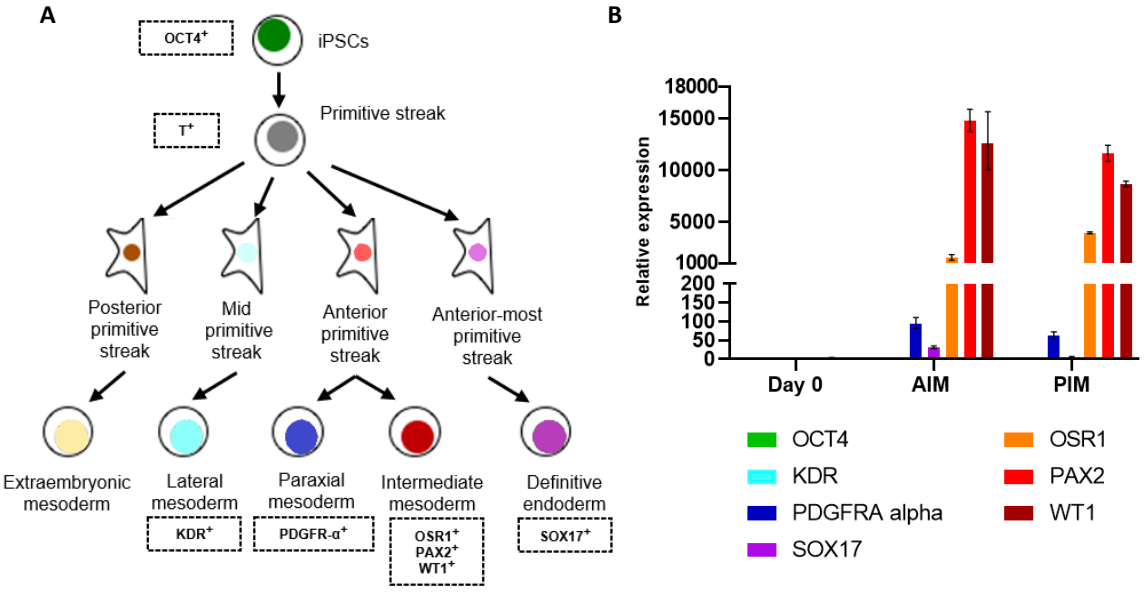

Figure 17 – (A) Schematic representation of iPSCs differentiation pathways into distinct primitive streak subtypes, each of which gives rise to a distinct mesoderm subtype or definitive endoderm. Adapted from Fowler et al., 2020. (B) Relative expression profiles of pluripotency, renal lineage, and different mesoderm markers during renal differentiation under monolayer conditions at day 7. Values are normalized to GAPDH expression and plotted relative to gene expression levels in iPSCs (D0). Data are represented as means ± SD from technical triplicates.

Results shown that in both AIM and PIM day-7 aggregates there is predominance of gene expression of IM makers, namely the early IM induction marker OSR1, also PAX2 and WT1 genes, which are vital for IM formation and later play a major role in kidney nephrogenesis (**Figure 17B**). However, in AIM and

PIM aggregates we can see also the expression of paraxial mesoderm marker PDGFRA-α (Sakurai et al., 2006). This indicates that there are some populations that in were not enough exposed to CHIR, the regulator mesendodermal patterning of iPSCs. This population is certainly difficult to avoid since paraxial mesoderm is derived from anterior primitive streak, just like IM. Interestingly, in AIM aggregates there is also expression of SOX17, a marker of definitive endoderm. This probably because some populations of cells were exposed high levels of activin A, which leads to endoderm differentiation (Wang et al., 2015). Overall, there is efficient IM induction in both AIM and PIM aggregates, the off-target populations are expected to be residual because of the low gene expression that they display.

Additionally, relative gene expression of GATA3 and HOXD11 was examined on day 7 of differentiation to confirm the anteroposterior fate of each population (**Figure 18B**). As expected, in the AIM aggregates had a strong expression of GATA3, but not HOXD11 (Uchimura et al., 2020). However, in PIM aggregates there was similar expression of the two markers. Suggesting that there is population of both progenitors of MM and UB. This is not totally unexpected as the original protocol from which PIM differentiation is based - Takasato protocol - reports the simultaneous induction of all progenitors of kidney lineage (Takasato et al., 2016). Additionally, relative gene expression can change in the course of the differentiation as RNA can still be degraded before being translated to a protein, and this can be resolved by analyzing resultant population in the kidney organoid.

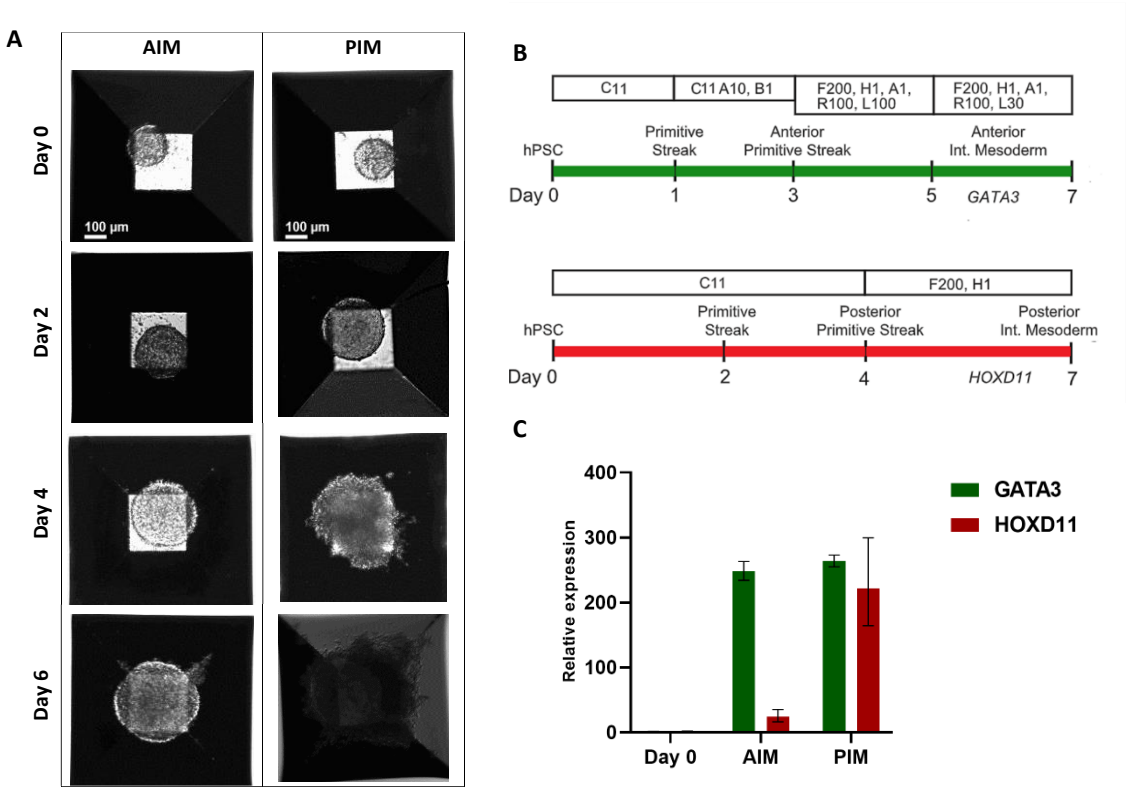

Figure 18 - (A) Brightfield images of human iPSCs aggregate at day 0 and differentiating cells in aggregates following the separate induction of AIM and PIM. (B) Outline of the Uchimura protocol from day 0 to day 7. A, activin (ng/mL); B, BMP4 (ng/mL); C, CHIR99021 (mM); F, FGF9 (ng/mL); H, heparin (mg/mL); L, LDN193189 (nM); R, nM retinoic acid. (C) Relative expression profiles of intermediate mesoderm markers during renal differentiation under monolayer conditions at day 7. Values are normalized to GAPDH expression and plotted relative to gene expression levels in iPSCs (D0). Data are represented as means ± SD from technical triplicates

3.2. Kidney Organoids

At day 7, the two populations (AIM and PIM) were mixed and seeded in transwell plates (**Figure 19A,B**) at a ratio of 3:1, with a total of $5x10^5$ cells per aggregate. Additionally, aggregates with only one of the cell lineages were also seeded. A 1-hour CHIR pulse was applied to all cell aggregates (**Figure 19C**) to optimize nephron formation, as the ureteric epithelium secretes WNT and stimulates nephron formation during kidney development (Takasato et al., 2015). Aggregates in the transwell filter stayed in air-liquid interface to maintain a 3D conformation.

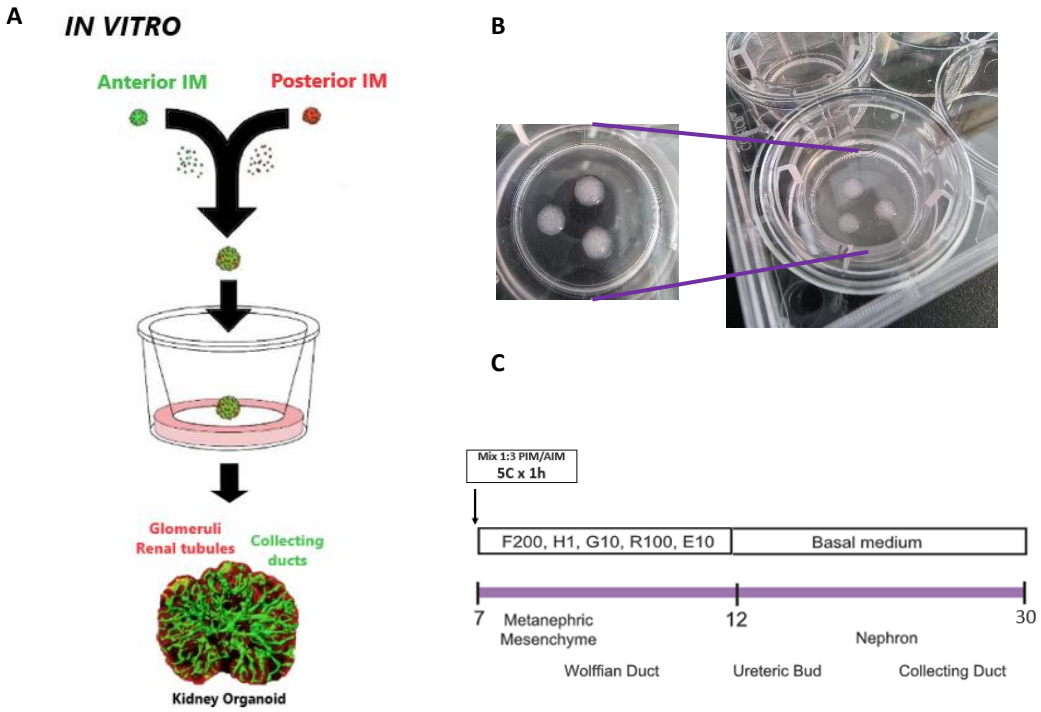

Figure 19 -(A) Schematic representation of the overall procedure of mixing of the two-progenitor population of renal tissue to achieve complex kidney organoids. (B) Photographs of the transwell with cell aggregates. (C) Outline of Uchimura protocol from day 7 to day 30 of differentiation. C, CHIR99021 (mM); E, EGF (ng/mL); F, FGF9 (ng/mL); G, GDNF (ng/mL); H, heparin (mg/mL); R, nM retinoic acid. Adapted from Uchimura et al, 2020.

The protocol was extended to day 30, rather than the initial 26 days, to allow the development of potentially more complex tissue structures (**Figure 20**). It was noted that during the rest of differentiation (from day 8 to 30) AIM aggregates had visibly different structure and type of tissues than PIM aggregates. AIM aggregates assumed a monolayered configuration and the nephron-like tubules were residual. Meanwhile, the PIM aggregates had a dense and multilayered 3D arrangement and exhibited a complex network of tubular nephron-like structures. Aggregates from the mix of the two populations were more similar to PIM aggregates and their nephron-like structures were less compact and dense.

It was observed a lot of heterogeneity between aggregates derived from the same cell types (only AIM or PIM or the mixture of AIM+PIM) in terms of size, shape and quantity of cells that were successfully incorporated to form the aggregate and future kidney organoid. This is probability due to cell death during or after seeding in the transwell. Another factor may be related with distribution of cells after

seeding: cells that assumed a more 2D conformation did not formed aggregates as successfully as the cells that were clustered together after seeding. Thus, this gave rise to smaller and bigger kidney organoids, with overall distinct and unique shapes.

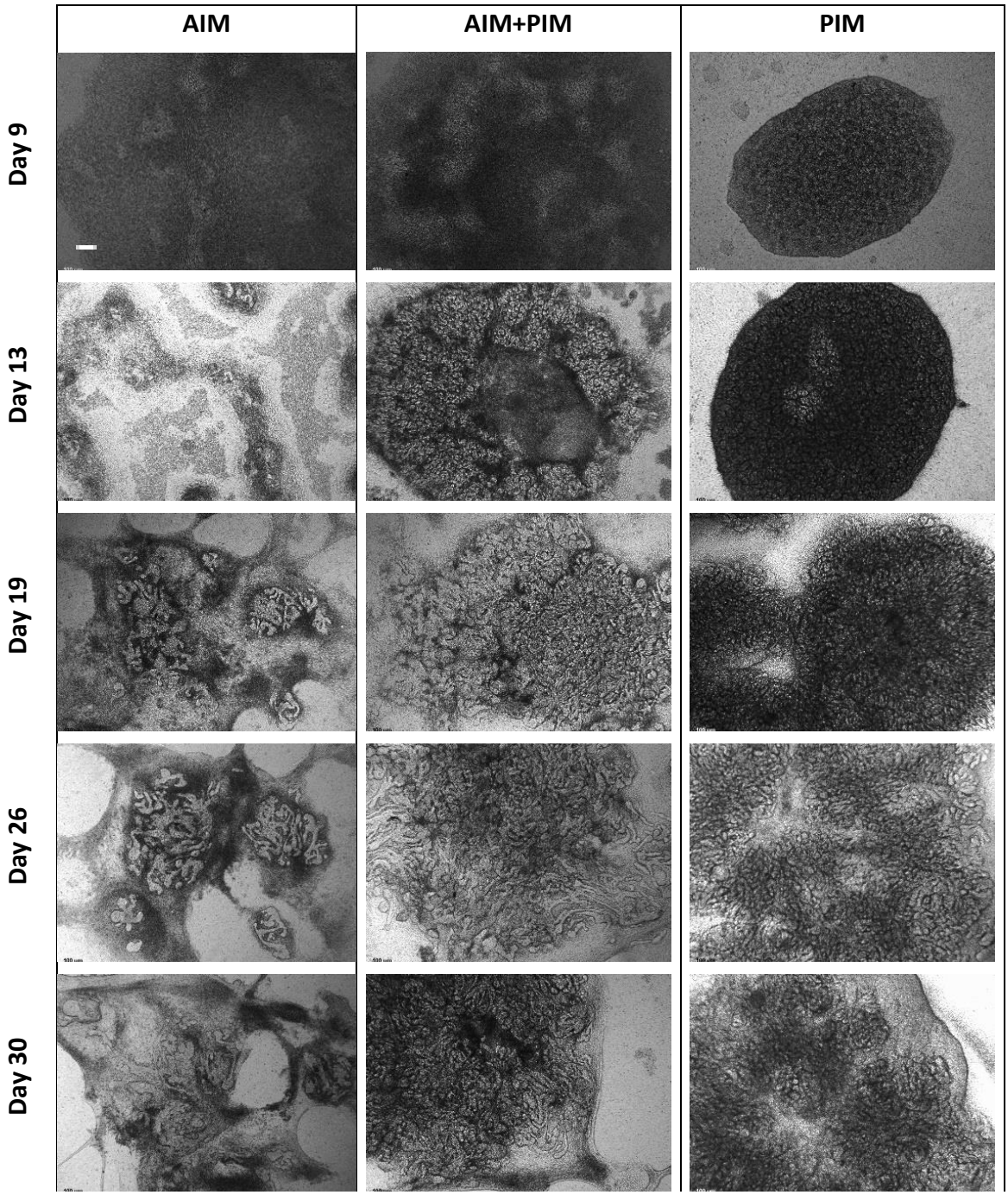

Figure 20 - Brightfield images of AIM aggregates, the mix of cells (AIM+PIM) and PIM in transwells during Uchimura protocol at days 9,13,19 26 and 30. Scale bars represent 200 µm.

Differentiation was halted at day 30 and immunofluorescence staining was performed in the sections of resulting kidney organoids to access which population were present. Unfortunately, only PIM and the

mix of AIM+PIM population aggregates-derived kidney organoids were possible to access by this method since the AIM kidney organoids were too thin for a successful cryosection.

In PIM aggregates, immunofluorescence shows PAX8 expression but not LHX1 (**Figure 21**). There is no confirmation of the presents of renal vesicles (PAX8+ LHX1+) but PAX8 is abundantly expressed by renal blastema cells during nephrogenesis (Bouchard et al., 2002). Additionally, PAX8 staining was previously reported in renal epithelial cells in all segments of renal tubules from the proximal tubules to the renal papillae in the adult kidney (Tong et al., 2009).

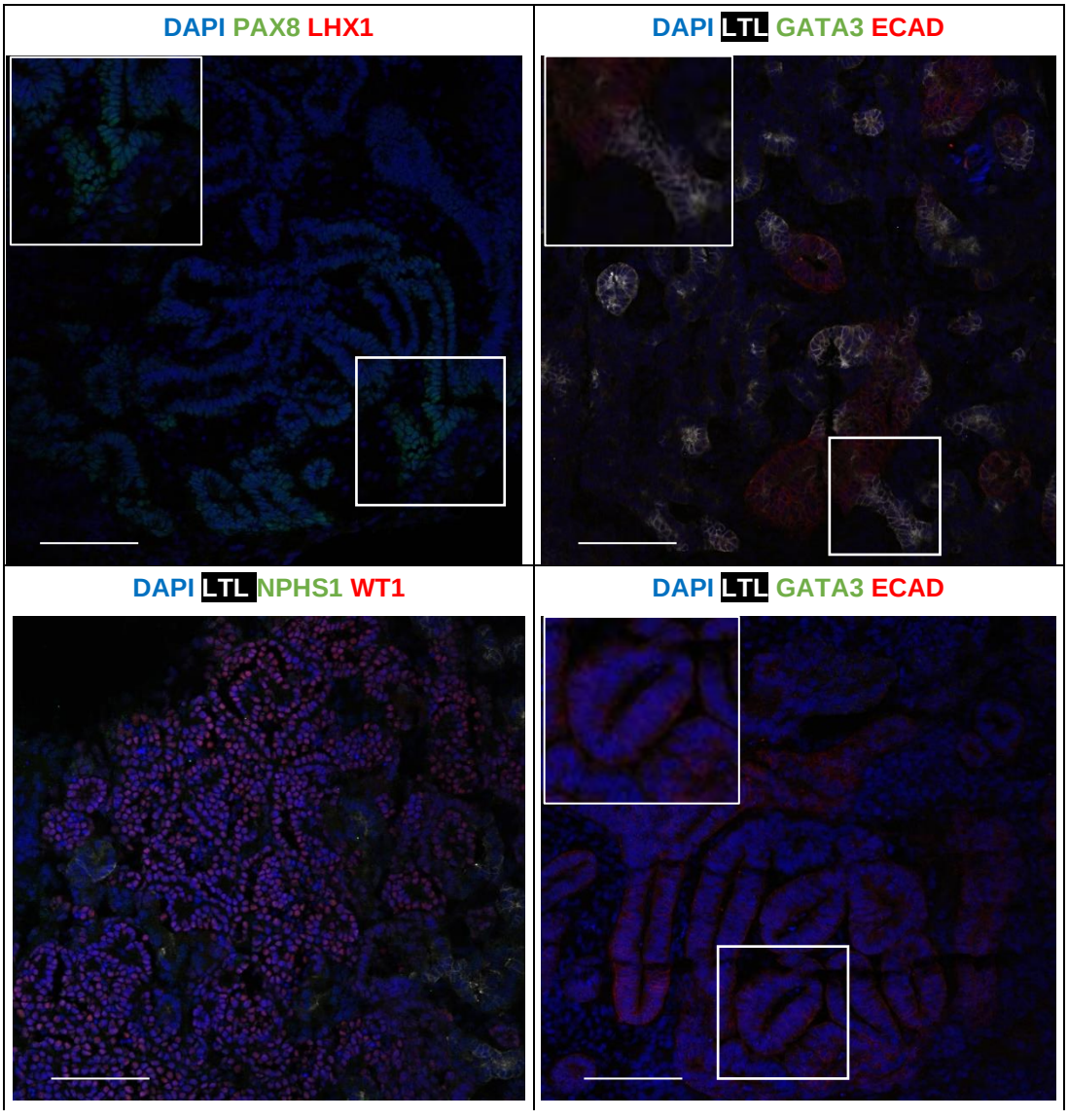

Figure 21 - Immunofluorescence staining in cryosections of PIM aggregate-derived kidney organoids at day 30 of Uchimura differentiation. Scale bars represent 100 µm.

For the same type of aggregate, absence of GATA3 expression indicates that collecting duct (GATA3+ ECAD+) formation is absent (**Figure 21**). Although gene expression of GATA3 was detected at day 7 of differentiation of the PIM population, probably this was not enough to induce AIM-derived structures.

There is the possibility of subsequent GATA3 gene downregulation, as in PIM differentiation is not expected to give rise to AIM derivates.

The expression of LTL in tubular structures and the lack of expression of ECAD marker confirms the rise of early proximal tube (LTL+ ECAD-). In contrast, tubular structures with only ECAD marker expression that lack both LTL and GATA3 staining point to early distal tube (LTL- GATA- ECAD+) formation (**Figure 21**) Interestingly, expression of both markers in the same tubular structure was noted but in distinct segments as there was never the simultaneous staining of LTL and ECAD. Nevertheless, ECAD marker is expressed both in immature proximal tube as well in the distal tube. Thus, it is difficult distinguish between these two structures.

WT1 and NPHS1 markers both stain podocytes but only WT1 expression can be seen in the cells around tubular-shaped cells (**Figure 21**), which is enough to suggest the presence of glomeruli cells.

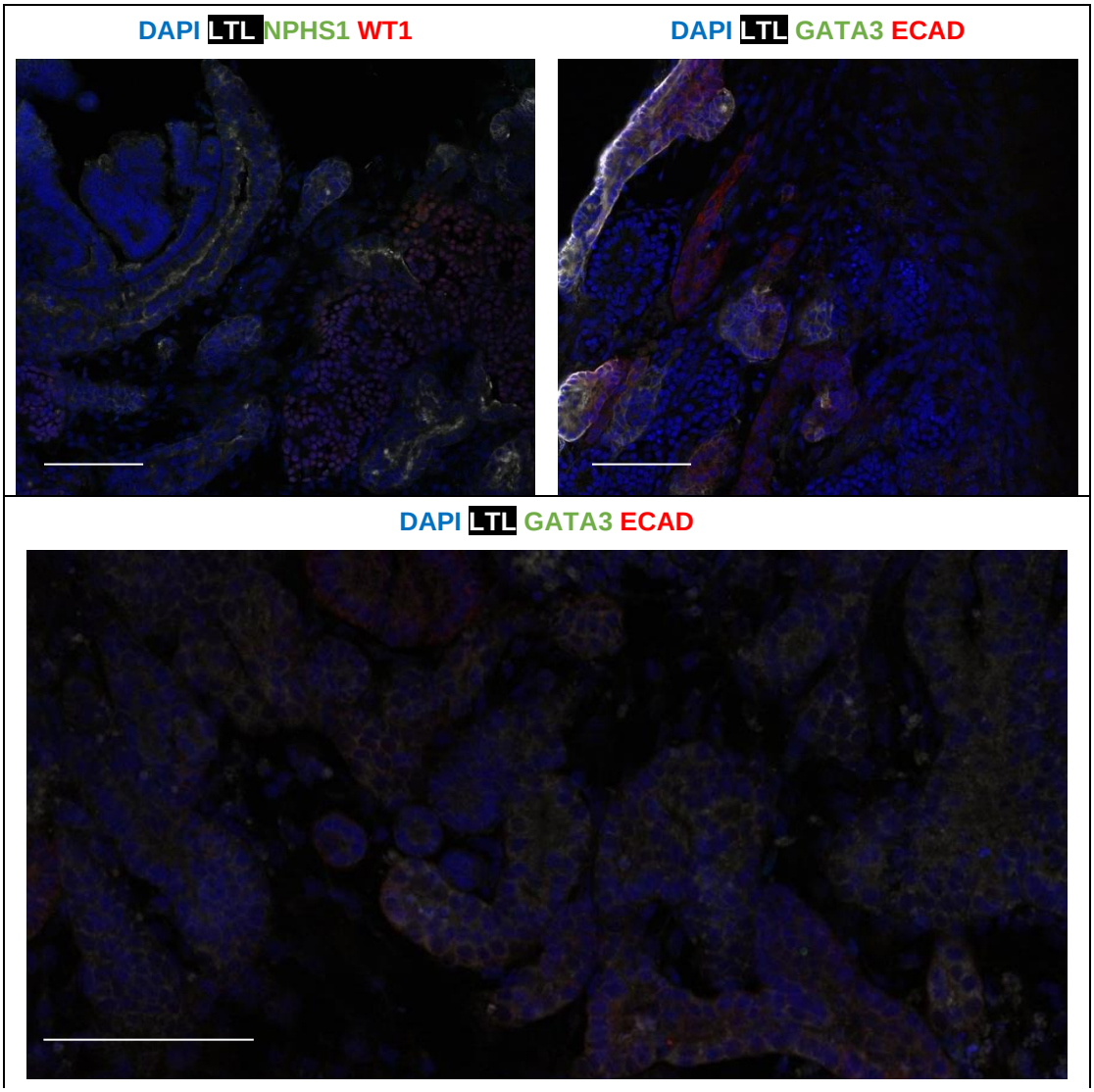

Figure 22 - Immunofluorescence staining in cryosections of AIM+PIM aggregate-derived kidney organoids at day 30 of Uchimura differentiation. Scale bars represent 100 µm.

Similarly to PIM-derived kidney organoids, kidney organoids generated from AIM+PIM aggregates expressed WT1 but not NPHS1 (**Figure 22**). WT1 staining was found in cells between LTL+ tubular structures, indicating the existence of glomeruli cells.

GATA3 staining was not detected (**Figure 22**), which means that there was no outgrowth of collecting duct (GATA3+ ECAD+). AIM gene expression at day 7 was not able to develop further into ureteric bud that would originate collecting ducts. Indeed, the has been much debate over the presence of collecting ducts in kidney organoids. While some studies employed genetic lineage analysis to confirm the presence of AIM derivates (Howden et al., 2019), other investigators were not able to detect the definitive AIM lineage (Subramanian et al., 2019). Nonetheless, presence of LTL+ tubular structures, together with the absence of ECAD marker expression, confirms the formation of the early proximal tube (LTL+ ECAD-). Tubular structures that only show the ECAD marker and neither LTL nor GATA3 staining, on the other hand, suggest early distal tube formation (LTL- GATA- ECAD+) (**Figure 22**).

3.3. Drug-injury model: cisplatin assay

On day 30 of differentiation, kidney organoids generated were treated with cisplatin (5 µM) for 24 hours to test their applicability as a model for research of drug-induced kidney injury. Cisplatin is an anti-cancer drug that was observed to cause proximal and distal tubular damage. It induces caspase-mediated acute apoptosis of proximal tubule cells in the kidney (Cummings & Schnellmann, 2002; Mese et al., 2000). Cisplatin nephrotoxicity assay is considered a maturation analysis on kidney organoids as nephrotoxicity is expected in mature kidney tubules.

PIM-derived kidney organoids were immunostained for kidney injury molecule-1 (KIM-1), a biomarker that is substantially upregulated in the proximal tubules following acute kidney injury (Vaidya et al., 2010), as well as LTL and ECAD to distinguish between the proximal and distal tubules.

In both control and exposed to cisplatin aggregates, there is LTL staining, which indicates the presence of early proximal tubes. However, there is no KIM-1 expression at the luminal surface of LTL+ tubules in organoids exposed to cisplatin that would indicate cisplatin-induced injury in proximal tubules (**Figure 23**). It was previously reported that only in mature proximal tubules (LTL+ ECAD+) was possible to detected cisplatin-induced apoptosis, whereas in the immature early proximal tubules (LTL+ ECAD-) do not undergo apoptosis (Takasato et al., 2015). From this it is concluded that the proximal tubules of the PIM-kidney organoids are immature.

Curiously, in organoids treated with cisplatin, there is almost no ECAD+ cells. Only a small cluster of ECAD+ cells can be seen in **Figure 23** and is enough to confirm that ECAD staining was successful. The observed absence of ECAD+ cells could indicate injury in distal tubules as it was previously reported that cisplatin causes ECAD suppression in kidney organoids generated (Morizane et al., 2015). However, the absence of ECAD+ cells might be due to organoid heterogeneity that cause differences in the structures that formed inside the kidney organoids.

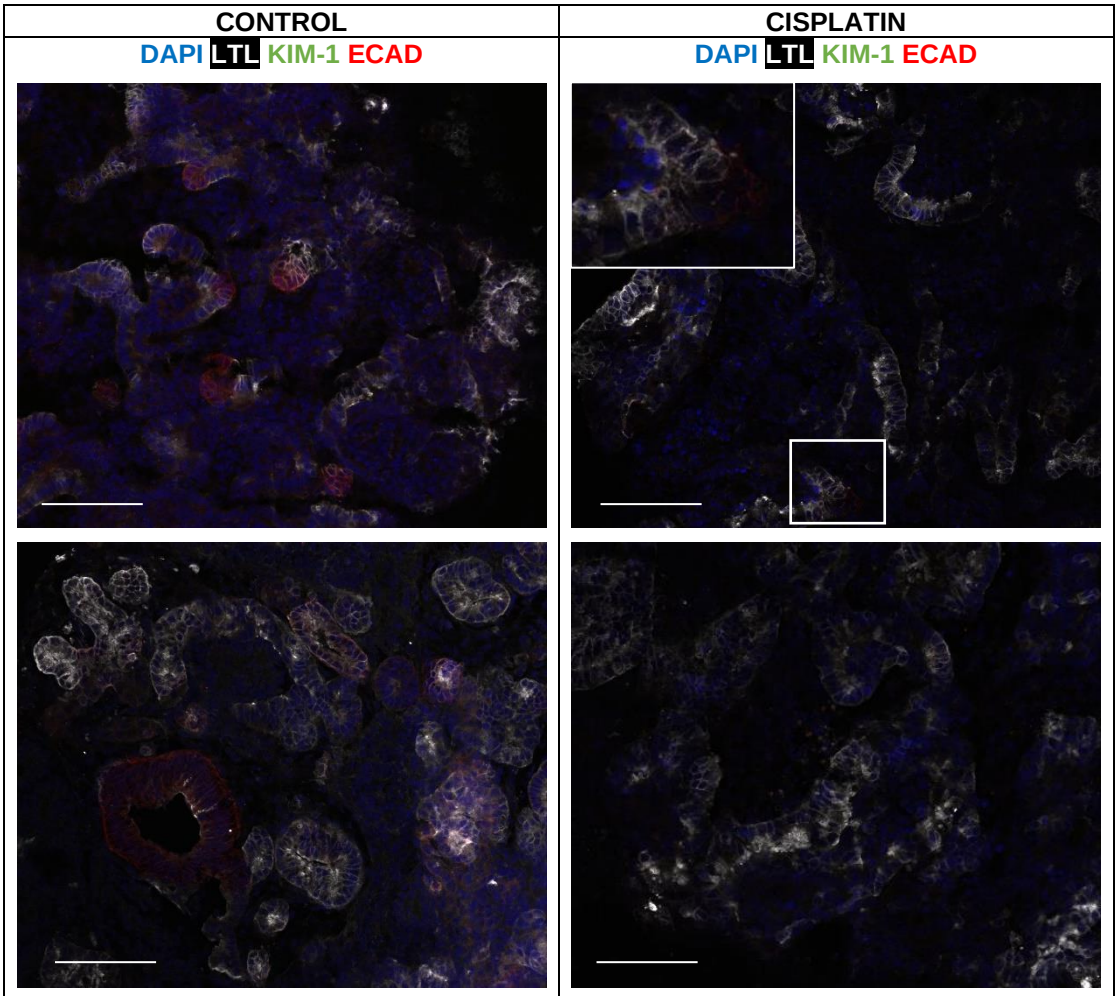

Figure 23 - Immunofluorescence staining in cryosections of control PIM aggregates derived kidney organoids at day 30 of Uchimura differentiation (left) and PIM aggregates derived kidney organoids at day 30 treated 24h with cisplatin (right). Scale bars represent 100 µm.

Additionally, in control and cisplatin-treated AIM+PIM kidney organoids, relative mRNA expression was assessed in different genes related to kidney structures and development PAX2, GATA3, CUBN and also the injury-related KIM-1 (**Figure 24**).

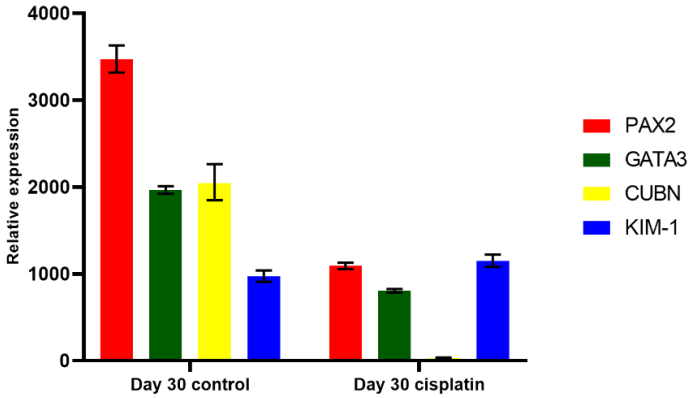

F**igure 24** - Relative expression profiles of renal markers at day 30 of differentiation in AIM+PIM aggregates treated with cisplatin and in control aggregates. Values are normalized to GAPDH expression and plotted relative to gene expression levels in iPSCs (D0). Data are represented as means ± SD from technical triplicates

PAX2 is considered a marker of renal tubules and collecting duct in kidney organoids, GATA3 is related to genesis of collecting ducts, besides being a marker of AIM in early stages of differentiation and CUBN is a gene expressed in proximal tubule of kidneys.

The levels of gene expression of PAX2, GATA3 and CUBN decreased significantly which in cisplatin-treated organoids, compared to the control organoids. This might be due to the cisplatin effect in the renal cells that might increase the renal cell stress response to a toxicant and thus, diminish the levels of genes related to synthesis of new structures inside the kidney. However, KIM-1 mRNA levels only increased slightly in cisplatin-treated organoids. In case proximal tubule injury, this molecule would be increased but this fact did not occur. A similar conclusion was reached after immunocytochemistry, in which KIM-1 staining was not detected. As discussed previously, results reveal that the proximal tubule injury is not detected by KIM-1 biomarker potentially because the proximal tubules developed in the organoids are still immature and do not sustain injury by cisplatin.

4. Development of “Morisato” protocol in fully 3D conditions

This chapter of the project aims to explore the possibility of the development of a protocol inspired in Uchimura protocol. The objective is to demonstrate the feasibility of the strategy of separate induction of AIM and PIM (the progenitor populations of ureteric bud and metanephric mesenchyme, respectively) and the subsequent combination of the two population to generate complex kidney organoids in fully 3D conditions.

4.1. Evaluation of cell lineage fate in different conditions

“Morisato” protocol uses Advanced RPMI medium as basis, the same as used in Morizane protocol. Furthermore, the novel “Morisato” protocol uses a limited set of small molecules (CHIR, Activin A, FGF9 and heparin) throughout differentiation to induce AIM and PIM populations, inspired by the protocols of Morizane and Takasato (Morizane & Bonventre, 2017; Takasato et al., 2016).

In order to assess the optimal conditions to differentiate AIM and PIM populations three main adaptations were subjected to modification: the initial size of the aggregate, the duration of CHIR exposure and the following supplementation of either Activin A (similarly to Morizane protocol) or supplementation of FGF9 and heparin (similarly to Takasato protocol) (**Figure 25**).

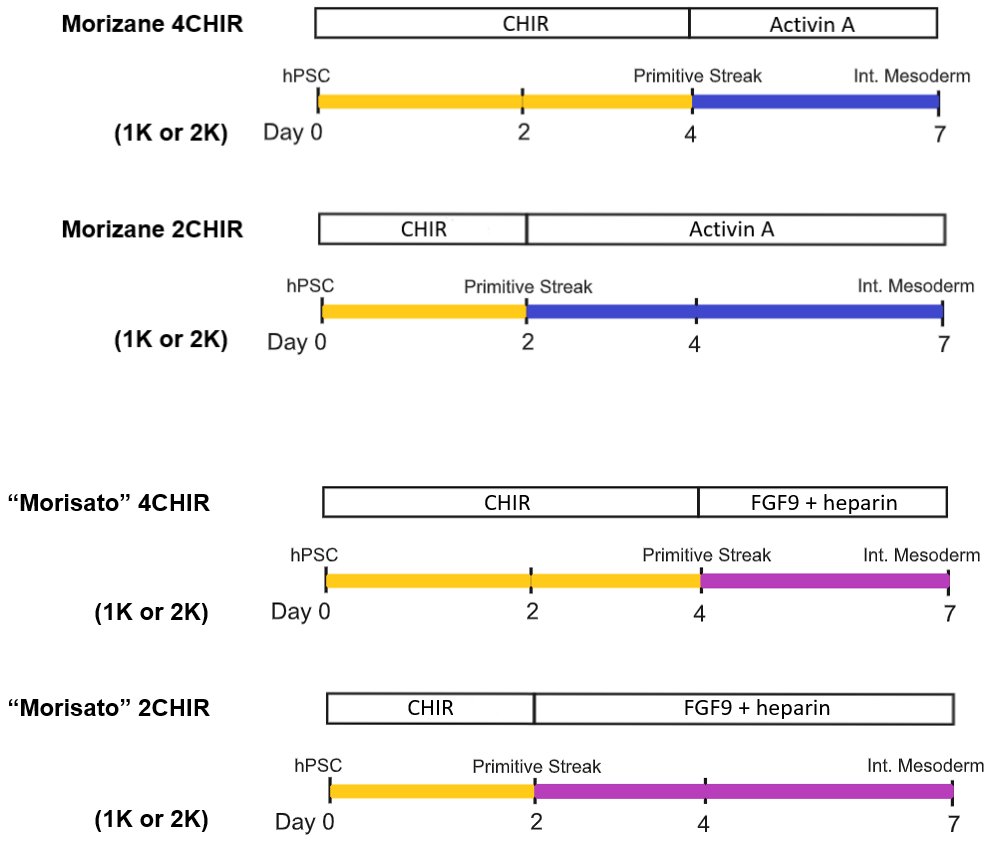

Figure 25 - Outline of modification to Morizane and “Morisato” protocols that rise from modifications of conditions, from day 0 to day 7 of differentiation.

Briefly, initial duration of WNT signaling was varied by manipulation of CHIR exposure length in the culture medium (2 or 4 days). After primitive streak induction with CHIR exposure, the next step of intermediate mesoderm induction was the addition of either Activin A (during Morizane protocol) or FGF9 and heparin (during “Morisato” protocol) until day 7 of differentiation. The initial size of the aggregate as 1,000 cells per aggregate (“1K”) or 2,000 cells per aggregate (“2K”) was also taken into consideration. These modifications yielded eight distinct conditions at day 7 of differentiation. To access off-target populations at day 4 and 7 of differentiation of each conditions considered, pluripotency marker OCT4, several mesoderm markers (KDR, PDGFRA-α, OSR1, PAX2 and WT1) and endoderm marker SOX17 were analyzed and represented in heatmap form (**Figure 26**).

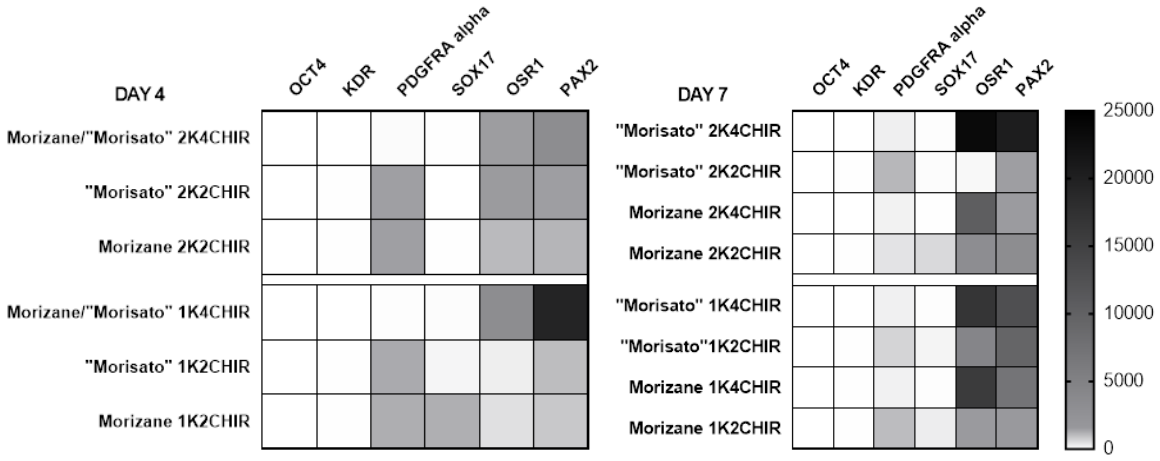

Figure 26 - Heatmap of the relative gene expression of different genes (OCT4, KDR, PDGFRA-α, OSR1, PAX2, WT1 and SOX17) in all possible variations of Morizane and “Morisato” differentiations at day 4 (left) and day 7 (right).

In day 4 as well in day 7 of differentiation, there is no OCT4 and KDR gene expression. SOX17 was slightly expressed at day 4 in the condition 1K2CHIR of Morizane protocol. In general, across all conditions, there is no significant gene expression of pluripotent cells, lateral mesoderm cells and endoderm cells.

It is interesting to note that cells that undertook 2 days of CHIR exposure (“2CHIR”) had higher levels of PDGFRA-α gene expression, comparing with the conditions with 4 days exposure (“4CHIR”) of the same molecule. This can be seen at day 4 and 7 of differentiation, but at day 4 the difference is more evident. Moreover, the timing of CHIR exposure seem to play a major role in the anteroposterior mesoderm fate in the conditions than the protocol itself applied: Morizane and “Morisato” protocols did not showed impact in this feature. Indeed, there is already expression of intermediate mesoderm markers OSR1 and PAX2 at day 4, and the highest expression this two markers happen to be in the conditions “1K4CHIR” and “2K4CHIR”, not regarding the protocol used. This appears to be a sign that 2 days of CHIR exposure did not cause total induction of intermediate mesoderm, as paraxial mesoderm gene expression is somewhat prevalent in those samples. At day 7, it is also worth noticing that conditions that have considerable expression of PDGFRA-α and SOX17, reveal less expression of renal markers

OSR1 and PAX2, this corroborates the hypothesis of insufficient CHIR induction. At the same day, results show that the conditions with higher OSR1 and PAX2 expression are “1K4CHIR” and “2K4CHIR” in both Morizane and “Morisato” protocols. Being the highest expression of the renal markers present in the condition “2K4CHIR” when “Morisato” protocol is applied.

To choose the best condition to continue the differentiation protocol further, relative expression of genes GATA3 and HOXD11 were assessed at day 7. The results confirm that the condition of “1K4CHIR” applied in the “Morisato” protocol is the best choice for PIM differentiation, as it revealed the highest expression of HOXD11, a marker of metanephic mesoderm progenitor PIM (**Figure 27**). “Morisato” protocol under “1K2CHIR”, “2K2CHIR” and also ““1K2CHIR” under Morizane showed the best results in terms of GATA3 expression, suitable for AIM differentiation (**Figure 27**). But ultimately, comparing with results of off-target populations, “1K2CHIR” Morizane condition was solidified as the chosen option to continue the differentiation.

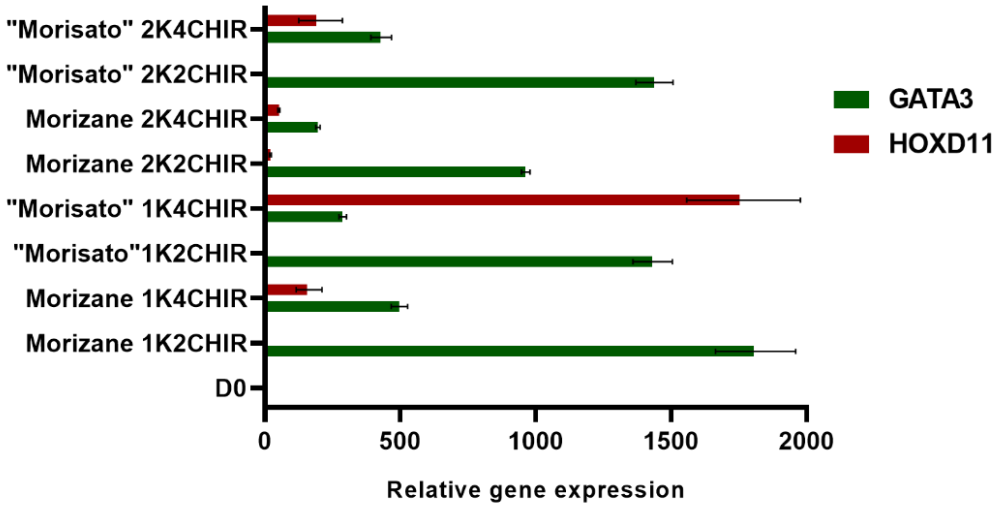

Figure 27 - Relative expression profiles of intermediate mesoderm markers during renal differentiation under distinct conditions at day 7 with Morizane or “Morisato” protocols. Values are normalized to GAPDH expression and plotted relative to gene expression levels in iPSCs (D0). Data are represented as means ± SD from technical triplicates.

4.2. Kidney Organoids

After the selection of the most suitable protocols and respective modifications, the differentiation was started by two separate but simultaneous differentiations in 3D environment: Morizane 1K2CHIR for the differentiation of AIM population and “Morisato” 1K4CHIR for the differentiation of PIM population (**Figure 28**). At day 7, the resulting aggregates were mixed and exposed to 5µM of CHIR pulse for 1h. Additionally, only AIM and PIM populations (without mixing) were also seeded in the transwell. FGF9 and heparin was supplemented until day 12 of differentiation and after that, only basal medium was supplied until day 30.

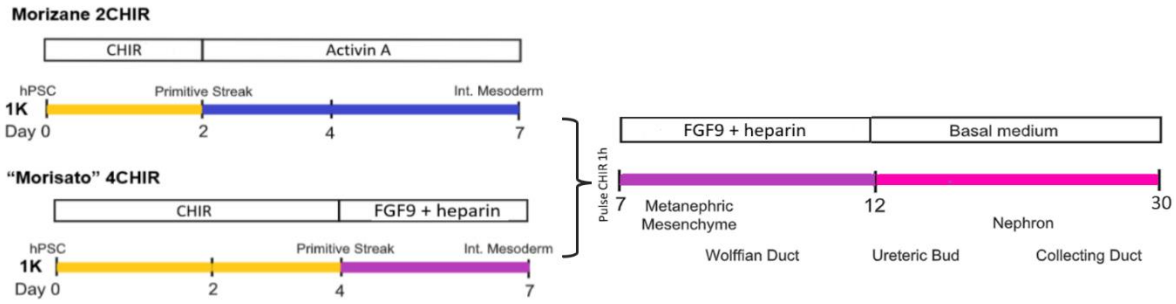

Figure 28 - Outline of modification to Morizane and "Morisato" protocols that rise from modifications of conditions, from day 0 to day 7 of differentiation.

After the seeding the transwell, only separate populations developed into microscopically visible structures associated with the starting of the nephrogenesis. AIM+PIM populations assumed a monolayer layer of cells with no complexity in the transwell and did not develop further. This translated to only organoids derived from only one of the populations: Morizane 1K2CHIR and "Morisato" 1K4CHIR. The resulting kidney organoids were heterogenous in size and shape (**Figure 29**).

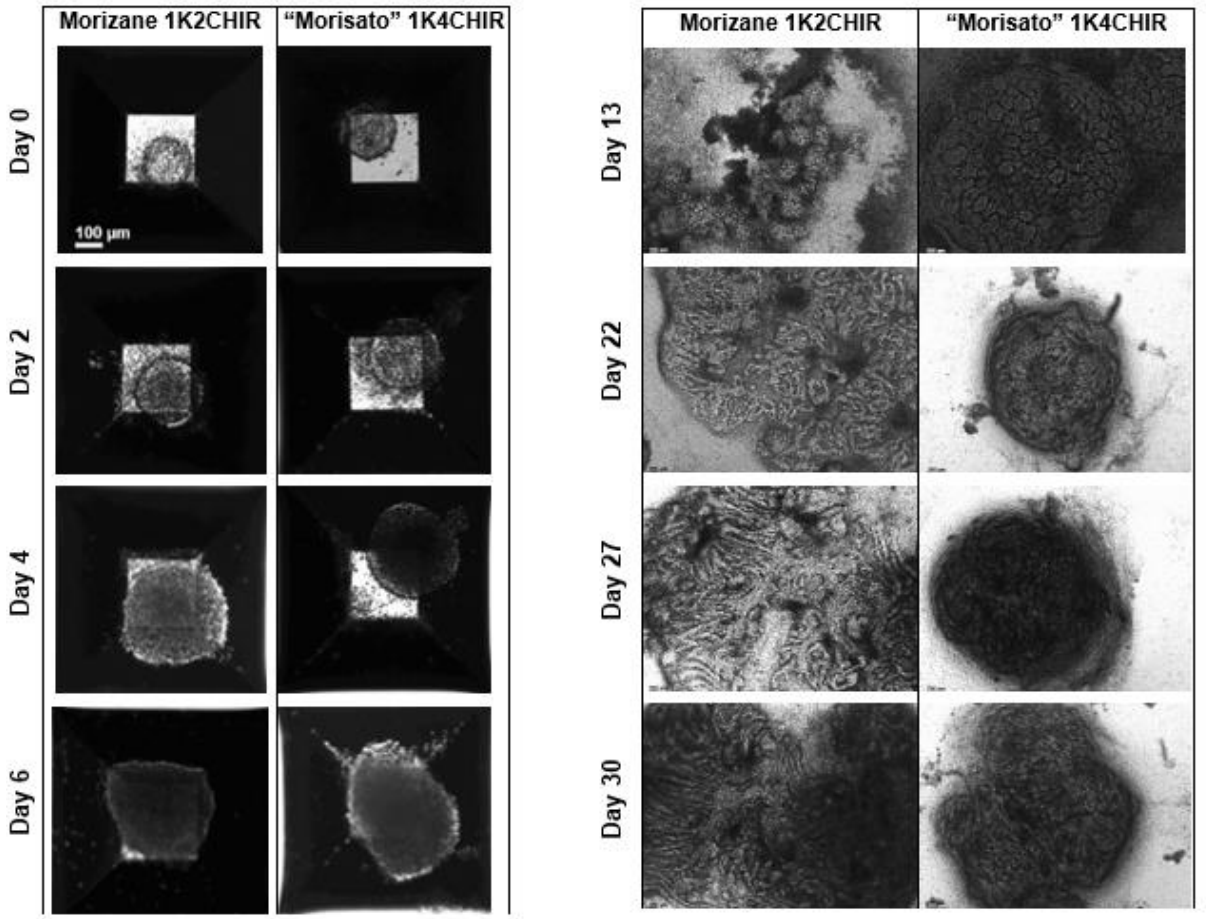

Figure 29 - Brightfield images of aggregates during "Morisato" protocol from day 0 to day 6 and developing kidney organoids in the transwell from day 13 until day 30. Scale bars represent 100 µm.

It was hypothesized that the failure to obtain organoids derived from the two populations (AIM+PIM) is due to inadequate number of cells ($5x10^5$ cells) during seeding in the transwell. This number of cells revealed to de too excessive to give rise of complex aggregates as it led to cell death, possibly because of inadequate supply of nutrients in the core of the aggregate in the transwell. When $2x10^5$ cells were applied, it revealed to be insufficient, and the cells did not amass to give rise to structures. Furthermore, the quality of cells grown in the aggrewells until day 7 also has a huge impact in the course of the rest of the differentiation.

The number of cells per aggregate and the ratio of Morizane 1K2CHIR/"Morisato" 1K4CHIR populations during transwell seeding should be the object of further investigation. This is only a preliminary study, as the full potential of the approach has not been proven.

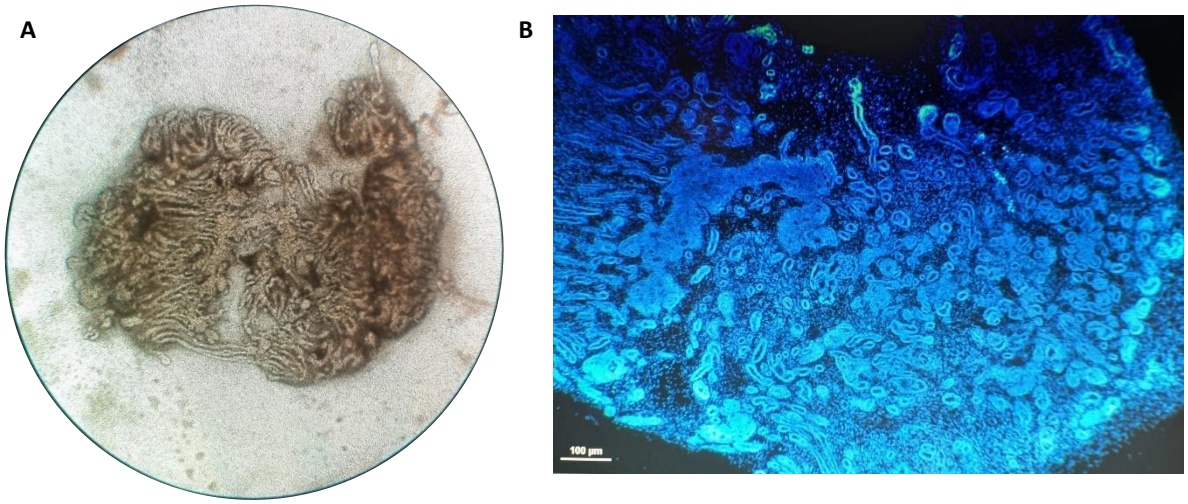

Figure 30 – (A) Brightfield image of a kidney organoid derived from Morizane 1K2CHIR aggregates at day 29 of differentiation. Image at 10x magnification. (B) Immunofluorescence staining with DAPI in a cryosection of the same 1K2CHIR Morizane-derived kidney organoid as in (A) at day 30 of differentiation. Scale bars represent 100 µm.

Nevertheless, resulting 1K2CHIR Morizane derived organoids revealed unexpected results, as the structures formed were suspected to not be originated from AIM population only (**Figure 30A**).

Only AIM-derived kidney organoids were possible to cryosection and immunostaing (**Figure 30B**). Interestingly, cells in the resulting kidney organoid expressed SIX2, a marker only found during kidney organogenesis in humans and is a marker specific of nephron progenitor cells, which are canonically originated from PIM. Furthermore, immunostaining revealed the presence of renal vesicles (PAX8+ LHX1+), early proximal tubules (LTL+ GATA3-) and distal tubules (LTL- ECAD+).

However, where was no WT1 and NPHS1 staining, suggesting no glomeruli generation. Similarly, the lack GATA3 expression indicates that collecting duct (GATA3+ ECAD+) formation is absent (**Figure 31**). Cells were also negative for the metanephric stromal progenitor marker FOXD1 (similar result was reported during the original Morizane protocol).

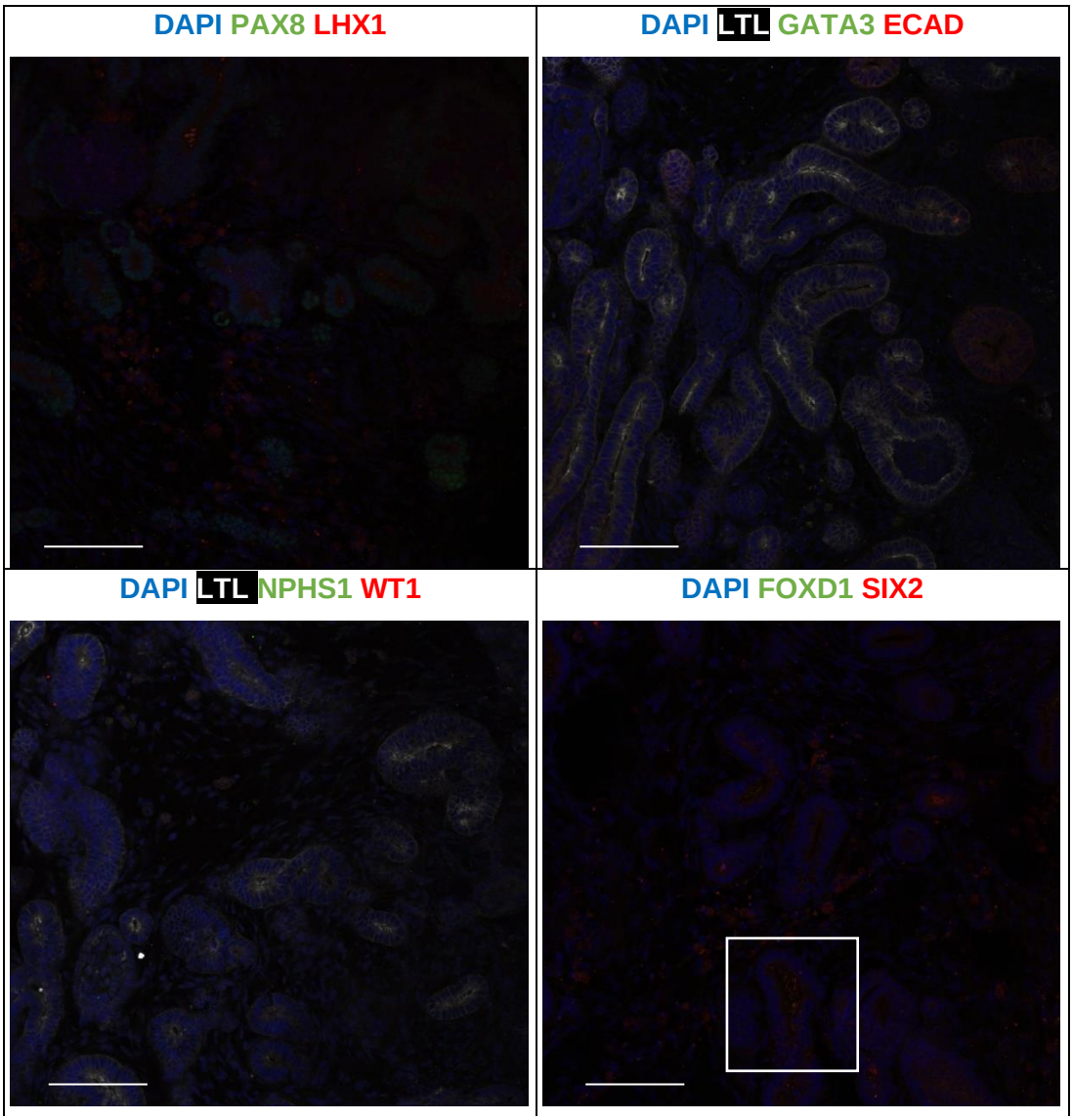

Figure 31 - Immunofluorescence staining in cryosections of AIM aggregate-derived kidney organoids at day 30 of "Morisato" differentiation. Scale bars represent 100 µm.

Structures like renal vesicles, proximal tubules, distal tubules and also the presence of nephron progenitor cells indicates that the gene expression AIM population at day 7 in 1K2CHIR Morizane-derived aggregates is not truly revealing in terms of future cell population inside the aggregate. The process of antero-posterior patterning in intermediate mesoderm is more dynamic than expected. Additionally, batch-to-batch heterogeneity between aggregates may play a role in the derivation of populations that ultimately bring distinct outcomes in terms of final cell populations inside the kidney organoid.

Conclusion & Future Remarks

In this thesis, protocols of Morizane, Takasato and the hybrid protocol “Morisato” were followed until the stage of intermediate (day 7) in both in 2D and 3D conditions. To induce primitive streak CHIR exposure was fixed as 4 days in all protocols, since it was previously established as the optimal timing to induce intermediate mesoderm. Thus, only the culture medium and the molecules supplemented after day 4 can explain the differences in gene expression that were assessed in day 7 of differentiation.

Early on, it was observed that the cells were more confluent in monolayer conditions when grown with STEMdiff APEL 2 medium (Takasato protocol) than cells grown in Advanced RPMI 1640 medium (Morizane and “Morisato” protocols). Indeed, STEMdiff APEL 2 medium is established as more robust medium, was specifically designed for ESCs and iPSCs differentiation and its formula is a trademark secret. Whereas Advanced RPMI 1640 medium is a quite simple basal medium that requires supplementation, generally used in a wide range of cell cultures but has an advantage of being more economically viable than STEMdiff APEL 2 medium.

Nevertheless, the confluence, the relative gene expression of GATA3 and HOXD11 unveiled similarities in “Morisato” and Takasato protocols, but set aside Morizane protocol, both in 2D and 3D conditions.

In the 2D application of Morizane protocol, there was more GATA3 expression, which is the opposite of cited in the original protocol, which expected induction of HOXD11, the progenitor population of nephron cells. It is known that gene expression standpoint is not totally accurate in translating accurate predictions in the cultures present, however, it can give a more general notion of genes that are more active at the time-point considered.

In 3D culture systems, there is a noticeable shift in the upregulation of posterior mesoderm gene expression marker HOXD11. Both “Morisato” and Takasato had more expression of HOXD11 than GATA3 in this culture system, and in case of Morizane, proportions gene expression of GATA3 and HOXD11 reach to be of similar level. It is interesting to note that higher concentration of CHIR applied in aggregate culture systems, allied with the 3D conformation favor the gene expression of more posterior populations. This fact goes in line with previous studies in which shorter periods of CHIR application induced the anterior intermediate mesoderm markers, LHX1 and GATA3, whereas longer periods increased the posterior intermediate mesoderm markers, HOXD11 and EYA1, at day 7 (Takasato et al., 2015).

In the adaptation of Uchimura protocol in fully 3D conditions revealed that in day 7, there was no significant gene expression of off-target genes in the differentiated populations AIM and PIM. However, unexpectedly the AIM population revealed both gene expression of markers characteristic of both AIM and PIM population. Indeed, it was observed the rise of some rudimentary tubular structures as early as in day 15 of differentiation in the AIM-derived kidney organoids. The identification of this structures requires more study since organoids did not survive cryosectioning method. Whole-mount immunohistochemistry is probably a better alternative to cryosectioning in this type of kidney organoids.

Kidney organoids derived from AIM+PIM population and PIM populations revealed impressive tubular structures that could be easily seen under the microscope. By immunostaining it revealed distal tube (LTL- GATA- ECAD+) and early proximal tube (LTL+ ECAD-) formation, surrounded by WT1+ glomeruli cells. With no GATA3 expression, it was concluded that kidney organoids obtained were still immature.

Furthermore, the cisplatin assay used to confirm organoid viability as proximal tubule injury model revealed no KIM-1 expression, it was hypothesized that this is due to the fact that the proximal tubules present in the kidney organoid are still immature. However, it is suspected that cisplatin halted the growth of distal tubules and down-regulated genes related with tubular genesis as revealed in the RT-PCR analysis.

In future experiments, I propose to access the gene expression of neutrophil gelatinase-associated lipocalin (NGAL). This could shed light into distal tubule injury by cisplatin, since NGAL is an early biomarker for nephrotoxic injury specifically in distal tubules of kidneys. NGAL protein expression was induced specifically in ECAD-positive distal tubules while subjected to cisplatin, as it was reported in Uchimura protocol article (Uchimura et al., 2020). Alternatively, apoptosis in cells treated by cisplatin can be detected by cleaved caspase-3 antibody-staining (CASP3) and give a more general answer about overall damage in the organoids (Takasato et al., 2015).

There is also the question if there is sufficient exposure of cisplatin in kidneys organoids, as a 24-hour exposure to 5 μM concentration of cisplatin may not be enough to assess significant injury in the tubules, but only the downregulation of genes related to tubule growth. Future research should certainly test further whether cisplatin injury is dose-dependent and at what threshold there is simultaneous distal tube and proximal tubes injury. Additionally, whole-mount immunostaining can potentially expand the understanding if there is specific zones or gradients that are damaged by cisplatin in the kidney organoids that are grown in transwell. Since air-liquid interface of transwells imply limited contact with the culture medium, where the cisplatin is supplemented.

Development of “Morisato” protocol is set out to be more economically viable option as Uchimura protocol, with less small molecules supplemented and at the same time using the same rationale of separate induction followed by co-culture. “Morisato” rises as a promising protocol but requires more optimization, namely in the number of cells of each population (AIM and PIM) seeded in the transwell and their respective ratio as well, as a response to the problem inviable populations seeded in transwell. Nevertheless, surviving AIM-derived kidney organoid at day 30 of differentiation shown structures canonically derived from PIM populations, such as renal vesicles (PAX8+ LHX1+), early proximal tubules (LTL+ GATA3-) and distal tubules (LTL- ECAD+). However, where was no WT1 and NPHS1 staining, suggesting no glomeruli generation.

Kidney organoids at day 30, both in Uchimura and “Morisato” protocols, revealed to be highly heterogenous in size and shape. This may be related with the number of cells that survive seeding in transwell and quality of the cell populations. This problem can be resolved by bioprinting that could allow precise manipulation of biophysical properties, including organoid size, cell number and conformation in the transwells. One example is the application of extrusion-based 3D cellular bioprinting that made

possible high-throughput generation of kidney organoids with highly reproducible cell number and viability (Lawlor et al., 2021).

Overall, the limitations of the present study include low number or absence of replicates in the performed experiments, as a greater number of replicates for each experiment would provide a more accurate comparison. Additionally, working with 2 or 3 different pluripotent stem cell lines would be beneficial to demonstrate proof-of-concept of the experiments.

References

Adewumi, O., Aflatoonian, B., Ahrlund-Richter, L., Amit, M., Andrews, P. W., Beighton, G., Bello, P. A., Benvenisty, N., Berry, L. S., Bevan, S., Blum, B., Brooking, J., Chen, K. G., Choo, A. B. H., Churchill, G. A., Corbel, M., Damjanov, I., Draper, J. S., Dvorak, P., … Zhang, W. (2007). Characterization of human embryonic stem cell lines by the International Stem Cell Initiative. *Nature Biotechnology*, *25*(7), 803–816. https://doi.org/10.1038/nbt1318

Akutsu, H., Cowan, C. A., & Melton, D. (2006). Human Embryonic Stem Cells. In *Methods in Enzymology* (Vol. 418, pp. 78–92). https://doi.org/10.1016/S0076-6879(06)18005-2

Barnett, L. M. A., & Cummings, B. S. (2018). *Nephrotoxicity and Renal Pathophysiology: A Contemporary Perspective*. https://doi.org/10.1093/toxsci/kfy159/5043549

Basson, M. A., Akbulut, S., Watson-Johnson, J., Simon, R., Carroll, T. J., Shakya, R., Gross, I., Martin, G. R., Lufkin, T., McMahon, A. P., Wilson, P. D., Costantini, F. D., Mason, I. J., & Licht, J. D. (2005). Sprouty1 is a critical regulator of GDNF/RET-mediated kidney induction. *Developmental Cell*, *8*(2), 229–239. https://doi.org/10.1016/j.devcel.2004.12.004

Batourina, E., Gim, S., Bello, N., Shy, M., Clagett-Dame, M., Srinivas, S., Costantini, F., & Mendelsohn, C. (2001). Vitamin A controls epithelial/mesenchymal interactionsthrough Ret expression. *Nature Publishing Group*, *27*, 74–78.

Bouchard, M., Souabni, A., Mandler, M., Neubüser, A., & Busslinger, M. (2002). Nephric lineage specification by Pax2 and Pax8. *Genes and Development*, *16*(22), 2958–2970. https://doi.org/10.1101/gad.240102

Bradley, A., Evans, M., Kaufman, M. H., & Robertson, E. (1984). Formation of germ-line chimaeras from embryo-derived teratocarcinoma cell lines. *Nature*, *309*, 255–256. https://doi.org/10.1038/309255a0

Carlson, B. M., & Kantaputra, P. N. (2018). *Human embryology and developmental biology* (6th ed.). Elsevier .

Carpenedo, R. L., & McDevitt, T. C. (2013). Stem Cells: Key Concepts. In *Biomaterials Science: An Introduction to Materials: Third Edition* (pp. 487–495). Elsevier Inc. https://doi.org/10.1016/B978-0-08-087780-8.00042-5

Carroll, T. J., Park, J. S., Hayashi, S., Majumdar, A., & McMahon, A. P. (2005). Wnt9b plays a central role in the regulation of mesenchymal to epithelial transitions underlying organogenesis of the mammalian urogenital system. *Developmental Cell*, *9*(2), 283–292. https://doi.org/10.1016/j.devcel.2005.05.016

Chagastelles, P. C., & Nardi, N. B. (2011). Biology of stem cells: An overview. In *Kidney International Supplements* (Vol. 1, Issue 3, pp. 63–67). https://doi.org/10.1038/kisup.2011.15

Chen, K. G., Mallon, B. S., McKay, R. D. G., & Robey, P. G. (2014). Human pluripotent stem cell culture: Considerations for maintenance, expansion, and therapeutics. In *Cell Stem Cell* (Vol. 14, Issue 1, pp. 13–26). Cell Press. https://doi.org/10.1016/j.stem.2013.12.005

Cook, D., Brown, D., Alexander, R., March, R., Morgan, P., Satterthwaite, G., & Pangalos, M. N. (2014). Lessons learned from the fate of AstraZeneca's drug pipeline: A five-dimensional framework. In *Nature Reviews Drug Discovery* (Vol. 13, Issue 6, pp. 419–431). Nature Publishing Group. https://doi.org/10.1038/nrd4309

Cruz, N. M., Song, X., Czerniecki, S. M., Gulieva, R. E., Churchill, A. J., Kim, Y. K., Winston, K., Tran, L. M., Diaz, M. A., Fu, H., Finn, L. S., Pei, Y., Himmelfarb, J., & Freedman, B. S. (2017). Organoid cystogenesis reveals a critical role of microenvironment in human polycystic kidney disease. In

Nature Materials (Vol. 16, Issue 11, pp. 1112–1119). Nature Publishing Group. https://doi.org/10.1038/NMAT4994

Cummings, B. S., & Schnellmann, R. G. (2002). *Cisplatin-Induced Renal Cell Apoptosis: Caspase 3-Dependent and-Independent Pathways*. http://jpet.aspetjournals.org

Davies, J. A. (2018). Organoids and mini-organs: Introduction, history, and potential. Introduction, history, and potential. In *Organoids and Mini-Organs* (pp. 3–23). Elsevier Inc. https://doi.org/10.1016/B978-0-12-812636-3.00001-8

de Miguel, M. P., Fuentes-Julián, S., & Alcaina, Y. (2010). Pluripotent Stem Cells: Origin, Maintenance and Induction. In *Stem Cell Reviews and Reports* (Vol. 6, Issue 4, pp. 633–649). https://doi.org/10.1007/s12015-010-9170-1

de Wert, G., & Mummery, C. (2003). Human embryonic stem cells: Research, ethics and policy. In *Human Reproduction* (Vol. 18, Issue 4, pp. 672–682). Oxford University Press. https://doi.org/10.1093/humrep/deg143

Deinsberger, J., & Weber, B. (2021). Induced pluripotent stem cells for vascular tissue engineering. *IPSCs in Tissue Engineering*, 77–97. https://doi.org/10.1016/B978-0-12-823809-7.00002-5

Draper, J. S., Pigott, C., Thomson, J. A., & Andrews, P. W. (2002). Surface antigens of human embryonic stem cells: changes upon differentiation in culture*. In *J. Anat* (Vol. 200).

Dressler, G. R. (2006). The cellular basis of kidney development. In *Annual Review of Cell and Developmental Biology* (Vol. 22, pp. 509–529). https://doi.org/10.1146/annurev.cellbio.22.010305.104340

Dressler, G. R., Deutsch, U., Chowdhury, K., Nornes, H. O., & Gruss, P. (1990). Pax2, a new murine paired-box-containing gene and its expression in the developing excretory system. *Development*, *109*(4), 787–795. https://doi.org/10.1242/dev.109.4.787

Dvela-Levitt, M., Kost-Alimova, M., Emani, M., Kohnert, E., Thompson, R., Sidhom, E. H., Rivadeneira, A., Sahakian, N., Roignot, J., Papagregoriou, G., Montesinos, M. S., Clark, A. R., McKinney, D., Gutierrez, J., Roth, M., Ronco, L., Elonga, E., Carter, T. A., Gnirke, A., … Greka, A. (2019). Small Molecule Targets TMED9 and Promotes Lysosomal Degradation to Reverse Proteinopathy. *Cell*, *178*(3), 521-535.e23. https://doi.org/10.1016/j.cell.2019.07.002

Forbes, T. A., Howden, S. E., Lawlor, K., Phipson, B., Maksimovic, J., Hale, L., Wilson, S., Quinlan, C., Ho, G., Holman, K., Bennetts, B., Crawford, J., Trnka, P., Oshlack, A., Patel, C., Mallett, A., Simons, C., & Little, M. H. (2018). Patient-iPSC-Derived Kidney Organoids Show Functional Validation of a Ciliopathic Renal Phenotype and Reveal Underlying Pathogenetic Mechanisms. *American Journal of Human Genetics*, *102*(5), 816–831. https://doi.org/10.1016/j.ajhg.2018.03.014

Fowler, J. L., Ang, L. T., & Loh, K. M. (2020). A critical look: Challenges in differentiating human pluripotent stem cells into desired cell types and organoids. In *Wiley Interdisciplinary Reviews: Developmental Biology* (Vol. 9, Issue 3). John Wiley and Sons Inc. https://doi.org/10.1002/wdev.368

Freedman, B. S., Brooks, C. R., Lam, A. Q., Fu, H., Morizane, R., Agrawal, V., Saad, A. F., Li, M. K., Hughes, M. R., Werff, R. vander, Peters, D. T., Lu, J., Baccei, A., Siedlecki, A. M., Valerius, M. T., Musunuru, K., McNagny, K. M., Steinman, T. I., Zhou, J., … Bonventre, J. v. (2015). Modelling kidney disease with CRISPR-mutant kidney organoids derived from human pluripotent epiblast spheroids. *Nature Communications*, *6*. https://doi.org/10.1038/ncomms9715

Georgas, K., Rumballe, B., Wilkinson, L., Chiu, H. S., Lesieur, E., Gilbert, T., & Little, M. H. (2008). Use of dual section mRNA in situ hybridisation/immunohistochemistry to clarify gene expression patterns during the early stages of nephron development in the embryo and in the mature nephron of the adult mouse kidney. *Histochemistry and Cell Biology*, *130*(5), 927–942. https://doi.org/10.1007/s00418-008-0454-3

Grobstein, C., & Dalton, A. J. (1956). *Kidney tubule induction in mouse metanephrogenic mesenchyme without cytoplasmic contact*.

Howden, S. E., Vanslambrouck, J. M., Wilson, S. B., Tan, K. S., & Little, M. H. (2019). Reporter-based fate mapping in human kidney organoids confirms nephron lineage relationships and reveals synchronous nephron formation. *EMBO Reports*, *20*(4). https://doi.org/10.15252/embr.201847483

Iberite, F., Gruppioni, E., & Ricotti, L. (2022). Skeletal muscle differentiation of human iPSCs meets bioengineering strategies: perspectives and challenges. In *npj Regenerative Medicine* (Vol. 7, Issue 1). Nature Research. https://doi.org/10.1038/s41536-022-00216-9

Kim, D., & Dressler, G. R. (2005). Nephrogenic factors promote differentiation of mouse embryonic stem cells into renal epithelia. *Journal of the American Society of Nephrology*, *16*(12), 3527–3534. https://doi.org/10.1681/ASN.2005050544

King, N. M., & Perrin, J. (2014). *Ethical issues in stem cell research and therapy*. http://stemcellres.com/content/5/4/85

Kinney, M. A., Saeed, R., & McDevitt, T. C. (2012). Systematic analysis of embryonic stem cell differentiation in hydrodynamic environments with controlled embryoid body size. *Integrative Biology (United Kingdom)*, *4*(6), 641–650. https://doi.org/10.1039/c2ib00165a

Kirby, A., Gnirke, A., Jaffe, D. B., Barešová, V., Pochet, N., Blumenstiel, B., Ye, C., Aird, D., Stevens, C., Robinson, J. T., Cabili, M. N., Gat-Viks, I., Kelliher, E., Daza, R., Defelice, M., Hůlková, H., Sovová, J., Vylet'al, P., Antignac, C., … Daly, M. J. (2013). Mutations causing medullary cystic kidney disease type 1 lie in a large VNTR in MUC1 missed by massively parallel sequencing. *Nature Genetics*, *45*(3), 299–303. https://doi.org/10.1038/ng.2543

Labastie, M.-C., Catala, M., Gregoire, J.-M., & Peault, B. (1995). The GATA-3 gene is expressed during human kidney embryogenesis. In *Kidney International* (Vol. 47).

Lancaster, M. A., & Huch, M. (2019). Disease modelling in human organoids. *DMM Disease Models and Mechanisms*, *12*(7). https://doi.org/10.1242/dmm.039347

Lancaster, M. A., & Knoblich, J. A. (2014). Organogenesisin a dish: Modeling development and disease using organoid technologies. In *Science* (Vol. 345, Issue 6194). American Association for the Advancement of Science. https://doi.org/10.1126/science.1247125

Lancaster, M. A., Renner, M., Martin, C. A., Wenzel, D., Bicknell, L. S., Hurles, M. E., Homfray, T., Penninger, J. M., Jackson, A. P., & Knoblich, J. A. (2013). Cerebral organoids model human brain development and microcephaly. *Nature*, *501*(7467), 373–379. https://doi.org/10.1038/nature12517

Lawlor, K. T., Vanslambrouck, J. M., Higgins, J. W., Chambon, A., Bishard, K., Arndt, D., Er, P. X., Wilson, S. B., Howden, S. E., Tan, K. S., Li, F., Hale, L. J., Shepherd, B., Pentoney, S., Presnell, S. C., Chen, A. E., & Little, M. H. (2021). Cellular extrusion bioprinting improves kidney organoid reproducibility and conformation. *Nature Materials*, *20*(2), 260–271. https://doi.org/10.1038/s41563-020-00853-9

Lengerke, C., Schmitt, S., Bowman, T. v., Jang, I. H., Maouche-Chretien, L., McKinney-Freeman, S., Davidson, A. J., Hammerschmidt, M., Rentzsch, F., Green, J. B. A., Zon, L. I., & Daley, G. Q. (2008). BMP and Wnt Specify Hematopoietic Fate by Activation of the Cdx-Hox Pathway. *Cell Stem Cell*, *2*(1), 72–82. https://doi.org/10.1016/j.stem.2007.10.022

Li, X., Ootani, A., & Kuo, C. (2016). An air-liquid interface culture system for 3D organoid culture of diverse primary gastrointestinal tissues. *Methods in Molecular Biology*, *1422*, 33–40. https://doi.org/10.1007/978-1-4939-3603-8_4

Liu, P., Wakamiya, M., Shea, M. J., Albrecht, U., Behringer, R. R., & Bradley, A. (1999). *Requirement for Wnt3 in vertebrate axis formation*. http://genetics.nature.com

Loh, Y. H., Wu, Q., Chew, J. L., Vega, V. B., Zhang, W., Chen, X., Bourque, G., George, J., Leong, B., Liu, J., Wong, K. Y., Sung, K. W., Lee, C. W. H., Zhao, X. D., Chiu, K. P., Lipovich, L., Kuznetsov, V. A., Robson, P., Stanton, L. W., … Ng, H. H. (2006). The Oct4 and Nanog transcription network regulates pluripotency in mouse embryonic stem cells. *Nature Genetics*, *38*(4), 431–440. https://doi.org/10.1038/ng1760

Lote, C. J. (2012). *Principles of Renal Physiology 5th Edition* (5th ed.). Springer. https://doi.org/https://doi.org/10.1007/978-1-4614-3785-7

Maddah, M., Shoukat-Mumtaz, U., Nassirpour, S., & Loewke, K. (2014). A System for Automated, Noninvasive, Morphology-Based Evaluation of Induced Pluripotent Stem Cell Cultures. *Journal of Laboratory Automation*, *19*(5), 454–460. https://doi.org/10.1177/2211068214537258

Marieb, E., Brady Wilhelm, P., & Mallatt, J. (2012). *Human Anatomy* (6th ed.). Pearson Education, Inc.

Martin, G. R., & Evans, M. J. (1975). *Differentiation of Clonal Lines of Teratocarcinoma Cells: Formation of Embryoid Bodies In Vitro (mouse tumors/tissue culture/pluripotent cells/cell determination/endoderm)* (Vol. 72, Issue 4).

Mese, H., Sasaki, A., Nakayama, S., Alcalde, R. E., & Matsumura, T. (2000). *The role of caspase family protease, caspase-3 on cisplatin-induced apoptosis in cisplatin-resistant A431 cell line*.

Miranda, C. C., Fernandes, T. G., Diogo, M. M., & Cabral, J. M. S. (2018). Towards multi-organoid systems for drug screening applications. In *Bioengineering* (Vol. 5, Issue 3). MDPI AG. https://doi.org/10.3390/bioengineering5030049

Moriya, N., Uchiyama, H., & Asashima, M. (1993). Development Induction of Pronephric Tubules by Activin and Retinoic Acid in Presumptive Ectoderm of Xenopus laevis. In *Develop. Growth & Differ* (Vol. 35, Issue 2).

Morizane, R., & Bonventre, J. v. (2017). Generation of nephron progenitor cells and kidney organoids from human pluripotent stem cells. *Nature Protocols*, *12*(1), 195–207. https://doi.org/10.1038/nprot.2016.170

Morizane, R., & Lam, A. Q. (2015). Directed differentiation of pluripotent stem cells into kidney. *Biomarker Insights*, *2015*, 147–152. https://doi.org/10.4137/BMI.S20055

Morizane, R., Lam, A. Q., Freedman, B. S., Kishi, S., Valerius, M. T., & Bonventre, J. v. (2015). Nephron organoids derived from human pluripotent stem cells model kidney development and injury. *Nature Biotechnology*, *33*(11), 1193–1200. https://doi.org/10.1038/nbt.3392

Morizane, R., Monkawa, T., & Itoh, H. (2009). Differentiation of murine embryonic stem and induced pluripotent stem cells to renal lineage *in vitro*. *Biochemical and Biophysical Research Communications*, *390*(4), 1334–1339. https://doi.org/10.1016/j.bbrc.2009.10.148

Moscona, A., & Moscona, H. (1952). *Organ Rudiments Of The Early Chick Embryo*.

Mugford, J. W., Sipilä, P., McMahon, J. A., & McMahon, A. P. (2008). Osr1 expression demarcates a multi-potent population of intermediate mesoderm that undergoes progressive restriction to an Osr1-dependent nephron progenitor compartment within the mammalian kidney. *Developmental Biology*, *324*(1), 88–98. https://doi.org/10.1016/j.ydbio.2008.09.010

Nusse, R. (2008). Wnt signaling and stem cell control. In *Cell Research* (Vol. 18, Issue 5, pp. 523–527). https://doi.org/10.1038/cr.2008.47

Osafune, K. (2021). iPSC technology-based regenerative medicine for kidney diseases. In *Clinical and Experimental Nephrology* (Vol. 25, Issue 6, pp. 574–584). Springer. https://doi.org/10.1007/s10157-021-02030-x

Peerani, R., Rao, B. M., Bauwens, C., Yin, T., Wood, G. A., Nagy, A., Kumacheva, E., & Zandstra, P. W. (2007). Niche-mediated control of human embryonic stem cell self-renewal and differentiation. *EMBO Journal*, *26*(22), 4744–4755. https://doi.org/10.1038/sj.emboj.7601896

Peli, J., Schmoll, F., Laurincik, J., Brem, G., & Schellande, K. (1996). *Comparison of aggregation and injection techniques in producing chimeras with embryonic stem cells in mice*.

Przepiorski, A., Sander, V., Tran, T., Hollywood, J. A., Sorrenson, B., Shih, J. H., Wolvetang, E. J., McMahon, A. P., Holm, T. M., & Davidson, A. J. (2018). A Simple Bioreactor-Based Method to Generate Kidney Organoids from Pluripotent Stem Cells. *Stem Cell Reports*, *11*(2), 470–484. https://doi.org/10.1016/j.stemcr.2018.06.018

Ramírez-Flores, C. J., & Knoll, L. J. (2021). Breakthroughs in microbiology made possible with organoids. *PLOS Pathogens*, *17*(11), e1010080. https://doi.org/10.1371/JOURNAL.PPAT.1010080

Rippon, H. J., & Bishop, A. E. (2004). Embryonic stem cells. In *Cell Prolif* (Vol. 37).

Rossi, G., Manfrin, A., & Lutolf, M. P. (2018). Progress and potential in organoid research. In *Nature Reviews Genetics* (Vol. 19, Issue 11, pp. 671–687). Nature Publishing Group. https://doi.org/10.1038/s41576-018-0051-9

Sainio, K., & Raatikainen-Ahokas, A. (1999). Mesonephric development and stem cell production Mesonephric kidney-a stem cell factory? Morphogenesis of the mammalian mesonephros. In *Int. J. Dev. Biol* (Vol. 43). www.ehu.es/ijdb

Sakurai, H., Era, T., Jakt, L. M., Okada, M., Nakai, S., Nishikawa, S., & Nishikawa, S.-I. (2006). *In Vitro* Modeling of Paraxial and Lateral Mesoderm Differentiation Reveals Early Reversibility. *Stem Cells*, *24*(3), 575–586. https://doi.org/10.1634/stemcells.2005-0256

Sato, T., Vries, R. G., Snippert, H. J., van de Wetering, M., Barker, N., Stange, D. E., van Es, J. H., Abo, A., Kujala, P., Peters, P. J., & Clevers, H. (2009). Single Lgr5 stem cells build crypt-villus structures *in vitro* without a mesenchymal niche. *Nature*, *459*(7244), 262–265. https://doi.org/10.1038/nature07935

Saxén, L. (1987). *Organogenesis of the Kidney*. Cambridge University Press.

Saxén, L., & Sariola, H. (1987). Early organogenesis of the kidney. In *Pediatr Nephrol* (Vol. 1).

Shamblott, M. J., Axelman, J., Wang, S., Bugg, E. M., Littlefield, J. W., Donovan, P. J., Blumenthal, P. D., Huggins, G. R., & Gearhart, J. D. (1998). Derivation of pluripotent stem cells from cultured human primordial germ cells (alkaline phosphataseembryoid bodyembryonic stem cellembryonic germ cell). In *Developmental Biology* (Vol. 95). www.pnas.org.

Staerk, J., Dawlaty, M. M., Gao, Q., Maetzel, D., Hanna, J., Sommer, C. A., Mostoslavsky, G., & Jaenisch, R. (2010). Reprogramming of human peripheral blood cells to induced pluripotent stem cells. *Cell Stem Cell*, *7*(1), 20–24. https://doi.org/10.1016/j.stem.2010.06.002

Stewart, C. E. (2021). Stem cells and regenerative medicine in sport science. In *Emerging Topics in Life Sciences* (Vol. 5, Issue 4, pp. 563–573). Portland Press Ltd. https://doi.org/10.1042/ETLS20210014

Subramanian, A., Sidhom, E. H., Emani, M., Vernon, K., Sahakian, N., Zhou, Y., Kost-Alimova, M., Slyper, M., Waldman, J., Dionne, D., Nguyen, L. T., Weins, A., Marshall, J. L., Rosenblatt-Rosen, O., Regev, A., & Greka, A. (2019). Single cell census of human kidney organoids shows reproducibility and diminished off-target cells after transplantation. *Nature Communications*, *10*(1). https://doi.org/10.1038/s41467-019-13382-0

Sweetman, D., Wagstaff, L., Cooper, O., Weijer, C., & Münsterberg, A. (2008). The migration of paraxial and lateral plate mesoderm cells emerging from the late primitive streak is controlled by different Wnt signals. *BMC Developmental Biology*, *8*. https://doi.org/10.1186/1471-213X-8-63

Taal, M. W., Brenner, B. M., & Rector, F. C. (2012). *Brenner & Rector's: The kidney* (9th ed., Vol. 2). Elsevier.

Taguchi, A., Kaku, Y., Ohmori, T., Sharmin, S., Ogawa, M., Sasaki, H., & Nishinakamura, R. (2014). Redefining the *in vivo* origin of metanephric nephron progenitors enables generation of complex kidney structures from pluripotent stem cells. *Cell Stem Cell*, *14*(1), 53–67. https://doi.org/10.1016/j.stem.2013.11.010

Taguchi, A., & Nishinakamura, R. (2015). Nephron reconstitution from pluripotent stem cells. In *Kidney International* (Vol. 87, Issue 5, pp. 894–900). Nature Publishing Group. https://doi.org/10.1038/ki.2014.358

Taguchi, A., & Nishinakamura, R. (2017). Higher-Order Kidney Organogenesis from Pluripotent Stem Cells. *Cell Stem Cell*, *21*(6), 730-746.e6. https://doi.org/10.1016/j.stem.2017.10.011

Takahashi, K., Tanabe, K., Ohnuki, M., Narita, M., Ichisaka, T., Tomoda, K., & Yamanaka, S. (2007). Induction of Pluripotent Stem Cells from Adult Human Fibroblasts by Defined Factors. *Cell*, *131*(5), 861–872. https://doi.org/10.1016/j.cell.2007.11.019

Takasato, M., Er, P. X., Chiu, H. S., & Little, M. H. (2016). Generation of kidney organoids from human pluripotent stem cells. *Nature Protocols*, *11*(9), 1681–1692. https://doi.org/10.1038/nprot.2016.098

Takasato, M., Er, P. X., Chiu, H. S., Maier, B., Baillie, G. J., Ferguson, C., Parton, R. G., Wolvetang, E. J., Roost, M. S., de Sousa Lopes, S. M. C., & Little, M. H. (2015). Kidney organoids from human iPS cells contain multiple lineages and model human nephrogenesis. *Nature*, *526*(7574), 564–568. https://doi.org/10.1038/nature15695

Takasato, M., & Little, M. H. (2016). A strategy for generating kidney organoids: Recapitulating the development in human pluripotent stem cells. In *Developmental Biology* (Vol. 420, Issue 2, pp. 210–220). Academic Press Inc. https://doi.org/10.1016/j.ydbio.2016.08.024

Takasato, M., & Wymeersch, F. J. (2020). Challenges to future regenerative applications using kidney organoids. In *Current Opinion in Biomedical Engineering* (Vol. 13, pp. 144–151). Elsevier B.V. https://doi.org/10.1016/j.cobme.2020.03.003

Thomson, J. A., Itskovitz-Eldor, J., Shapiro, S. S., Waknitz, M. A., Swiergiel, J. J., Marshall, V. S., & Jones, J. M. (1998). Embryonic Stem Cell Lines Derived from Human Blastocysts. In *New Series* (Vol. 282, Issue 5391).

Tong, G. X., Yu, W. M., Beaubier, N. T., Weeden, E. M., Hamele-Bena, D., Mansukhani, M. M., & O'Toole, K. M. (2009). Expression of PAX8 in normal and neoplastic renal tissues: An immunohistochemical study. *Modern Pathology*, *22*(9), 1218–1227. https://doi.org/10.1038/modpathol.2009.88

Tsujimoto, H., Kasahara, T., Sueta, S. ichi, Araoka, T., Sakamoto, S., Okada, C., Mae, S. ichi, Nakajima, T., Okamoto, N., Taura, D., Nasu, M., Shimizu, T., Ryosaka, M., Li, Z., Sone, M., Ikeya, M., Watanabe, A., & Osafune, K. (2020). A Modular Differentiation System Maps Multiple Human Kidney Lineages from Pluripotent Stem Cells. *Cell Reports*, *31*(1). https://doi.org/10.1016/j.celrep.2020.03.040

Uchimura, K., Wu, H., Yoshimura, Y., & Humphreys, B. D. (2020). Human Pluripotent Stem Cell-Derived Kidney Organoids with Improved Collecting Duct Maturation and Injury Modeling. *Cell Reports*, *33*(11). https://doi.org/10.1016/j.celrep.2020.108514

Unbekandt, M., & Davies, J. A. (2010). Dissociation of embryonic kidneys followed by reaggregation allows the formation of renal tissues. *Kidney International*, *77*(5), 407–416. https://doi.org/10.1038/ki.2009.482

Ungrin, M. D., Joshi, C., Nica, A., Bauwens, C., & Zandstra, P. W. (2008). Reproducible, ultra high-throughput formation of multicellular organization from single cell suspension-derived human embryonic stem cell aggregates. *PLoS ONE*, *3*(2). https://doi.org/10.1371/journal.pone.0001565

Vaidya, V. S., Ozer, J. S., Dieterle, F., Collings, F. B., Ramirez, V., Troth, S., Muniappa, N., Thudium, D., Gerhold, D., Holder, D. J., Bobadilla, N. A., Marrer, E., Perentes, E., Cordier, A., Vonderscher,

J., Maurer, G., Goering, P. L., Sistare, F. D., & Bonventre, J. v. (2010). Kidney injury molecule-1 outperforms traditional biomarkers of kidney injury in preclinical biomarker qualification studies. *Nature Biotechnology*, *28*(5), 478–485. https://doi.org/10.1038/nbt.1623

van den Brink, S. C., Baillie-Johnson, P., Balayo, T., Hadjantonakis, A. K., Nowotschin, S., Turner, D. A., & Arias, A. M. (2014). Symmetry breaking, germ layer specification and axial organisation in aggregates of mouse embryonic stem cells. *Development (Cambridge)*, *141*(22), 4231–4242. https://doi.org/10.1242/dev.113001

Votteler, M., Kluger, P. J., Walles, H., & Schenke-Layland, K. (2010). Stem Cell Microenvironments - Unveiling the Secret of How Stem Cell Fate is Defined. In *Macromolecular Bioscience* (Vol. 10, Issue 11, pp. 1302–1315). https://doi.org/10.1002/mabi.201000102

Wang, Z., Li, W., Chen, T., Yang, J., Wen, Z., Yan, X., Shen, T., & Liang, R. (2015). Activin A can induce definitive endoderm differentiation from human parthenogenetic embryonic stem cells. *Biotechnology Letters*, *37*(8), 1711–1717. https://doi.org/10.1007/s10529-015-1829-x

Weitzer, G. (2006). Embryonic Stem Cell-Derived Embryoid Bodies: An *In Vitro* Model of Eutherian Pregastrulation Development and Early Gastrulation. In *HEP* (Vol. 174).

Wellik, D. M. (2011). Hox genes and kidney development. *Pediatric Nephrology*, *26*(9), 1559–1565. https://doi.org/10.1007/s00467-011-1902-1

Wesselschmidt, R. L. (2011). The teratoma assay: An *in vivo* assessment of pluripotency. *Methods in Molecular Biology*, *767*, 231–241. https://doi.org/10.1007/978-1-61779-201-4_17

Wilson, H. v. (1910). DEVELOPMENT OF SPONGES FROM TISSUE CELLS OUTSIDE THE BODY OF THE PARENT. In *Source: Journal of the Elisha Mitchell Scientific Society* (Vol. 26, Issue 2). https://www.jstor.org/stable/24331171

Wu, H., & Humphreys, B. D. (2020). Single Cell Sequencing and Kidney Organoids Generated from Pluripotent Stem Cells. *Clinical Journal of the American Society of Nephrology : CJASN*, *15*(4), 550–556. https://doi.org/10.2215/CJN.07470619

Wu, J., & Izpisua Belmonte, J. C. (2016). Stem Cells: A Renaissance in Human Biology Research. In *Cell* (Vol. 165, Issue 7, pp. 1572–1585). Cell Press. https://doi.org/10.1016/j.cell.2016.05.043

Xia, Y., Nivet, E., Sancho-Martinez, I., Gallegos, T., Suzuki, K., Okamura, D., Wu, M. Z., Dubova, I., Esteban, C. R., Montserrat, N., Campistol, J. M., & Izpisua Belmonte, J. C. (2013). Directed Differentiation of Human Pluripotent Cells to Ureteric Bud Kidney Progenitor-Like Cells. *Nature Cell Biology*, *15*(12), 1507–1515. https://doi.org/10.1038/ncb2872

Xu, J., Wong, E. Y. M., Cheng, C., Li, J., Sharkar, M. T. K., Xu, C. Y., Chen, B., Sun, J., Jing, D., & Xu, P. X. (2014). Eya1 interacts with Six2 and Myc to regulate expansion of the nephron progenitor pool during nephrogenesis. *Developmental Cell*, *31*(4), 434–447. https://doi.org/10.1016/j.devcel.2014.10.015

Yoshimura, Y., Taguchi, A., Tanigawa, S., Yatsuda, J., Kamba, T., Takahashi, S., Kurihara, H., Mukoyama, M., & Nishinakamura, R. (2019). Manipulation of nephron-patterning signals enables selective induction of podocytes from human pluripotent stem cells. *Journal of the American Society of Nephrology*, *30*(2), 304–321. https://doi.org/10.1681/ASN.2018070747

Yu, J., Vodyanik, M. A., Smuga-Otto, K., Antosiewicz-Bourget, J., Frane, J. L., Tian, S., Nie, J., Jonsdottir, G. A., Ruotti, V., Stewart, R., Slukvin, I. I., & Thomson, J. A. (2007). *Induced Pluripotent Stem Cell Lines Derived from Human Somatic Cells*. www.sciencemag.org